http://researchcommons.waikato.ac.nz/

Research Commons at the University of Waikato

Copyright Statement:

The digital copy of this thesis is protected by the Copyright Act 1994 (New Zealand).

The thesis may be consulted by you, provided you comply with the provisions of the Act and the following conditions of use:

- Any use you make of these documents or images must be for research or private study purposes only, and you may not make them available to any other person.
- Authors control the copyright of their thesis. You will recognise the author's right to be identified as the author of the thesis, and due acknowledgement will be made to the author where appropriate.
- You will obtain the author's permission before publishing any material from the thesis.

Synthesis of Platinum Complexes Containing Bidentate N,O-donor Ligands

A thesis submitted in partial fulfilment

of the requirements for the degree

of

Masters of Science in Chemistry

at

The University of Waikato

by

Sophie Anne Sim

The University of Waikato

2014

THE UNIVERSITY OF
WAIKATO
Te Whare Wānanga o Waikato

Abstract

The reaction of N,O-donor ligands hippuric acid and *N*-phenylanthranilic acid with $[PtCl_2(COD)]$ (COD = 1,5-cyclooctadiene) in dichloromethane and in the presence of silver(I) oxide yields the complexes $[Pt\{OC(O)CH_2N(COPh)\}(COD)]$ and $[Pt\{OC(O)(C_6H_4)N(Ph)\}(COD)]$. Several ligand-substitution reactions were performed using complex $[Pt\{OC(O)CH_2N(COPh)\}(COD)]$ and a variety of phosphines, to produce $[Pt\{OC(O)CH_2N(COPh)\}(PPh_3)_2].1.5.CH_2Cl_2$, $[Pt\{OC(O)CH_2N(COPh)\}(dppe)]$ [dppe = 1,2-bis(diphenylphosphino)ethane], $[Pt\{OC(O)CH_2N(COPh)\}(PTA)_2]$ (PTA = 1,3,5-triaza-7-phosphaadamantane) and $[Pt\{OC(O)CH_2N(COPh)\}(dppf)]$ [1,1'-bis(diphenylphosphino)ferrocene]. The X-ray crystal structure of $[Pt\{OC(O)CH_2N(COPh)\}(COD)]$ was obtained which showed the hippurate ligand coordinated to platinum via the nitrogen and oxygen atoms. Attempts were made to synthesise two N,O-coordinated gold(III) complexes, however characterisation showed the resulting products to be a mixture of compounds.

All new complexes were characterised by elemental analysis, melting point, electrospray ionisation mass spectrometry (ESI-MS), nuclear magnetic resonance (NMR) and infra-red (IR) spectroscopy. In particular, a range of various 1D (^1H, ^{13}C, ^{31}P, DEPT and selective NOESY) and 2D (COSY, NOESY, HSQC, HMBC and H2BC) NMR experiments were used to provide full spectral assignment of each complex.

Acknowledgements

I would like to thank my supervisors Bill Henderson and Jo Lane for all the time and effort they have put into helping me with this process. Bill, I am immensely appreciative of your efficiency, advice and prompt responses to any questions throughout my MSc. I am especially appreciative of your commitment to supervision through the period where you were sick. To Jo Lane, thank you for not only being an excellent supervisor but also a great mentor. The advice you have given me on both computational chemistry and life in general has been very beneficial.

I don't quite know how to express my thanks to Alistair Wilkins for the invaluable knowledge and time given when helping me with my thesis NMR experiments, particularly in aiding me with the recovery of a great deal of lost data. Alistair, your expertise and enthusiasm has instilled in me a great love of NMR spectroscopy.

I would also like to thank Dr. Graham Saunders for the X-ray crystal structure determination he carried out for this thesis.

A special thanks to Wendy Jackson and Pat Gread for always answering my silly questions, helping me source much-needed (and ever-missing) equipment and always having an excellent sense of humour.

Thank you to my friends, family and parents for all the support and encouragement for the duration of this thesis. Your reassurance in times of uncertainty picked me up and kept me going. Henry, thank you for cheering me up and for making me laugh on the not-so-good days.

Lastly, thank you to The University of Waikato for a Masters Fees Award and a Masters Research Scholarship.

Table of Contents

List of Figures

List of Tables

List of Abbreviations

NMR	Nuclear Magnetic Resonance
IR	Infra-Red
ESI-MS	Electrospray Ionisation Mass Spectrometry
m/z	mass-to-charge ratio (ESI-MS)
vs	very strong (IR)
s	singlet (NMR)/strong (IR)
d	doublet
t	triplet
m	multiplet (NMR)/medium (IR)
br	broad (NMR, IR)
cm^{-1}	wavenumber
υ	frequency (IR) (in cm^{-1})
asym.	asymmetric (IR)
Hz	Hertz
J	Coupling Constant (in Hz)
ppm	parts-per-million
δ	chemical shift (in ppm)
MHz	MegaHertz
COSY	Correlation Spectroscopy
DEPT	Distortionless Enhancement by Polarisation Transfer
NOESY	Nuclear Overhauser Effect Spectroscopy
HSQC	Heteronuclear Single Quantum Coherence
HMBC	Heteronuclear Multiple Bond Correlation

H2BC	Heteronuclear 2-Bond Correlation
COD	1,5-cyclooctadiene
Bz	benzoyl
dppm	1,1-bis(diphenylphosphino)methane
dppe	1,2-bis(diphenylphosphino)ethane
dppp	1,3-bis(diphenylphosphino)propane
dppb	1,4-bis(diphenylphosphino)butane
PTA	1,3,5-triaza-7-phosphaadamantane
dppf	1,1'-bis(diphenylphosphino)ferrocene
$H_2{}^tBA^FPh$	2-(2-trifluoromethyl)aniline-4,6-di-*tert*-butylphenol
bipy	2,2'-bipyridine
mp	melting point
decomp.	decomposes
mL	millilitre
mmol	millimole
mg	milligram
GoF	Goodness-of-Fit
Å	Angström unit
DFT	Density Functional Theory
CSD	Cambridge Structural Database
anp	anilinopyridyl
bp	benzylpyridyl

Chapter 1: Introduction

1.1 Platinum Compounds Containing N,O-Donor Ligands

There has been much interest in platinum(II) compounds as anti-cancer agents following the discovery - and subsequent use of - *cis*-platin, *cis*-[$PtCl_2(NH_3)_2$], as a powerful anti-tumour drug by Rosenberg et al.[1] While a great deal of attention has been placed on platinum(II) complexes containing amino acids, less compounds of this type containing bidentate, dianionic N,O-donor ligands (typically substituted amino acids) have been reported. In these complexes both the nitrogen and oxygen become deprotonated and bond to the platinum(II) centre, forming a metallacycle ring in the process. This thesis investigates two such N,O-donor ligands, the first being hippuric acid **1** which coordinates to platinum(II) to form complexes of the type **2** (Figure 1.1). The reaction of **2** with phosphine ligands produces complexes of the type **3** (Figure 1.1).

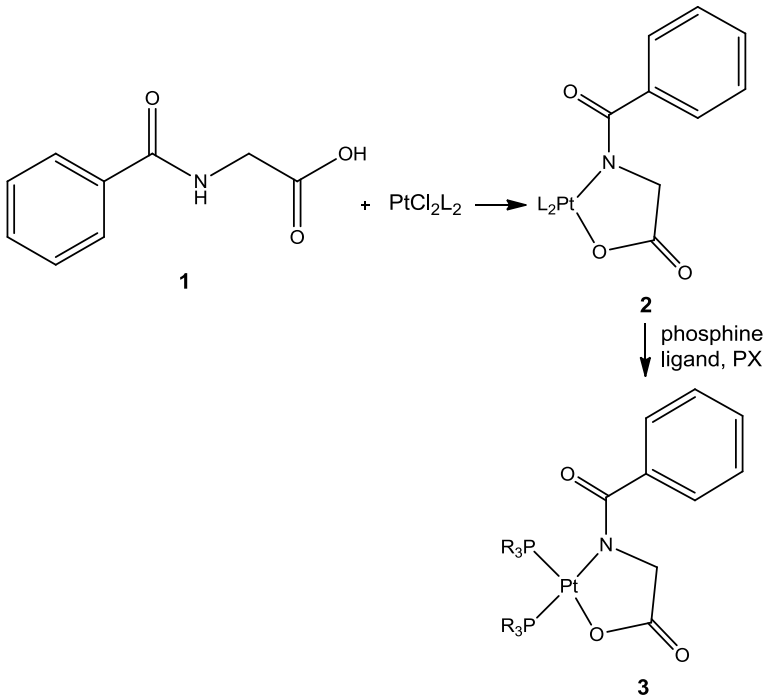

Figure 1.1: The reaction of hippuric acid with the Pt(II) complex Pt_2Cl_2 affords complexes of the type 2. Further reaction with phosphine ligands gives complexes of the type 3.

The second N,O-donor ligand being examined in this thesis is *N*-phenylanthranilic acid **4**, and its coordination to platinum(II) produces complexes of the type **5** outlined in Figure 1.2.

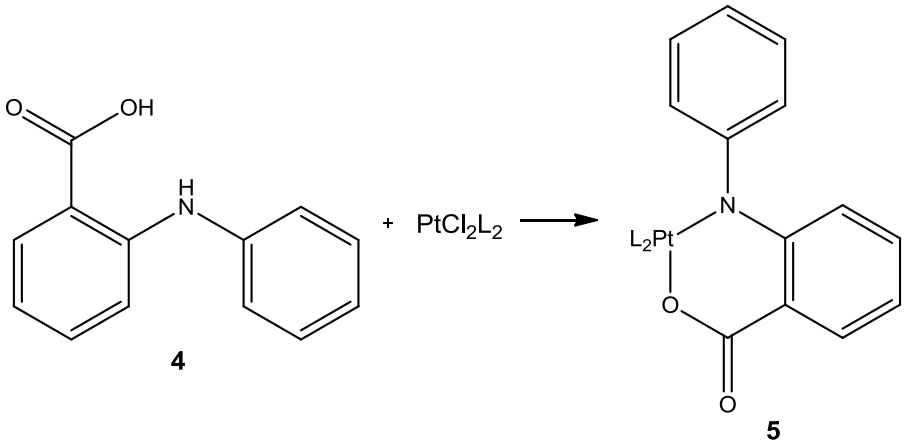

Figure 1.2: Reaction of the N,O-donor ligand *N*-phenylanthranilic acid 4 with the platinum(II) complex Pt_2Cl_2 affords complexes of the type 5.

The purpose of the remainder of this introduction is to review the relevant literature of compounds – and the N,O-donor ligands which coordinate to platinum to form such compounds – which are similar to complexes of the type **2**, **3** and **5**.

1.1.1 Platinum Complexes with Bidentate N,O-Ligands Forming a 5-membered Ring, and Pt-C Bonds

Complexes similar to type **2** (but without the phenyl group) may be synthesised by reacting $PtCl_2L_2$ (where L = a ligand in which carbon binds Pt) with N,O-donor ligands. The first published example of such platinum complexes was in 1976 .[2] Nance & Frye reacted the dipeptides L-val-L-val, L-leu-L-val and L-val-L-leu (where val = valine, leu = leucine, both amino acids) with Zeise's salt, $K[Pt(C_2H_4)Cl_3]$, to form the tetradentate complexes **6**, **7** and **8**. The nitrogen and

oxygen groups of each dipeptide acted as bis(bidentate) ligands to achieve coordination. IR spectroscopy was used for characterisation, and the crystal structure for **6** was obtained, confirming tetradentate coordination.[2]

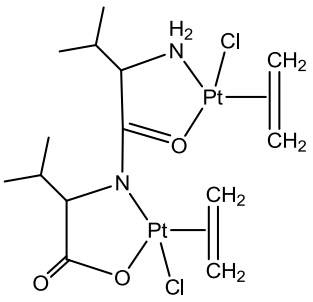

6

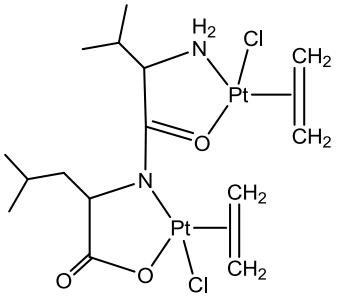

7

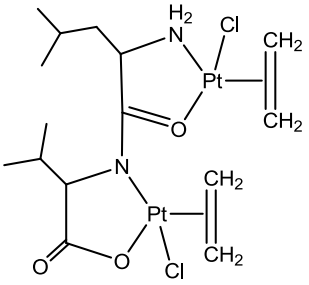

8

In 1992, Kemmitt et al. published two similar bidentate platinum complexes containing Pt-N, Pt-O and Pt-C bonds, [Pt{N(COMe)CH_2C(O)O}(COD)] **9** and [Pt{N(COMe)CH(CH_2Ph)C(O)O}(COD)] **10**.[3] These both contain the COD ligand, which has also been used to synthesise two novel platinum complexes in this thesis. However, complexes **9** and **10** do not appear to have been characterised by X-ray crystallography as their crystal structures cannot be located in the Cambridge Structural Database (CSD, Version 1.15). *N*-Acetylglycine **11** and *N*-acetyl-L-phenylalanine **12** were reacted with [$PtCl_2$(COD)] **13** to produce **9** and **10**, respectively.[3] Interestingly, complex **9** was remade and patented by Fehn in 2006 as a catalyst for crosslinking reactions to prepare silicone elastomers.[4] [$PtCl_2$(COD)] **13** is an important starting material in this thesis, as it has been reacted with various N,O-donor ligands to produce other novel platinum complexes containing the COD ligand.

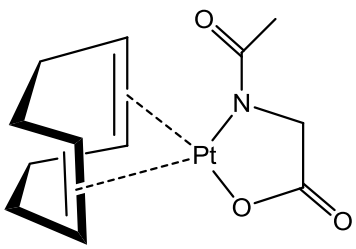

9

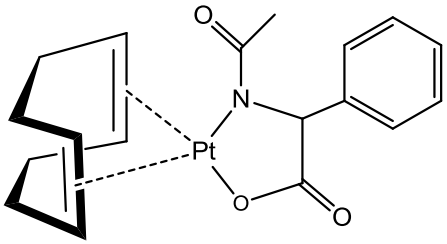

10

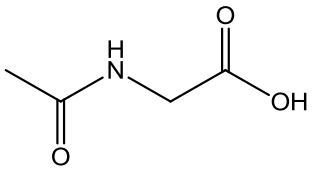

11

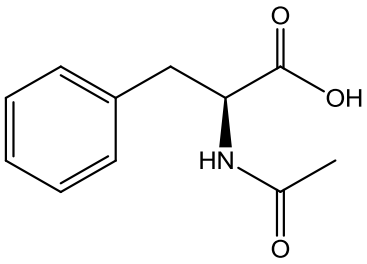

12

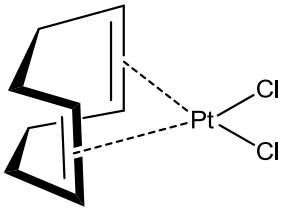

13

Several other examples of such complexes containing both N,O-donor ligands and COD were published by Boyer et al. in 2009.[5] A number of platinum complexes containing the N,O-donor precursor **14** have been synthesised and characterised, several of them crystallographically.

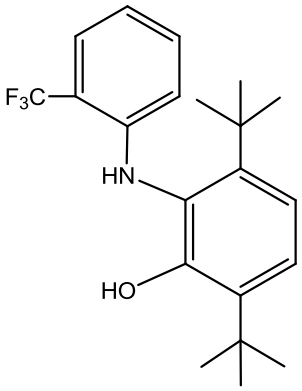

14

Recently, Laurent et al. published the only other known example of a COD-containing platinum complex with bidentate N,O-coordination, [(COD)Pt{OSi-(O^{t}Bu)$_3$}(N(SiMe$_3$)] (complex **15**).[6] This was designed to create silica-supported

platinum nanoparticles, which have applications in the fields of medical imaging [7], electronics [8] and as catalysts for various reactions.[9]

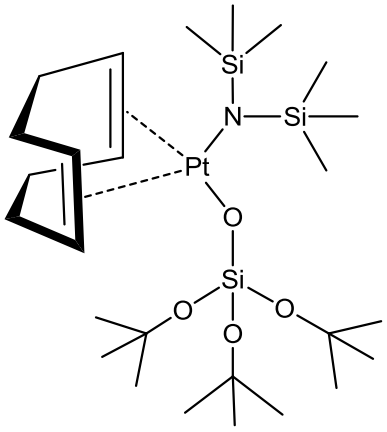

15

1.1.2 Platinum Complexes with Bidentate N,O-Ligands Containing an N-Substituted Acetyl Group Which Form a 5-Membered Ring, and Pt-P Bonds

There are a great deal more platinum complexes containing Pt-P bonds compared to platinum complexes containing N,O-ligands which form a 5-membered metallacycle ring and Pt-C bonds. Complexes such as these are similar to the type **3**. Several such complexes have been synthesised and characterised in this thesis.

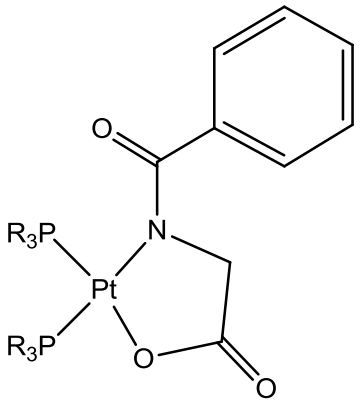

3

In 1991, Kemmitt et al. pioneered this research by publishing 13 of these types of complex **16**-**28**.[10] The group used the starting materials *cis*-[$PtCl_2L_2$] [where L = PPh_3, PMePh, PMe_2Ph, $PBzPh_2$ (Bz = benzyl); L_2 = $Ph_2PCH_2PPh_2$ (dppm), $Ph_2P(CH_2)_2PPh_2$ (dppe), $Ph_2P(CH_2)_3PPh_2$ (dppm), $Ph_2P(CH_2)_4PPh_2$ (dppb)] and the acids α-acetamidocinammic acid **29** (to produce **16**-**23**) and 2-acetamidoacrylic acid **30** (to produce **24**-**28**) and reacted these with silver(I) oxide to form complexes **16**-**28**. No X-ray crystal structures were obtained for any of these complexes. Remarkably, the ^{31}P NMR spectra of complexes **25** and **26** indicate that upon reaction of *cis*-[$PtCl_2L_2$] (L = $PMePh_2$ and PMe_2Ph) and 2-acetamidoacrylic acid with silver(I) oxide, originally complexes **25** and **26** are formed, before being isolated later as only complexes **27** and **28**, respectively.[10] The driving force of this isomerisation is the formation of a strong Pt-C bond in both complex **27** and **28**.[11]

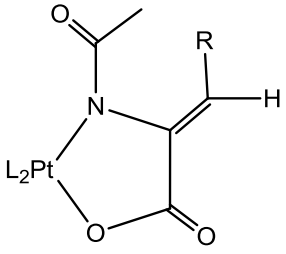

(**16**-**23**: R = Ph, **16**, L = PPh_3; **17**, L = PMePh; **18**, L = PMe_2Ph; **19**, L = $PBzPh_2$; **20**, L_2 = dppm; **21**, L_2 = dppe; **22**, L_2 = dppp; **23**, L_2 = dppb)

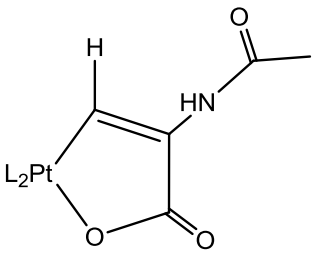

(**27**, L = $PMePh_2$; **28** L = PMe_2Ph)

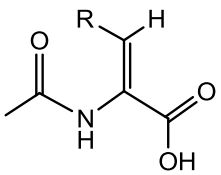

(**24**-**26**: R = H, **24**, L_2 = dppm; **25**, L = $PMePh_2$; **26**, L = PMe_2Ph

(**29**, R = Ph; **30**, R = H)

The same research group published a further 35 complexes containing bidentate dianionic N,O-ligands and phosphine moieties (**31**-**65**) in the following year, which then inspired them to create an additional 6 complexes **66**-**71** using substrates with acidic protons, in the same paper.[3] They succeeded in making all complexes by once again reacting *cis*-[$PtCl_2L_2$] [L & L_2 = the same phosphines used to prepare complexes **23**-**28**, as well as $P(CH_2Ph)Ph_2$, COD and $(PPh_3)_2$] with 1 molar equivalent of various amino acid derivatives [*N*-acetylglycine **11** (to produce **31**-**38**), *N*-acetyl-DL-alanine **72** (to produce **39**-**45**), *N*-acetyl-DL-methionine **73** (to produce **46**-**52**), *N*-acetyl-L-phenylalanine **12** (to produce **53**-**60**), *N*-formylglycine **74** (to produce **61**), *N*-trifluoroacetylglycine **75** (to produce **62**), L-proline **76** (to produce **63**-**65**), 2-acetamidophenol **77** (to produce **66**), pyrrole-2-carboxylic acid **78** (to produce **67**) and oxamic acid **79** (to produce **68**-**71**)] using an excess of silver(I) oxide as a mediating reagent.[3]

The methods of Kemmitt et al. played a large role in this thesis, as similar methods were employed in the production of ligand-substituted complexes during this research.

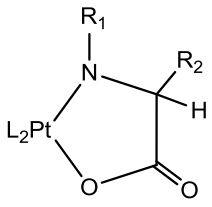

[**31-38**: R_1 = COMe, R_2 = H, **31**, L = PPh_3; **32**, L = $PMePh_2$; **33**, L = $P(CH_2Ph)Ph_2$; **34**, L_2 = dppm; **35**, L_2 = dppe; **36**, L_2 = dppp; **37**, L_2 = dppb; **38**, L_2 = COD]

[**39-45**: R_1 = COMe, R_2 = Me, **39**, L = PPh_3; **40**, L = $PMeCH_2$; **41**, L = $P(CH_2Ph)Ph_2$; **42**, L_2 = dppm; **43**, L_2 = dppe; **44**, L_2 = dppp; **45**, L_2 = dppb]

[**46-52**: R_1 = COMe, R_2 = CH_2CH_2SMe, **46**, L = PPh_3; **47**, L = $PMeCH_2$; **48**, L = $P(CH_2Ph)Ph_2$; **49**, L_2 = dppm; **50**, L_2 = dppe; **51**, L_2 = dppp; **52**, L_2 = dppb]

[**53-60**: R_1 = COMe, R_2 = CH_2Ph, **53**, L = PPh_3; **54**, L = $PMePh_2$; **55**, L = PMe_2Ph; **56**, L_2 = dppm; **57**, L_2 = dppe; **58**, L_2 = dppp; **59**, L_2 = dppb; **60**, L_2 = COD]

[**61**: R_1 = CHO, R_2 = H, **61**, L = $(PPh_3)_2$]

[**62**: R_1 = $COCF_3$, R_2 = H, **62**, L = $(PPh_3)_3$]

[**63-65**: R_1, R_2 = ring -$CH_2CH_2CH_2$-, **63**, L = PPh_3; **64**, L_2 = dppp; **65**, L_2 = dppb]

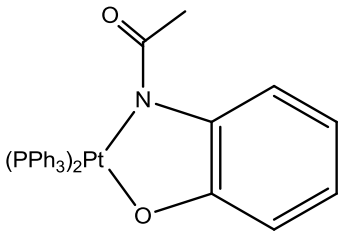

66

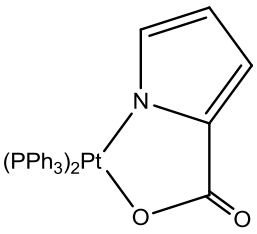

67

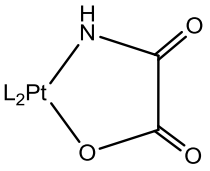

(**68-71**: **68**, L = PPh_3; **69**, L_2 = dppe; **70**, L_2 = dppp; **71**, L_2 = dppb)

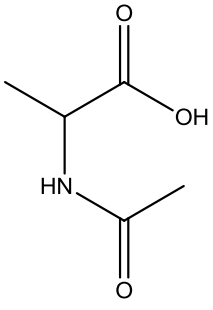

72

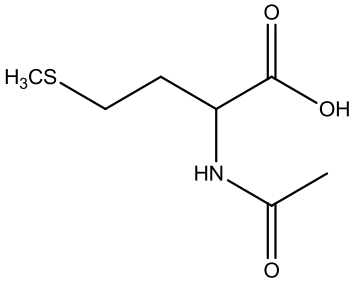

73

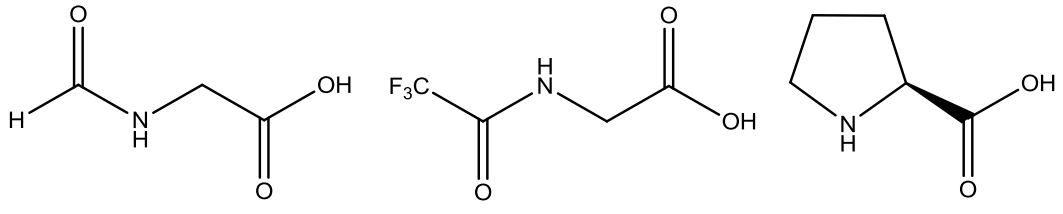

74 **75** **76**

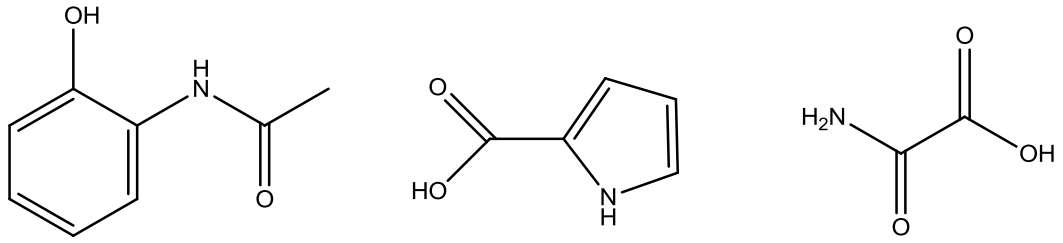

77 **78** **79**

In 1998, Bauer et al. produced 3 heterobimetallic complexes containing Pt-P bonds.[12] Using the same general method as Kemmitt et al., the N,O-donor ligands **80**-**82** were reacted with 1 molar equivalent of $(PPh_3)_2PtCl_2$ along with excess silver(I) oxide to create complexes **83**-**85**. Two diastereoisomers of **83** and four isomers of **84** and **85** were seen in the ^{31}P NMR spectra. None of these were characterised by X-ray crystallography.[12] Complexes **83**-**85** differ from the other complexes containing Pt-P bonds as they contain a piano-stool with an Fe metal centre.

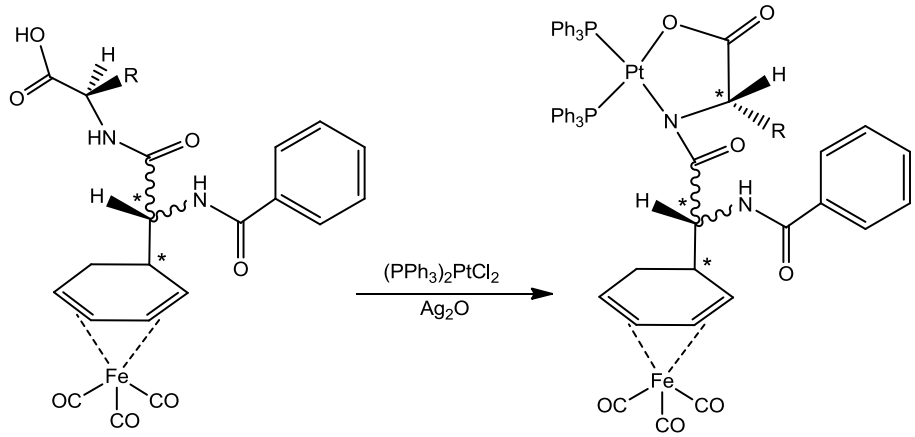

(**80**-**82**: **80**, R = H;
81, R = CH_2Ph;
82, R = CH_2CH_2SMe)

(**83**-**85**: **83**, R = H;
84, R = CH_2Ph;
85, R = CH_2CH_2SMe)

More recently, Chaudhuri et al. reacted the bis(triphenylphosphine)carbonatoplatinum(II) complex $[Pt(CO_3)(PPh_3)_2]$ **86** with 1 molar equivalent of several non-substituted (L-alanine **87**, DL-valine **88** and L-leucine **89**) and substituted amino acids (*N*-methylglycine **90**, *N*-ethylglycine **91**, *N*-acetylglycine **11**, *N*-phenylglycine **92**) in methanol to produce various platinum complexes containing N,O-donor ligands and phosphine groups **93**-**99**.[13]

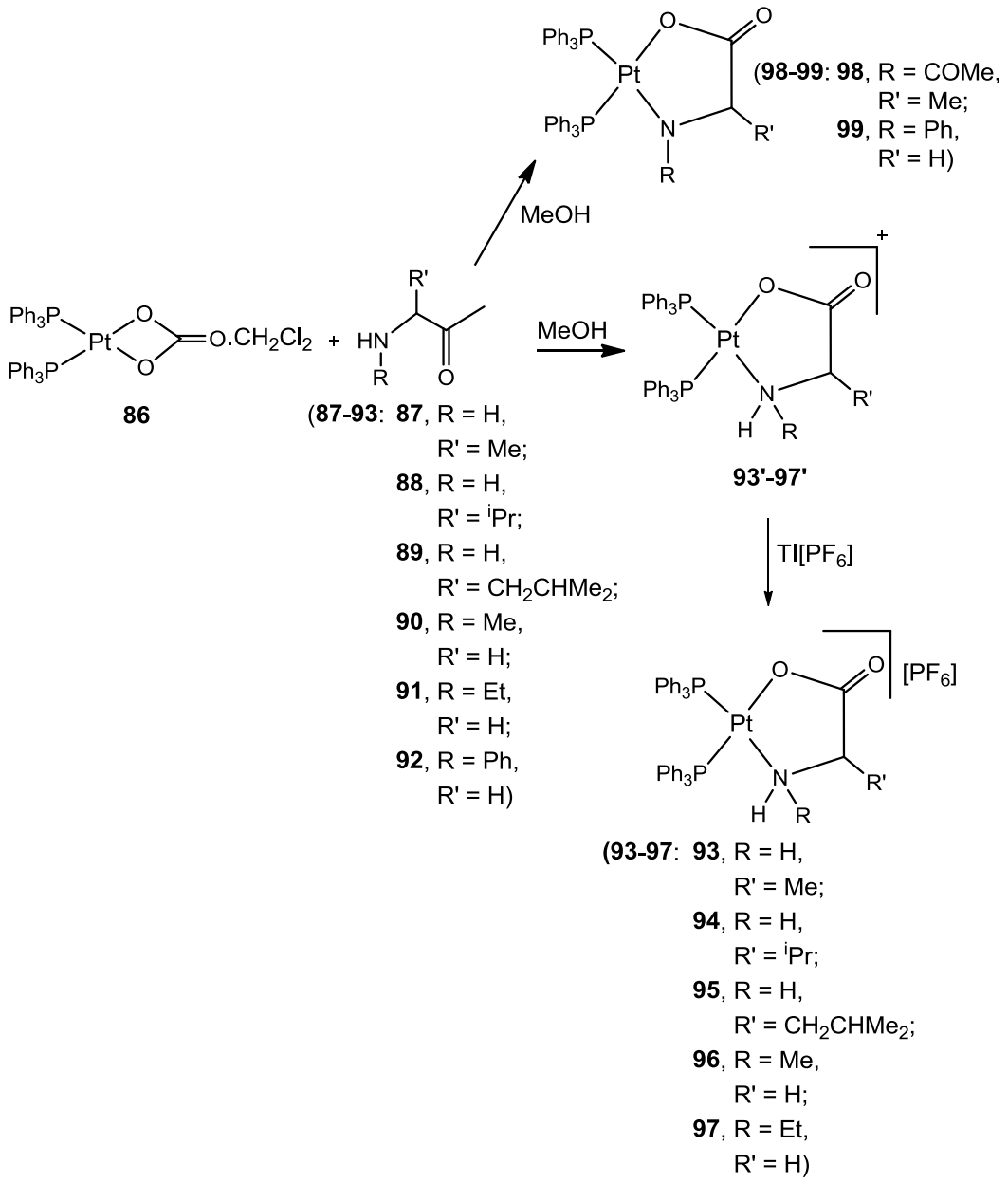

The crystal structure of complex **96** was determined, which showed platinum in a square planar configuration. Cytotoxicity studies against assorted human tumour cell lines (from thyroid, ovarian, epithelial, breast and colon cancers) indicated that complex **98** had the highest activity of the complexes listed, and induced apoptosis (programmed cell-death of affected cells). Further studies on cell cycle perturbation showed that complex **98** also induced cell death more rapidly than *cis*-platin.[13]

1.1.3 Platinum Complexes with Bidentate N,O-Ligands Containing an N-Substituted Phenyl Ketone Group Which Form a 5-membered Ring

Of particular interest to this thesis are the syntheses of platinum complexes containing dianionic N,O-donor ligands, with 5 atoms in the metallacycle, a ring carbonyl, and an N-substituted benzoyl group **2**. Complexes of this type are formed by reacting $PtCl_2L_2$ with N,O-donor ligands (various substituted amino acids). One such N,O-donor ligand is hippuric acid **1**, which has been utilised to produce several further novel bidentate platinum complexes in this thesis, as discussed in Chapters 2-4.

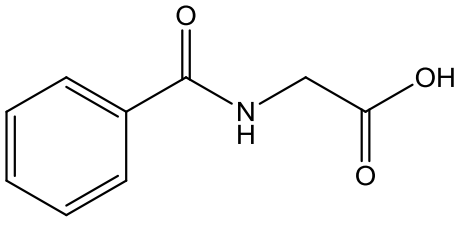

1

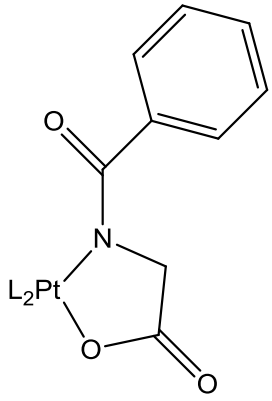

2

In 1997, Gong et al. reacted N-benzoyl-DL-α-valine **99** with Pt(bipy)Cl_2 (bipy = 2,2-bipyridine) in a 1:2 ratio to produce complex **100**.[14] The crystal structure of this complex was not determined.

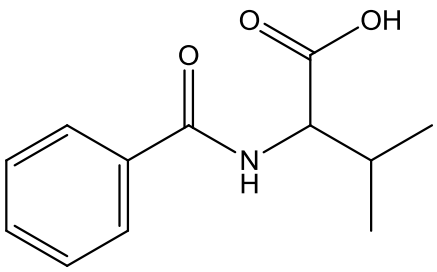

99

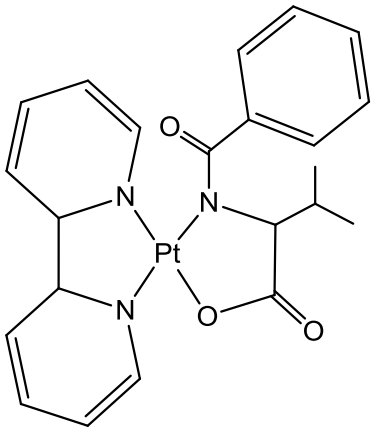

100

Several additional ring-substituted complexes were patented by Zeng in 2004.[15] These benzisoselenazol ketone derivatives were shown to have anti-inflammatory, anti-tumour and anti-thrombotic activity. Various substituted ebselen-glycine derivatives were reacted with diaminocyclohexane platinum to produce complexes **101**-**106**. Zeng patented complex **101** again in 2009 as a continuation of the 2004 patent.[16]

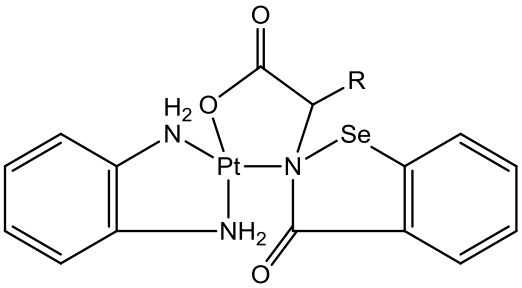

(**101-106**: **101**, R = H_2;
102, R = Me;
103, R = Et;
104, R = CH_2Ph;
105, R = CH_2SH;
106, R = CH_2CH_2SMe)

In 2005, Gabano et al. reacted a novel estrogen-like ligand **107** with $[(NH_3)_2PtI_2]$ to synthesise a new platinum complex **108**.[17] The structural isomer of complex **108** (**109**) contains a dianionic N,O estrogenic ligand, and is formed very slowly, with NMR showing a 6:1 ratio of **108**:**109**. This slow conversion is due to steric hindrance, and the fact that the amidic nitrogen in **109** is less favourable for platinum coordination than the oxygen in **108**.[17]

The majority of mammary tumours express estrogen receptors,[18] so in order to target these cancers the estrogen-like moiety in complex **108** (or its structural isomer, **109**) may deliver the platinum fragment to target the cancerous cells only, enabling the healthy cells to remain unaffected in chemotherapy. However, testing determined that, while the complex maintained its biological activity, (particularly against MCF-7 and MDA-MB-231 breast cancer cell lines), the estrogen-type ligands in the compound caused proliferation of the entire molecule.[17]

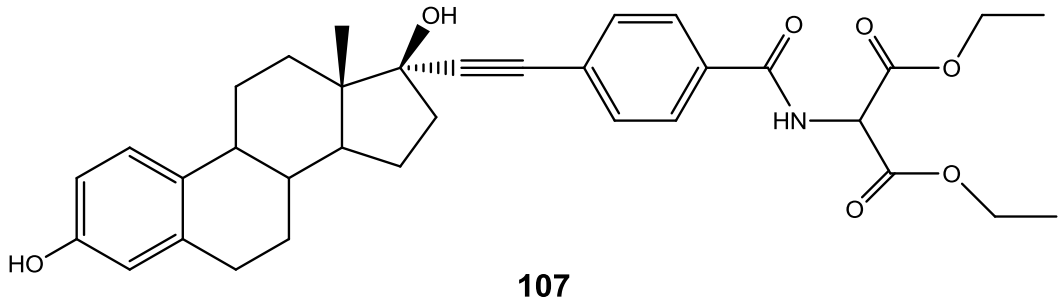

107

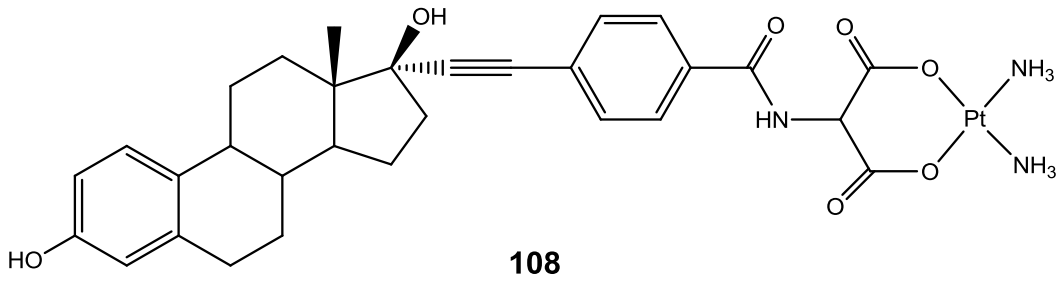

108

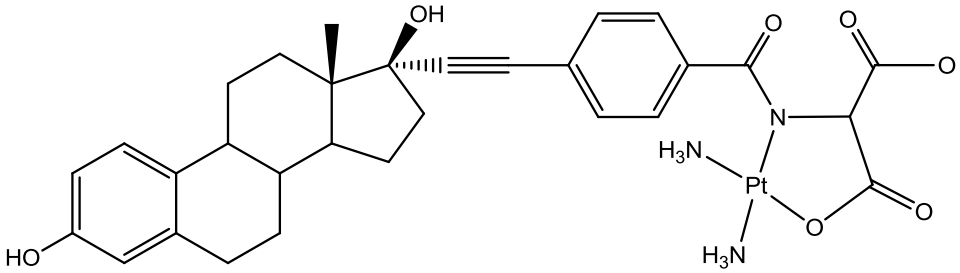

109

Zhang et al. reacted four amino acids (L-leucine **89**, phenylalanine **110**, L-valine **111** and L-tryptophan **112**) with K_2PtCl_4 to produce a further twelve platinum complexes **113-124**, and these were patented in 2010 as precursors for the preparation of anti-tumour drugs.[19] Interestingly, Zhang (along with a new group of researchers) re-patented complexes **113**, **114**, **115** and **118** more recently in 2012.[20]

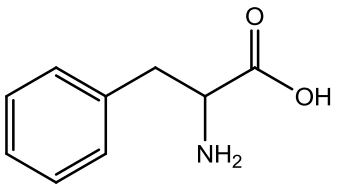

110

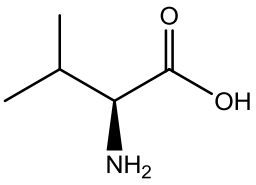

111

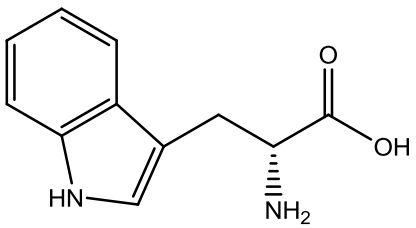

112

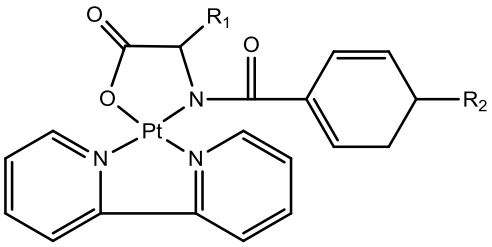

113-118: (**113**, R_1 = ^{i}Bu, R_2 = H;
114, R_1 = CH_2Ph, R_2 = H;
115, R_1 = 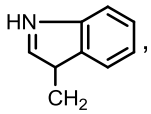 , R_2 = H;
116, R_1 = CH(Me)Et, R_2 = H;
117, R_1 = CH(Me)Et, R_2 = Me;
118, R_1 = ^{i}Pr, R_2 = H)

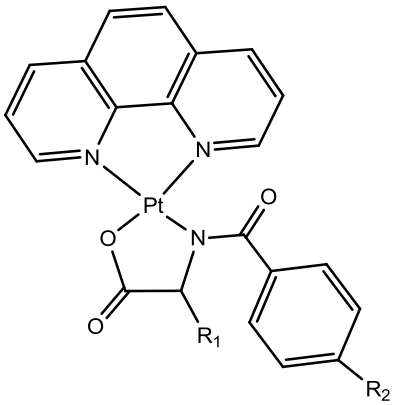

119-124: (**119**, R_1 = ^{i}Bu, R_2 = H
120, R_1 = CH_2Ph, R_2 = H;
121, R_1 = 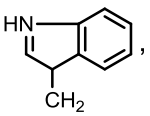 , R_2 = H;
122, R_1 = CH(Me)Et, R_2 = H;
123, R_1 = ^{i}Pr, R_2 = H;
124, R_1 = ^{i}Pr, R_2 = Me)

1.1.4 Platinum Complexes with Bidentate N,O-Ligands Forming a 6-membered Ring

An additional N,O-donor ligand which is investigated in this thesis is *N*-phenylanthranilic acid **4**, which forms a 6-membered ring upon coordination to platinum, producing complexes of the type below **5**. *N*-Phenylanthranilic acid was used to synthesise a new complex which is discussed in Chapter 4.

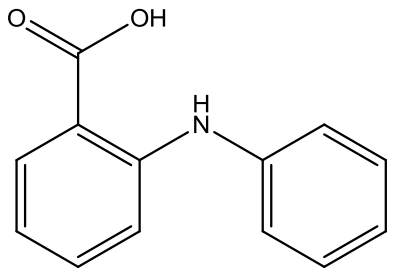

4

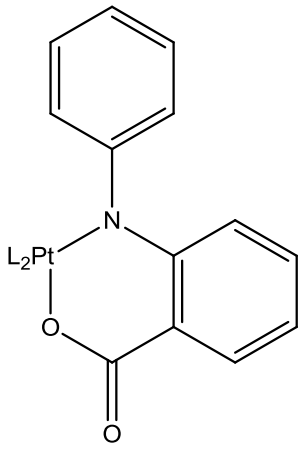

5

A number of similar complexes (without the nitrogen-attached phenyl ring) have been synthesised, dating back to the 1970s. In 1979 Sankhla et al. published another such platinum complex **125**, which was prepared by reacting platinum(II) with o-(2-pyrrolylmethyleneimino)benzoic acid **126** and α-picoline.[21] Magnetic moments, conductance and spectral data suggest that complex **125** has a square planar geometry.

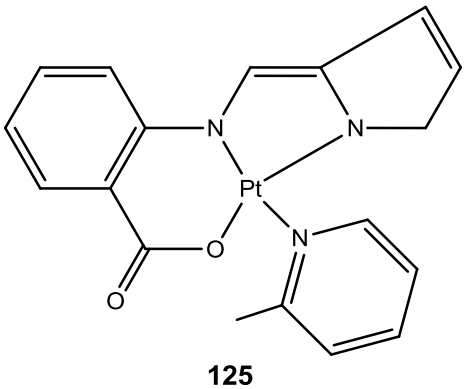

125

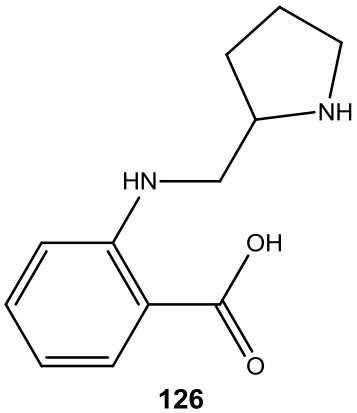

126

Later in 1980, Singh et al. prepared the octahedral platinum(IV) complex **127**, which was then characterised by electrical conductivity, electronic and IR spectra and magnetic studies.[22]

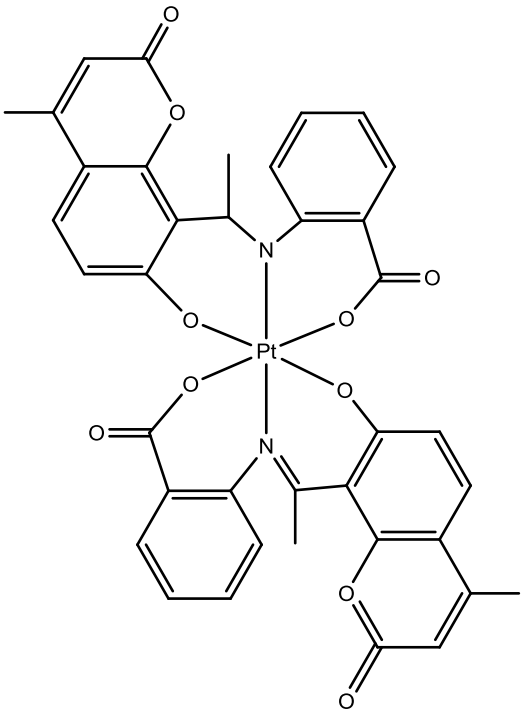

127

Further work was published by Pokhariyal in 1985, which included the divalent platinum complex **128**.[23] This was characterised by molecular conductivity, magnetic, studies, electronic, IR and NMR (^{1}H) spectroscopy as a square planar platinum(II) complex.

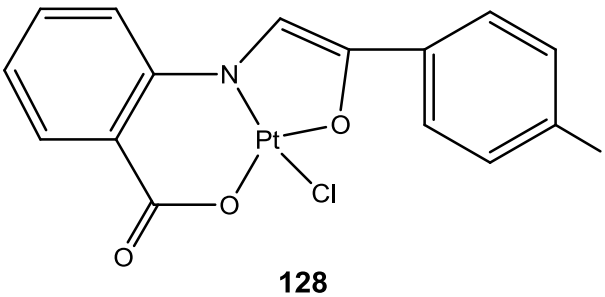

128

In 1985 Gade & Puri reacted three substituted amino acids [2-(acetylamino)benzoic acid **129**, 2-(benzoylamino)benzoic acid **130** and 2-(2-aminobenzoylamino)benzoic acid **131**] with platinum(II) to produce three novel divalent platinum complexes, **132**, **133** and **134** respectively.[24] These were

characterised by molar conductivity, thermal studies and electronic, IR and NMR spectroscopy. The NH and NH_2 groups in complexes **132**, **133** and **134** are expected to bond in a deprotonated form, however no access to the paper was obtained to confirm this (only access to the chemical abstract was available), hence whether **132**, **133** and **134** are actually dianionic N,O-donor ligands may be questionable.

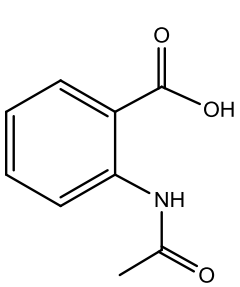

129

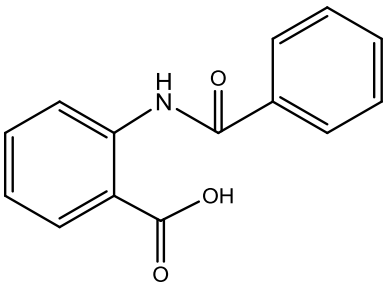

130

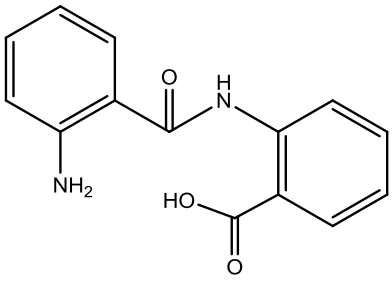

131

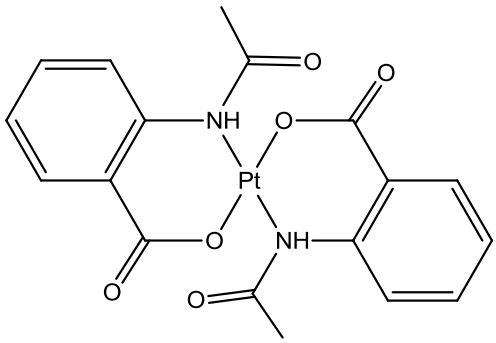

132

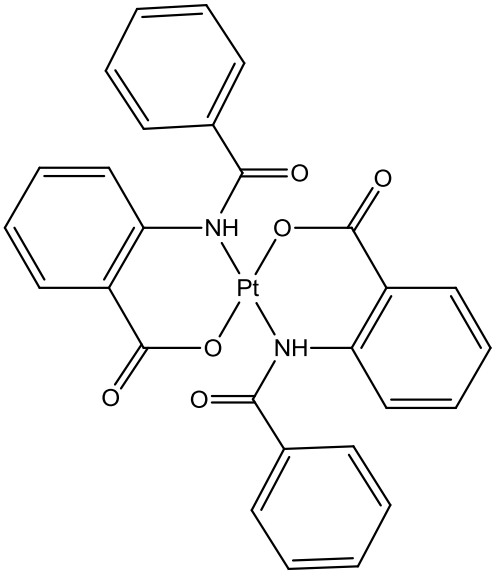

133

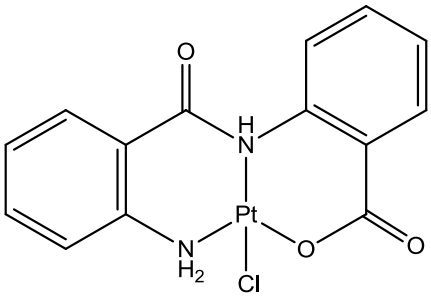

134

The most recent complex of this type was published in 2011. Xie et al. reacted a novel triazene ligand, 1-[(2-carboxymethyl)benzene]-3-[o-aminobenzoic

acid]triazene **135** in a mixture of methanol and dichloromethane with $Pt(PPh_3)_2Cl_2$ in the presence of triethylamine to form the divalent platinum complex **136**.[25] This was characterised by cyclic voltammetry, and ^{31}P NMR, electronic and IR spectra. The X-ray crystal structure of **136** was also determined, which displayed Pt-N and Pt-O bond distances comparable to similar platinum(II) complexes.[26]

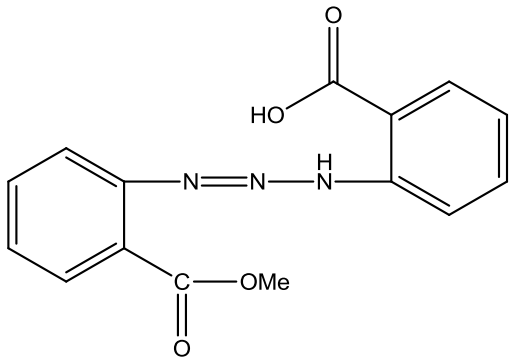

135

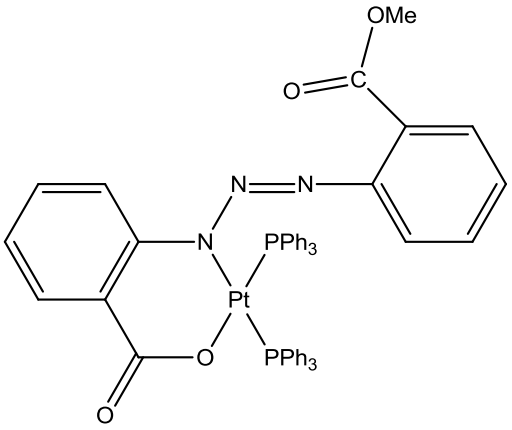

136

1.2 Scope of Investigation

The aims of this thesis were to investigate the synthesis and characterisation of two different dianionic N,O-donor ligand systems coordinated to primarily platinum and gold metal centres, with ancillary phosphine ligands for some complexes. The N,O-donor ligands examined in this thesis include hippuric acid **1** and *N*-phenylanthranilic acid **4**. These were characterised by a number of different techniques, including elemental analyses, melting point, ESI-MS, IR and NMR spectroscopy.

Chapter 2: Synthesis and Characterisation of Platinum Hippurate Complexes

Note:

There are 2 sets of compound numbers; complexes **2a**-**2e** discussed in chapters 2-4 are separate from compound **2** mentioned in the introduction.

2.1 Experimental

2.1.1 Synthesis of [Pt{OC(O)CH$_2$N(COPh)}(COD)] (2a)

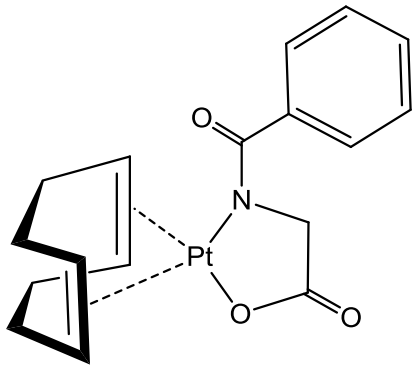

2a

Silver(I) oxide (611.1 mg, excess) was added to a mixture of [PtCl$_2$(COD)] (201.2 mg, 0.538 mmol) and hippuric acid (96.7 mg, 0.540 mmol) in dichloromethane (30 mL), and the mixture was refluxed for 3.5 h giving a brown suspension. After cooling to room temperature the mixture was filtered through glass fibre filter paper giving a pale purple solution. Petroleum spirits (60 mL) was added and the mixture allowed to crystallise, giving pale purple crystals which were filtered off, washed with petroleum spirits (~10 mL) and dried under vacuum overnight to give 124.3 mg (48%) of **2a**.

mp = 157-168°C (decomp.)

Found: C, 42.5; H, 4.0; N, 2.9%. $C_{17}H_{19}NPtO_3$ requires C, 42.5; H, 4.0; N, 2.9%.

IR: υ(C=O) = 1690 cm^{-1}(vs) & 1604 cm^{-1}(vs).

ESI-MS: (capillary exit voltage = 250 V) *m/z* 480.97 (50%, $[M+H]^+$), calculated *m/z* 481.11.

NMR: Refer to Figure 2.3 for the atom numbering scheme of **2a**.

^{1}H δ 7.36-7.18 (m, 5H, H21-H26), 6.51 (s, 2H, H1/H2, $^2J_{Pt-H}$ ~ 70.1 Hz), 5.43 (m, 2H, H5/H6, $^2J_{Pt-H}$ ~ 56.7 Hz), 4.01 (s, 2H, H9a & H9b, $^3J_{Pt-H}$ ~ 18.1 Hz), 2.77-2.23 (m, 8H, H3, H4, H7 & H8) ppm.

^{13}C-{^{1}H} δ 184.4 (s, C10), 176.7 (s, C11, $^2J_{Pt-C}$ ~ 31.7 Hz), 138.5 (s, C21, $^3J_{Pt-C}$ ~ 42.4 Hz), 128.6 (d, overlapping s + s, C23/C25 & C24), 125.5 (s, C22/C26), 98.5 [s, C5/C6$_{(trans\ N)}$, $^1J_{Pt-C}$ = 140.2 Hz], 96.0 [s, C1/C2$_{(trans\ O)}$, $^1J_{Pt-C}$ = 159.9 Hz], 56.9 [s, C9, $^2J_{Pt-C}$ ~ 15.4 Hz], 32.4 [s, C3/C8], 28.2 [s, C4/C7] ppm.

^{13}C-^{1}H (excluding aromatic region) δ 184.4 (t, C10, $^1J_{C-H}$ = 5.6 Hz), 176.7 (s, C11), 138.6 (t, C21, $^1J_{C-H}$ = 6.8 Hz), 98.5 [d, C5/C6$_{(trans\ N)}$, $^1J_{C-H}$ = 164.8 Hz], 96.0 [d, C1/C2$_{(trans\ O)}$, $^1J_{C-H}$ = 165.5 Hz], 56.9 (t, C9, $^1J_{C-H}$ = 140.1 Hz), 32.4 (t, C3/C8, $^1J_{C-H}$ = 130.5 Hz), 28.2 (t, C4/C7, $^1J_{C-H}$ = 131.8 Hz) ppm.

2.1.2 Synthesis of [Pt{OC(O)CH$_2$N(COPh)}(PPh$_3$)$_2$].1.5.CH$_2$Cl$_2$ (2b.1.5CH$_2$Cl$_2$)

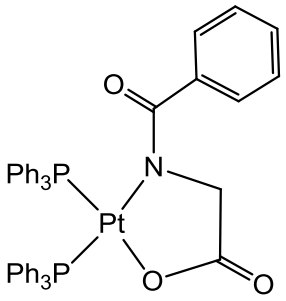

2b

Complex **2b.1.5CH$_2$Cl$_2$** was prepared by a ligand substitution reaction.[27] A mixture of triphenylphosphine (51.8 mg, 0.197 mmol) and **2a** (46.5 mg, 0.097 mmol) was dissolved in dichloromethane (4 mL) and left for 5 min, then filtered through a cotton-plugged glass Pasteur pipette and washed through with a further 0.5 mL dichloromethane to remove any silver impurities. Petroleum spirits (25 mL) was added to precipitate the white needle crystals on standing overnight. Upon subsequent evaporation to 2/3 volume, further product formed which, following removal of the supernatant, was washed with petroleum spirits (~2 mL) and dried under vacuum for 3 hours to give 95.7 mg (97%) of **2b.1.5CH$_2$Cl$_2$**.

mp = 174-178°C

Found: C, 54.3; H, 4.0; N, 1.4%. $C_{45}H_{37}NPtO_3P_2.1.5CH_2Cl_2$ requires C, 54.5; H, 4.0; N, 1.4%.

IR: υ(C=O) = 1647 cm^{-1}(vs).

ESI-MS (added NaCl): (capillary exit voltage = 160 V) *m/z* 919.18 (100%, $[M+Na]^+$), calculated *m/z* for $C_{45}H_{37}NPtO_3P_2.Na$ = 919.18.

NMR: ^{1}H δ 7.81-6.75 (m, 35H, Ph), 5.32 (s, CH_2Cl_2), 4.16 (d, 2H, CH_2, $^3J_{Pt\text{-}H}$ ~ 40.8 Hz) ppm.

^{31}P-{^{1}H} δ 9.2 [d, $P_{A(trans\ N)}$, $^1J_{Pt\text{-}P}$ = 3058 Hz, $^2J_{P\text{-}P}$ = 23.7 Hz], 4.8 [d, $P_{B(trans\ O)}$, $^1J_{Pt\text{-}P}$ = 4031 Hz, $^2J_{P\text{-}P}$ = 22.7 Hz] ppm.

2.1.3 Synthesis of [Pt{OC(O)CH$_2$N(COPh)}(dppe)] (2c)

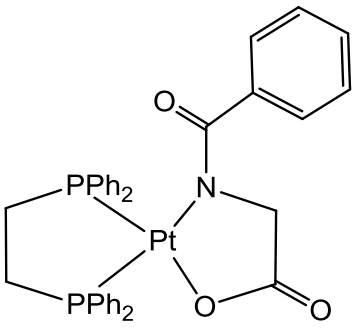

2c

Complex **2c** was prepared by a ligand substitution reaction,[27] following the same procedure as for **2b**, with a mixture of dppe (37.9 mg, 0.095 mmol) and **2a** (44.4 mg, 0.092 mmol) in dichloromethane (4 mL) giving fluffy white crystals [41.1 mg (57%)] of **2c**.

mp = 276-278°C

Found: C, 54.7; H, 4.1; N, 1.8%. $C_{35}H_{31}NPtO_3P_2$ requires C, 54.6; H, 4.1; N, 1.8%.

IR: υ(C=O) = 1652 cm^{-1}(vs).

ESI-MS (added NaCl): (capillary exit voltage = 160 V) *m/z* 793.13 (100%, $[M+Na]^+$), calculated *m/z* for $C_{35}H_{31}NPtO_3P_2$.Na = 793.13.

NMR: ^{1}H δ 7.99-6.77 (m, 25H, Ph), 4.03 [d, 2H, CH_2(metallacycle ring), $^3J_{Pt\text{-}H}$ ~ 18.3 Hz], 2.39-1.99 [m, 4H, CH_2(dppe)] ppm.

^{31}P-{^{1}H} δ 37.4 [d, $P_{A(trans\ N)}$, $^1J_{Pt\text{-}P}$ = 3085 Hz, $^2J_{P\text{-}P}$ = 12.4 Hz], 28.1 [d, $P_{B(trans\ O)}$, $^1J_{Pt\text{-}P}$ = 3876 Hz, $^2J_{P\text{-}P}$ = 12.1 Hz] ppm.

2.1.4 Synthesis of [Pt{OC(O)CH$_2$N(COPh)}(PTA)$_2$] (2d)

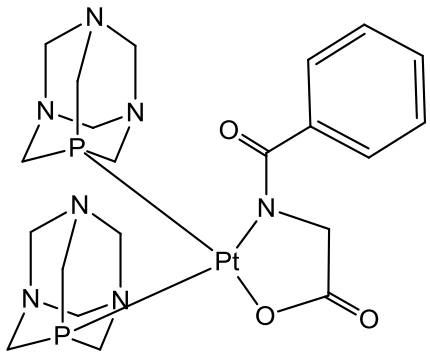

2d

Complex **2d** was prepared by a ligand substitution reaction.[27] A mixture of PTA (28.9 mg, 0.184 mmol) and **2a** (45.7 mg, 0.095 mmol) was dissolved in dichloromethane (4 mL) and left for 5 min. Fluffy white crystals started to form immediately, and petroleum spirits (25 mL) was added to further precipitate this overnight. Following removal of the supernatant, the product was washed with petroleum spirits (~2 mL) and dried under vacuum for 3 hours to give 58.5 mg (90%) of **2d**.

mp = 250-265°C (decomp.)

Found: C, 35.9; H, 4.8; N, 13.7%. $C_{21}H_{21}NPtO_2$ requires C, 36.7; H, 4.6; N, 14.3%.

IR: υ(C=O) = 1638 cm^{-1}(vs).

ESI-MS (added NaCl): (capillary exit voltage = 160 V) *m/z* 709.10 (100%, [M+Na]$^+$), calculated *m/z* for $C_{21}H_{31}N_7PtO_3P_2$.Na = 709.15.

NMR: ^{1}H δ 7.35-7.27 (m, 5H, Ph), 5.28 (s, CH_2Cl_2), 4.58-4.27 [m, 24H, CH_2(PTA)], 4.07 (d, 2H, CH_2(metallacycle ring), $^3J_{Pt\text{-}H}$ = 19.0 Hz) ppm.

^{31}P-{^{1}H} δ -67.0 [d, $P_{A(trans\ N)}$, $^1J_{Pt\text{-}P}$ = 2800 Hz, $^2J_{P\text{-}P}$ = 22.0 Hz], -67.4 [d, $P_{B(trans\ O)}$, $^1J_{Pt\text{-}P}$ = 3484 Hz, $^2J_{P\text{-}P}$ = 21.7 Hz] ppm.

2.1.5 Synthesis of [Pt{OC(O)CH$_2$N(COPh)}(dppf)] (2e)

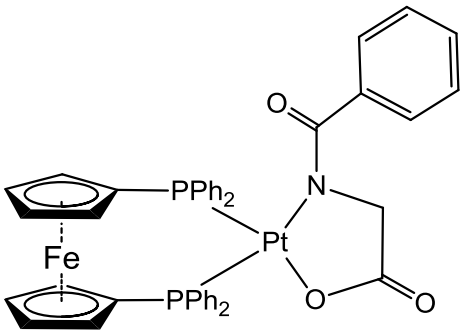

2e

Complex **2e** was prepared by a ligand substitution reaction,[27] using a similar procedure to **2b**. A mixture of dppf (55.0 mg, 0.099 mmol) and **2a** (46.0 mg, 0.096 mmol) was used in the same process as **2b**, however additional petroleum spirits (10 mL) was added to further precipitate the product overnight. Reduction of volume by 1/3 followed by addition of extra petroleum spirits (~1 mL) was repeated once more and the yellow product, after removal of the supernatant, was washed with petroleum spirits (~2 mL) and dried under vacuum for 3 hours to give 69.5 mg (77%) of **2e**.

mp = 204.5-210°C (decomp.)

Found: C, 55.8; H, 4.4; N, 1.4%. $C_{43}H_{35}NPtO_3FeP_2$ requires C, 55.7; H, 3.8; N, 1.5%.

IR: υ(C=O) = 1654 cm^{-1} (s).

ESI-MS (added NaCl): (capillary exit voltage = 160 V) *m/z* 949.10 [100%, $(M+Na)^+$], calculated *m/z* for $C_{43}H_{35}NPtO_3FeP_2$.Na = 949.10.

NMR: Refer to Figure 2.15 for the atom numbering scheme of **2e**.

^{1}H ($CDCl_3$) δ 7.91-6.58 (m, 29H, Ph), 5.00 [br s, 2H, ferrocene Fe(C_5H_4)$_2$], 4.46 [s, 2H, ferrocene Fe(C_5H_4)$_2$], 4.18 [s, 2H, ferrocene Fe(C_5H_4)$_2$], 3.96 (d, 2H, H9a & H9b, $^{3}J_{Pt\text{-}H}$ ~ 20.1 Hz), 3.58 [d, 2H, ferrocene Fe(C_5H_4)$_2$] ppm.

^{1}H (DMSO) δ 7.90-6.50 (m, 29H, Ph), 5.09 [br s, 2H, ferrocene Fe(C_5H_4)$_2$], 4.60 [s, 2H, ferrocene Fe(C_5H_4)$_2$], 4.36 [s, 2H, ferrocene Fe(C_5H_4)$_2$], 3.75 (br s, 2H, H9a & H9b, $^{3}J_{Pt\text{-}H}$ ~ 50.7 Hz) ppm (fourth ferrocene CH signal not observed due to solvent overlap).

^{31}P-{^{1}H} ($CDCl_3$) δ 9.44 [d, $P_{A(trans\ N)}$, $^{1}J_{Pt\text{-}P}$ = 3131 Hz, $^{2}J_{P\text{-}P}$ = 22.2 Hz], 6.47 [d, $P_{B(trans\ O)}$, $^{1}J_{Pt\text{-}P}$ = 4102 Hz, $^{2}J_{P\text{-}P}$ = 22.6 Hz] ppm.

^{13}C-{^{1}H} (DMSO) δ 182.1 (d, C10), 171.6 (s, C11), 138.4-127.2 (m, Ph), 76.8 [s, ferrocene Fe(C_5H_4)$_2$], 75.1 [d, ferrocene Fe(C_5H_4)$_2$], 74.8 [d, ferrocene Fe(C_5H_4)$_2$], 73.7 [d, ferrocene Fe(C_5H_4)$_2$], 56.5 (s, C9, $^{2}J_{Pt\text{-}C}$ = 47.2 Hz) ppm.

2.1.6 Crystal Structure of 2a

The product was dissolved in minimal dichloromethane, filtered through a glass Pasteur pipette plugged with 0.5 cm cotton wool and 0.5 cm Filter Aid (medium) and recrystallised by vapour diffusion with ether to produce cloudy cream block-shaped crystals of crystallographic quality, and crystallographic data was collected on these.

Crystal Data: $C_{17}H_{19}NO_3Pt$, M_r = 480.42 g mol^{-1}, monoclinic, space group $P2_1/n$, *a* = 12.306(8), *b* = 9.411(6), *c* = 12.545(7)Å, β = 94.59(6), V = 1448.15(16)Å^3, T = 173(2)K, Z = 4, D_c = 2.204 gcm^{-1}, μ(Cu-*K*α) = 18.237 mm^{-1}, F(000) 920; 27882 reflections collected with 4.8° < 2θ < 73.6°, 2917 unique (R_{int} = 0.0481) used after correction for absorption ($T_{max,min}$ = 0.4075, 0.2002). Crystal

dimensions = 0.13 x 0.10 x 0.06 mm. Refinement on F^2_o converged at $R_1 = 0.0207$ [$I > 2\sigma(I)$] and $wR^2 = 0.0544$, GoF = 1.128.

Details of the diffractometer used are given in Appendix I. The structure of **2a** is illustrated in Figures 2.21-2.24, and selected bond-lengths and angles are summarised in Table 2.5.

2.2 Results & Discussion

2.2.1 Syntheses

The reaction of [$PtCl_2$(COD)] with hippuric acid in the presence of silver(I) oxide (Ag_2O) in refluxing dichloromethane gives, in reasonable yield and purity, the novel complex **2a** (Figure 2.1), which is stable in both air and water (as expected, since water is a by-product of this reaction). It crystallises as a white solid with a slight purple tinge, due to slight contamination by colloidal silver metal.

The ligand substitution reaction of **2a** with triphenylphosphine, dppe, PTA and dppf gives, in high yield and reasonable purity, dianionic N,O-metallacyclated platinum complexes with various phosphine ligands (**2b-e**, Figure 2.1). These crystallise as white or yellow solids and also melt at high temperatures (generally >170°C, with the PTA complex melting at >320°C).

The percentage compositions obtained in the elemental analyses of complexes **2a**, **2c**, **2d** and **2e** matched the calculated percentages within 1%; however that of complex **2b** did not match those required within experimental error limits. This

inconsistency may have been due to co-crystallisation with an amount of dichloromethane during crystallisation. Reasonable agreement between observed and calculated values was obtained for 1.5 moles of CH_2Cl_2 per mole of **2b**. The presence of CH_2Cl_2 was confirmed in the proton NMR spectrum; integration showed roughly 1:1.5 moles of **2b**:CH_2Cl_2.

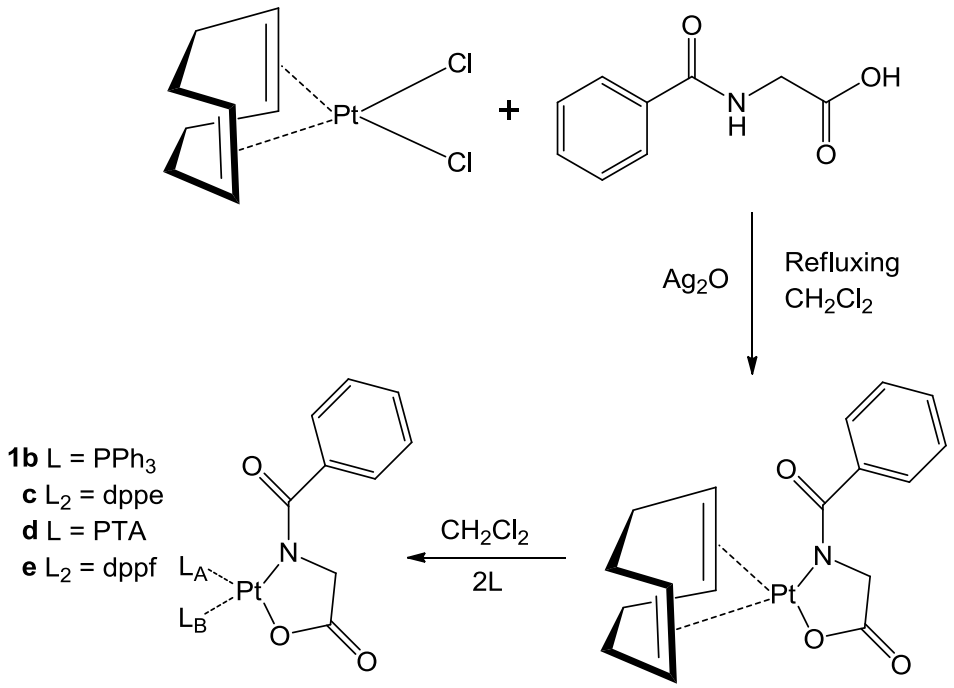

Figure 2.1: Synthesis of complex 2a and various subsequent ligand substitution reactions to the resulting platino-hippurate complexes (2b-e).

All complexes were initially characterised by ^{1}H NMR spectroscopy. This gave a good indication as to whether or not the desired complex had been synthesised, and whether it was pure enough to carry out full characterisation. All NMR spectroscopy was recorded using $CDCl_3$ as the solvent, unless otherwise stated in the experimental section. The ^{1}H NMR for complex **2e** was recorded in both $CDCl_3$ and DMSO. This was because ^{13}C NMR for this complex needed to be recorded in DMSO as the ferrocene CH signals appeared around the same region

as the $CDCl_3$ peak (~77 ppm), therefore the proton spectrum also needed to be recorded in DMSO in order to obtain the correct correlations in the 2D spectra. The proton spectrum was also recorded in $CDCl_3$, since in DMSO the water peak masked the fourth ferrocene CH signal.

The ligand-substituted complexes **2b-e** were also characterised by ^{31}P NMR, which is an equally rapid and convenient technique to gain information on structure and purity of phosphorus-containing complexes. In particular, the $^{1}J_{Pt-P}$ coupling constants seen in the phosphorus NMR emphasised the *trans*-influence differences of the nitrogen and oxygen donors of the dianionic ligand exerted on the *trans* phosphorus atoms. Hence ^{31}P NMR made it simple to distinguish between phosphines (one *trans* to N, the other to O) attached to the platinum centre.

Complexes **2a** and **2e** were characterised by additional 2D NMR experiments as the ^{1}H and ^{13}C alone spectra proved inconclusive. A more comprehensive analysis of the NMR spectra obtained is discussed in section 2.2.

Each complex, with the exception of **2a**, was also successfully characterised using ESI-MS. The ESI mass spectrum of **2a** showed a very weak $[M+H]^+$ ion at *m/*z 481, despite several attempts with varied ionisation conditions and solvents (both methanol and acetonitrile). It is not clear why this is the case, as the phosphine-substituted complexes (**2b**-**2e**) and other similar complexes containing a COD moiety show strong ions in ESI-MS results.[28]

2.2.2 Silver(I) Oxide as a Mediating Agent

In the synthesis of **2a**, silver(I) oxide was used to mediate the reaction. Ag_2O is well-recognised as a facilitating reagent for the formation of new platinum-carbon bonds, with the first known example of this occurring in 1977.[29] Although silver(I) oxide was originally used to form Pt-C bonds, a wide variety of other platinum-ligand bonds have been prepared subsequently using this reagent.[3,28,30] It acts as both a base (O^{2-}) which removes acidic protons from electron-withdrawing groups on the organic ligand, and a halide abstractor (Ag^{+}) which abstracts the chloride ions from the $PtCl_2L_2$ starting complex as insoluble AgCl.[29]

Although silver(I) oxide is now widely established as a mediator for metallacyclic reactions, it can result in the product having a slight purple tinge. This may be due to colloidal silver, originating from decomposition of soluble silver-containing complexes which form during the reaction and cannot be removed by filtration through fine glass fibre filter paper. Thus an investigation into alternative bases (using copper(I) oxide and calcium hydroxide in the place of silver(I) oxide) was carried out in two reactions using all the same conditions as were used with silver(I) oxide but substituting the base. However, both reactions did not appear to produce the desired product, hence silver oxide was the base of choice for all following reactions.

An alternative technique used to overcome the silver(I) oxide contamination during recrystallisation was dissolving the end product in the desired solvent (e.g. dichloromethane or chloroform) and filtering through a glass Pasteur pipette which was packed with 0.5 cm of cotton wool and 0.5 cm of filter-aid. This

method was utilised to eventually recrystallise **1** to produce crystallographic-quality crystals.

2.2.3 NMR Spectroscopic Analysis

2.2.3.1 NMR Spectroscopic Characterisation of **2a**

^{1}H NMR

The ^{1}H NMR spectrum (Figure 2.2) of the platino-hippurate complex **2a** (containing the COD moiety) affords a great deal of structural information on the complex.

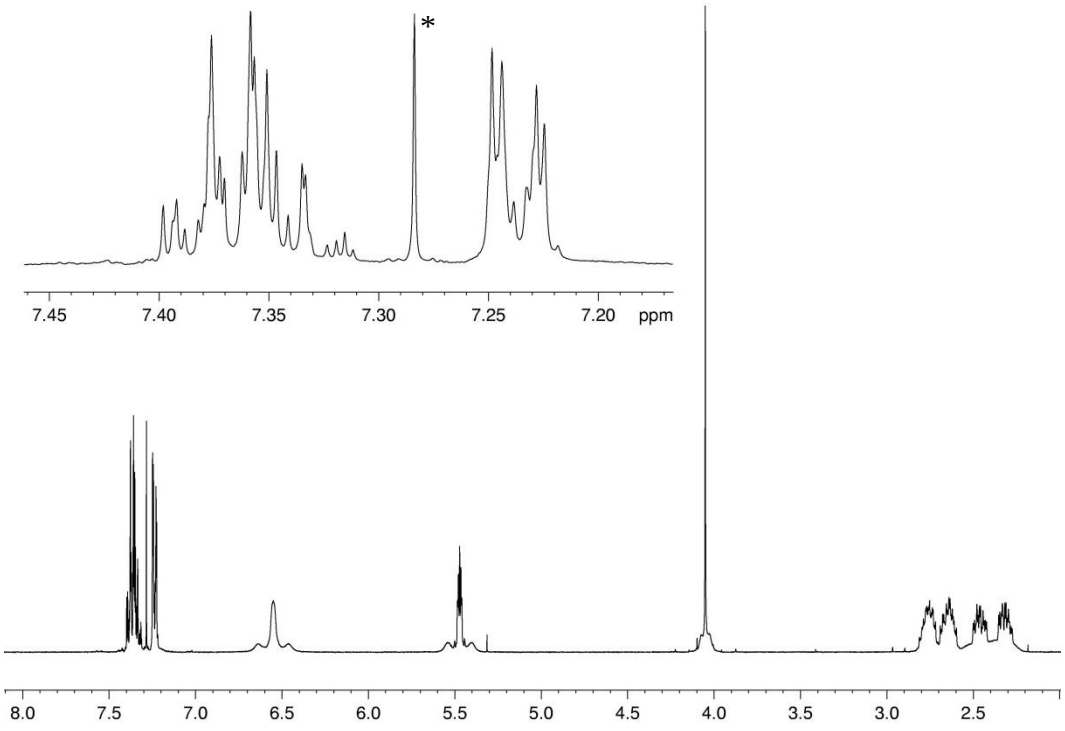

Figure 2.2: The ^{1}H NMR spectrum of complex 1 with $CDCl_3$ as the solvent (* represents traces of $CHCl_3$ in the $CDCl_3$ solvent). In the top left of the figure is an expansion of the aromatic region.

The signals which correspond to the various proton and carbon environments on Figure 2.3 are summarised in Table 2.1 at the end of this section.

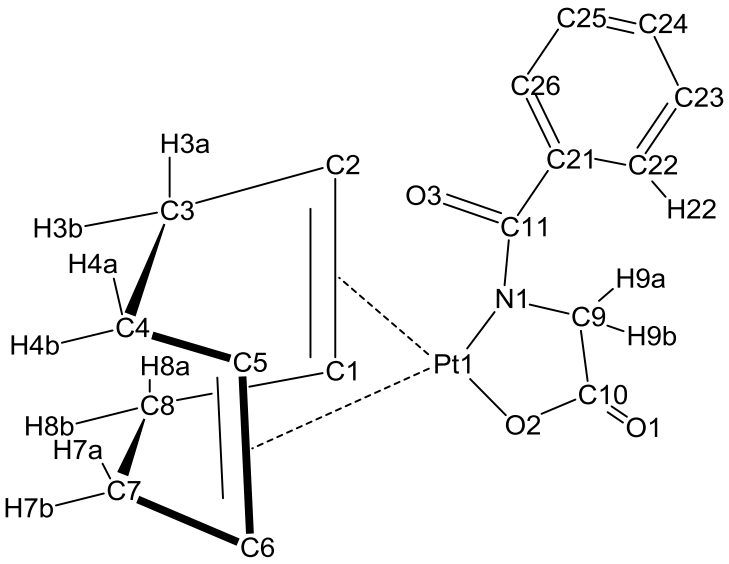

Figure 2.3: The various different carbon and proton environments of 2a leading to signals in the ^{1}H and ^{13}C NMR spectra. The COD moiety (on the left-hand side of platinum) is present in the boat conformation required for coordination.

Although there are four methyne (CH) protons present in the COD complex, only two ^{1}H signals are observed in the proton NMR spectrum. This is due to symmetry in the COD moiety as it is present in the boat (gauche) conformation required for coordination (Figure 2.3), which renders C1 and C2, and C5 and C6 spectroscopically equivalent. Consequently, H1 & H2 and H5 & H6 are also equivalent. The resulting two COD methyne protons occur at 6.51 ppm and 5.43 ppm, and each of these has broad shoulders attributable to platinum satellites arising from coupling to ^{195}Pt as illustrated in Figure 2.4 ($^{2}J_{Pt\text{-}H}$ ~ 70.1 Hz and $^{2}J_{Pt\text{-}H}$ ~ 56.7 Hz, respectively).

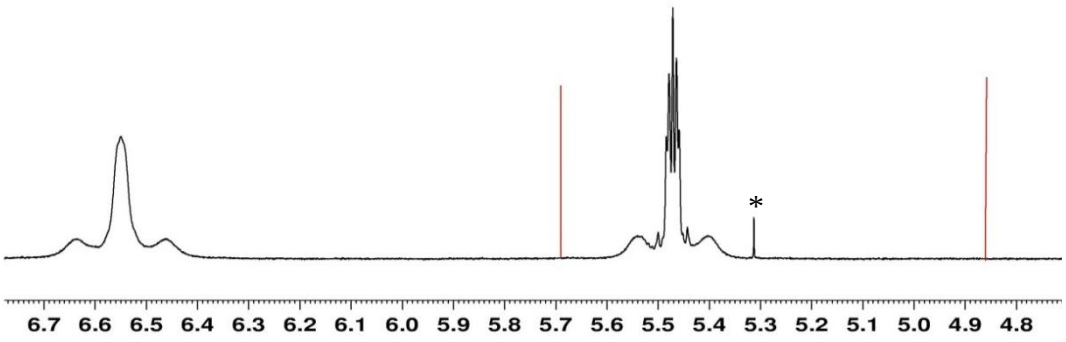

Figure 2.4: An expansion of the 4.8-6.8 ppm region in the ^{1}H NMR spectrum of complex 2a (* represents traces of dichloromethane). The sharp red lines indicate the two DFT-calculated chemical shifts.

The hippurate nitrogen and oxygen atoms on Pt-attached atoms exert an influence on atoms *trans* to these. This *trans* influence allows differentiation between carbon atoms *trans* to nitrogen/oxygen, based on their $^{1}J_{Pt\text{-}C}$ coupling constants.[31] The CH(COD) signal at 6.51 ppm can be assigned as the environment attributed to H1 & H2, as it has the larger $^{2}J_{Pt\text{-}H}$ coupling constant of ~ 70.1 Hz, indicating that the carbon environment it is attached to (at 96.0 ppm, from the HSQC) is *trans* to the metallacycle oxygen atom. Similarly, the signal at 5.43 ppm can be assigned as the environment which arises from H5 & H6 as it has the smaller $^{2}J_{Pt\text{-}H}$ coupling constant of ~ 56.7 Hz, which suggests that the carbon environment it is attached to (at 98.5 ppm, from the HSQC) is *trans* to the metallacycle nitrogen atom. There are also remarkable differences between the two CH(COD) signals in terms of chemical shift, multiplicity and broadness. In particular, the broadness of the signal at 6.51 ppm may be attributable to a proximity to lone pair electron density such as that on the N-C=O group on the hippurate moiety[32]. This is consistent with the data, as the H1 & H2 signal at 6.51 ppm is broader and downfield, while the H5 & H6 signal at 5.43 ppm is sharper and more upfield. It is intuitive to expect the methyne proton environment nearest the nitrogen to be

further downfield, as nitrogen is less electronegative than the metallacycle oxygen therefore is less shielding.[33] Density functional theory (DFT) was used to calculate theoretical NMR shifts, and further detail on the methods used for this is given in the general experimental section (Appendix I). From the DFT-calculated NMR data (shown by the sharp red lines in Figure 2.4), there are two different environments which, when averaged to account for vibrational motion on the time-scale of NMR spectroscopy, show a difference of 0.84 ppm. This is fairly consistent with the experimental NMR, which shows a difference of 1.1 ppm between the signals for H1/H2 and H5/H6. The calculated resonance which corresponds to H1/H2 is 5.69 ppm and is closest to the nitrogen, while the calculated signal arising from H5/H6 is at 4.86 ppm. Although these differ from the experimental resonances of 6.51 and 5.43 ppm by 0.8 and 0.6 ppm respectively, they still suggest that the proton closest to the nitrogen is that in the H1/H2 environment, therefore assignment of the ^{1}H spectrum can be fully confirmed with H1 & H2 corresponding to the signal at 6.51 ppm and H5 & H6 to 5.43 ppm.

Assuming that the two protons in the H22/H26 environment are identical due to free rotation about the C11-C21 bond, there are three aromatic proton environments from the hippurate moiety (corresponding to H22 & H26, H23 & H25, and H24 in Figure 2.3). These appear in the region from 7.36-7.18 ppm, and an expansion of this can be seen in the top left of the ^{1}H NMR spectrum (Figure 2.2). Only one of the three aromatic proton environments was adequately resolved in the proton spectrum. The signal which appears at ~7.19 ppm essentially as a doublet of doublets (^{3}J = 8.0, ^{4}J = 1.7 Hz) can be uniquely attributed to the H22/H26 environment, since of the aromatic proton environments

only this proton is expected to show a ^{3}J coupling to its nearest neighbour (H6) and a smaller ^{4}J coupling to H7. A NOESY experiment confirmed this, showing an NOE from the H22/H26 protons at ~7.19 ppm to the H9 protons at 4.01 ppm which is consistent with H22/H26 being the closest of the aromatic protons to H9. The H24 and H23/H25 proton environments occur in the 7.36-7.27 ppm region as complex second-order overlapped multiplets. In principle, each of these signals would be expected to occur as a ^{3}J coupled doublet of doublets (approximate triplet). Notwithstanding the complex nature of the overlapped signal, it is apparent in the high resolution COSY spectrum (Figure 2.5) that the initial more intense correlation peaks are attributable to the larger ^{3}J couplings between H22 at ~7.19 and the protons at ~7.31 ppm, and later the smaller ^{4}J coupling correlations develop to the proton at ~7.34. This allows tentative assignment for the higher chemical shift as H24 and the lower as the H23/H25 environment.

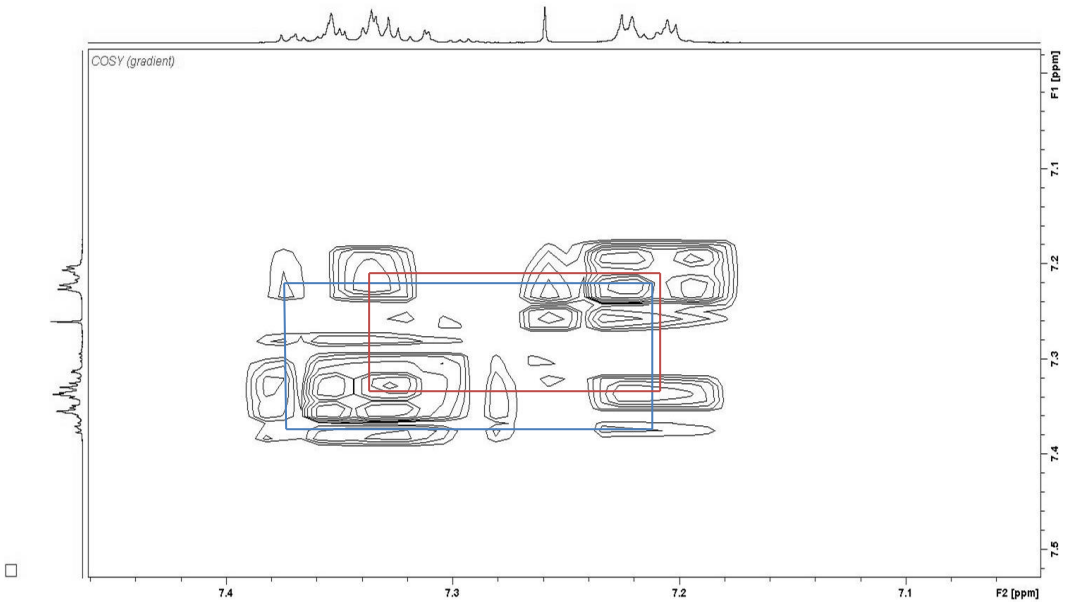

Figure 2.5: The high-resolution COSY spectrum of complex 2a, showing ^{1}H-^{1}H correlations in the aromatic region. Strong initial ^{3}J correlations from ~7.19 to ~7.31 ppm are shown in red, while later weaker ^{4}J couplings to ~7.34 ppm are illustrated in blue.

The hippurate ring CH_2 signal at 4.01 ppm ($^3J_{Pt\text{-}H}$ ~ 18.1 Hz) also shows significant coupling to ^{195}Pt, as expected. It is clearly recognisable as a methylene signal in the DEPT135 experiment (Appendix II). The fact that the proton spectrum shows a single peak for this CH_2 indicates that the hippurate ligand lies in a plane of symmetry, which makes both protons chemically equivalent.

The signals attributable to the COD CH_2 protons are also easily distinguished as methylenes in the DEPT135 experiment, and are observed as complex multiplets in the region 2.80-2.58 ppm. The extensive coupling seen in these signals is due to two factors. Firstly, when COD coordinates to platinum it is forced into the normal gauche boat confirmation seen in metal-attached COD. This gives the COD moiety such symmetry that, although there are four methyne protons, only two methyne signals are seen, which means they are chemically equivalent pairs. Similarly, there are eight methylene protons, however only four methylene resonances occur in the proton spectrum, indicating that the protons are paired up due to symmetry as depicted in Figure 2.3 (H3a & H8a, H3b & H8b, H4a & H7a and H4b & H7b are chemically equivalent pairs). In addition, in the COD moiety there is both germinal ^2J coupling (between Ha and Hb for the CH_2 protons) and ^3J coupling between methylene and methyne protons, leading to complicated overlapping signals. Furthermore, each COD methylene couples to ^{195}Pt which adds to the complexity of the signals.

In the COSY spectrum (Appendix III) the alkene proton at 6.51 ppm correlates to the protons at ~2.72 and ~2.42 ppm, whereas the proton at 5.43 ppm shows correlations to the protons at ~2.60 and ~2.28 ppm. In addition the high-resolution COSY spectrum (Figure 2.6) shows mutual correlations between the 4 adjacent

methylene signals. Axial protons are generally higher in chemical shift than equatorial protons[32]. This allows assignment of the following environments with the corresponding signals: H3a & H8a at ~2.72 ppm, H3b & H8b at ~2.42 ppm, H4a & H7a at ~2.60 ppm, and H4b & H7b at ~2.28 ppm.

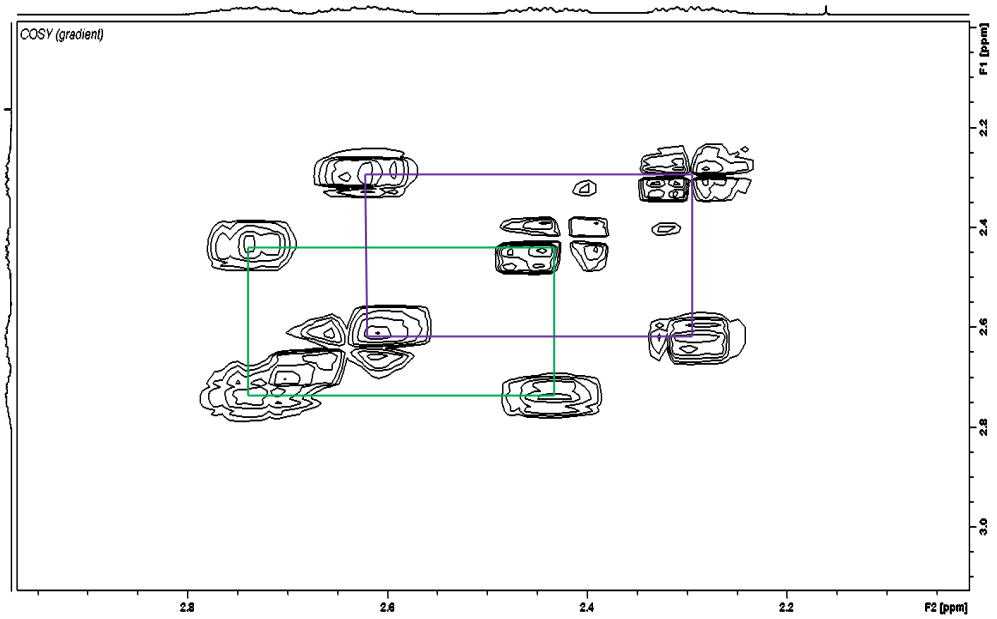

Figure 2.6: The high-resolution COSY spectrum of complex 2a, showing ^{1}H-^{1}H correlations in the COD CH_2 region. Correlations from protons at ~2.72 to ~2.22 ppm are presented in green, while couplings from protons at ~2.60 and ~2.28 ppm are demonstrated in purple.

Table 2.1: The ^{1}H and ^{13}C chemical shifts of the various environments in complex 2a. Refer to Figure 2.3 for the atom numbering scheme.

Atoms	^{1}H chemical shift (ppm)	^{13}C chemical shift (ppm)
1, 2	6.51	96.0
3, 8	~2.72 (**a**), ~2.42 (**b**)	32.4
4, 7	~2.60 (**a**), ~2.28 (**b**)	28.2
5, 6	5.43	98.5
9	4.01	56.9
10	-	184.4
11	-	176.7
21	-	138.5
22, 26	~7.19	125.5
23, 25	~7.31	128.58
24	~7.34	128.61

^{13}C NMR

The ^{1}H-decoupled ^{13}C NMR spectrum of complex **2a** (Figure 2.7) displays several key signals which can be assigned to the 11 different carbon environments (Figure 2.3) which exist in the complex, and these are detailed in Table 2.1.

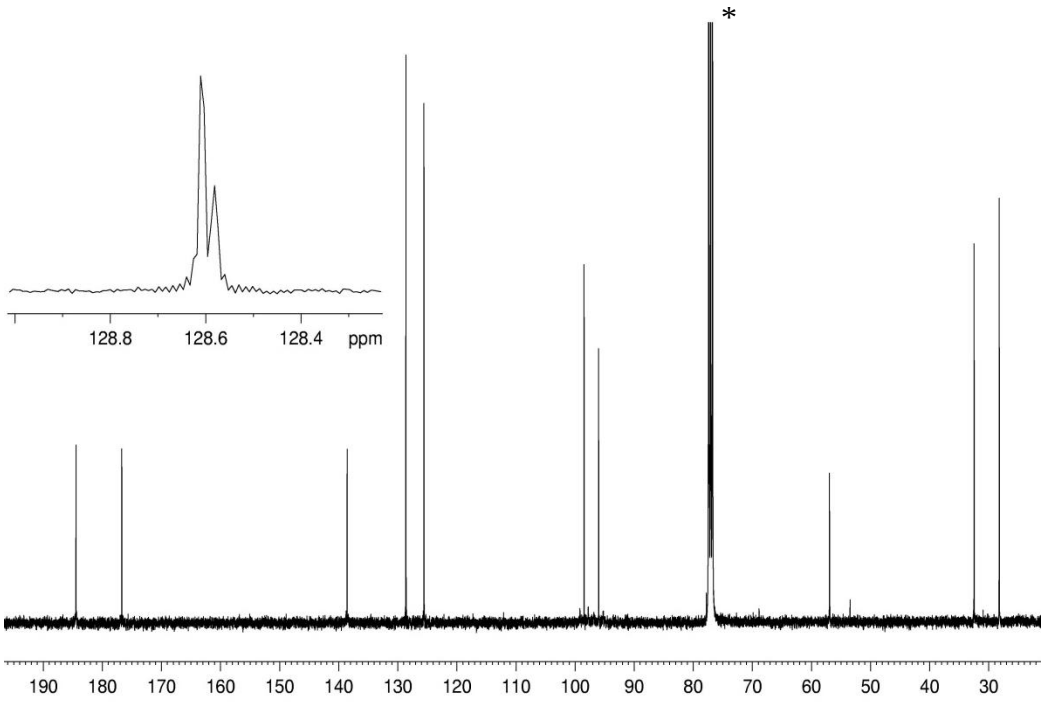

Figure 2.7: The quantitative proton-decoupled ^{13}C NMR spectrum of complex 2a with $CDCl_3$ as the solvent (* represents the $CDCl_3$ solvent line). The top left of the figure shows an expansion of the aromatic region to show the superimposed aromatic resonances at 128.6 ppm.

In this experiment, the NOEs were cancelled to selectively enhance the two carbonyl signals, and to try to identify any ^{195}Pt-satellites. The nitrogen-attached carbonyl signal (C11 on Figure 2.3) occurs at 176.7 ppm and has slightly broad shoulders from coupling to ^{195}Pt ($^2J_{Pt\text{-}C}$ ~ 31.7 Hz), while the metallacycle ring carbonyl signal (C10) comes slightly upfield at 184.4 ppm. No ^{195}Pt coupling could be resolved for the signal at 184.4 ppm. The HMBC spectrum (Appendix IV) confirms these shifts since it shows correlations from the nitrogen-attached carbonyl to the aromatic protons, whereas the ring carbonyl displays no coupling to ^{1}H as it is too far away. The ^{1}H-coupled ^{13}C spectrum (Figure 2.8) shows further evidence, with C10 appearing as a triplet at 184.4 ppm ($J_{C\text{-}H}$ = 5.9 Hz) due to splitting by its neighbouring CH_2, while the nitrogen-attached carbonyl appears as a singlet at 176.7 ppm.

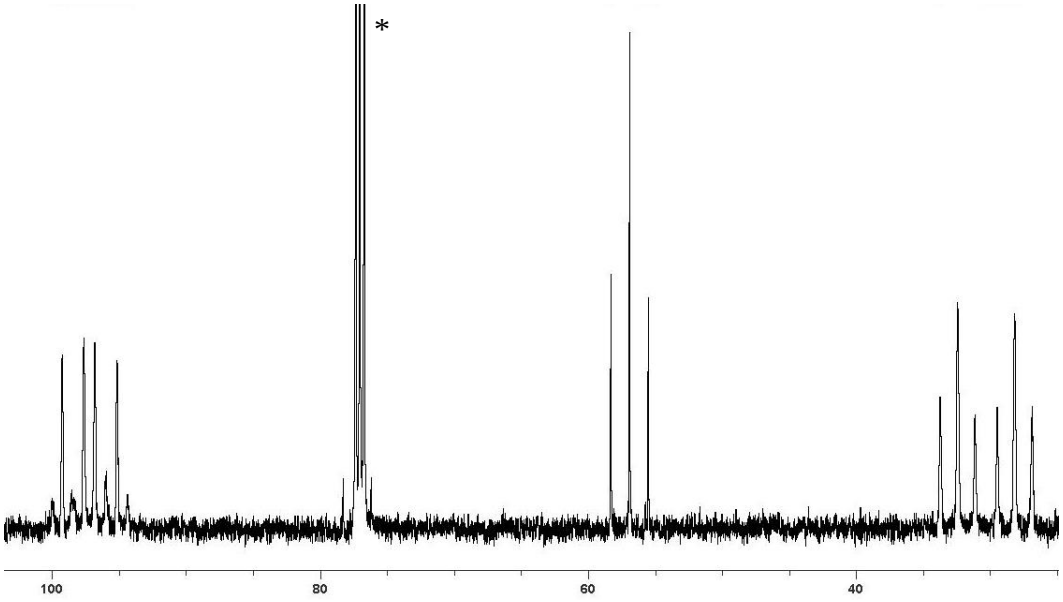

Figure 2.8: The 25-100 ppm region of the proton-coupled ^{13}C NMR spectrum of 2a, showing the COD CH and CH_2 $^1J_{C\text{-}H}$ couplings (* represents the $CDCl_3$ solvent line).

Similarly, the quaternary carbon of the phenyl (C21) exhibits broad shoulders due to coupling to ^{195}Pt ($^3J_{Pt\text{-}C}$ ~ 42.4 Hz). It is further upfield in the aromatic region as expected at 138.5 ppm and can be assigned due to its low intensity and the fact that it shows no correlations to protons in the HSQC. Also in the aromatic region, two of the environments appear to overlap as a doublet at 128.6 ppm, while the final signal occurs at 125.5 ppm. The latter is assigned as the C22/C26 environment due to its correlation to the H22/H26 signal at ~7.19 ppm in the HSQC (Figure 2.9). As seen in the expansion of the aromatic region (Figure 2.7), the peaks at 128.6 ppm can be almost fully separated to see the intensity ratio of 2:1. This enables clear assignment of environment C24 as the signal with the lower chemical shift at 128.58 ppm since it has a lower intensity attributable to its single carbon. In contrast, the signal with the higher chemical shift of 128.61 ppm has a doubled intensity therefore must arise from 2 carbons, hence corresponds to the C23/C25 environment.

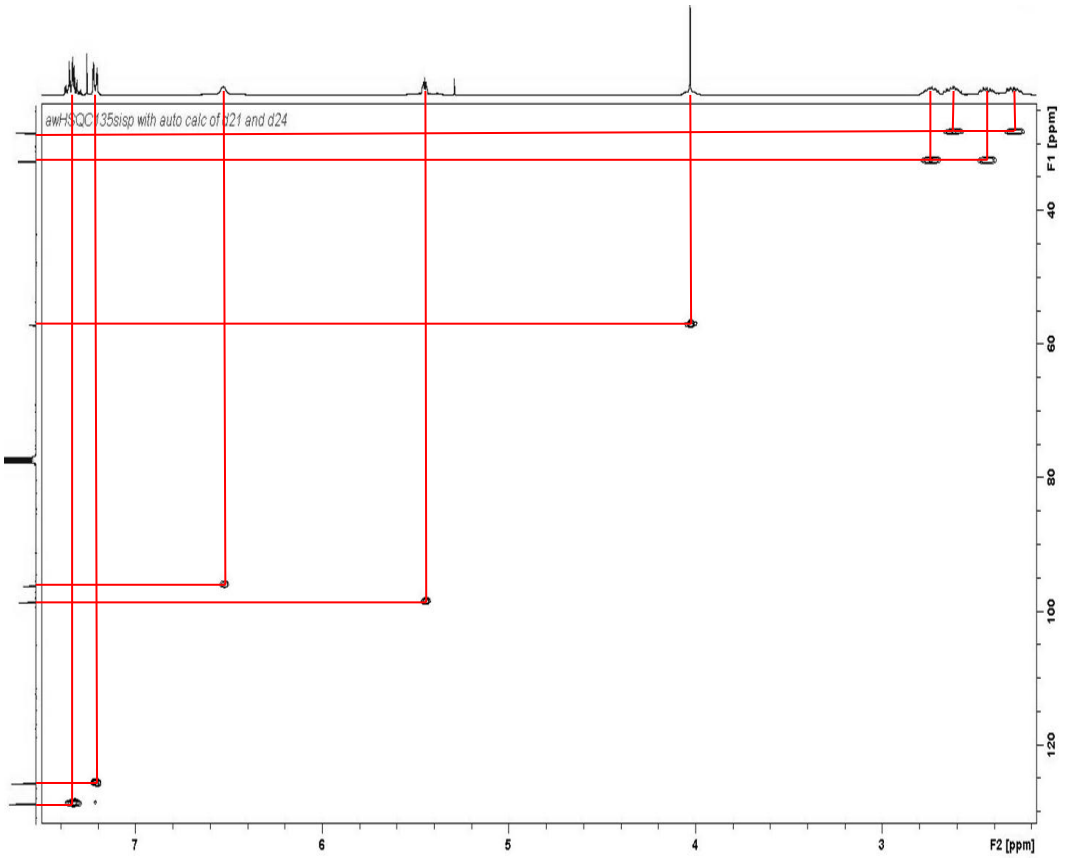

Figure 2.9: The HSQC NMR spectrum of complex 2a showing ^{13}C-^{1}H correlations in red.

The two CH resonances arising from the COD moiety (the C1/C2 and C5/C6 environments in Figure 2.3) are both seen in the ^{13}C-{^{1}H} spectrum as singlets at 98.5 ($^{1}J_{Pt\text{-}C}$ = 140.2 Hz) and 96.0 ($^{1}J_{Pt\text{-}C}$ = 159.9 Hz) ppm, and both display substantial coupling to ^{195}Pt. The HSQC (Figure 2.9) shows that these are attached to the protons at 5.43 and 6.51 ppm, respectively. The signal at 96.0 ppm can be assigned as the C1 & C2 environment due to its higher $^{1}J_{Pt\text{-}C}$ coupling constant of 159.9 Hz which shows that it is *trans* to the metallacycle oxygen atom, while the 98.5 ppm shift can be attributed to the C5 & C6 environment by its smaller $^{1}J_{Pt\text{-}C}$ coupling constant of 140.2 Hz, which indicates that it is *trans* to the metallacycle nitrogen atom. In the proton-coupled carbon spectrum, the C1/C2 environment appears as a doublet at 96.0 ppm ($J_{C\text{-}H}$ = 165.5 Hz) while the C3/C4 signal is also

seen as a doublet at 98.5 ppm (J_{C-H} = 164.8 Hz). These J_{C-H} coupling constants are typical values for CH environments of this type.[34]

The COD methylene environments (C3 & C8, and C4 & C7) occur at 32.4 and 28.2 ppm in the proton-decoupled carbon spectrum (Figure 2.7). In the proton-coupled spectrum, the C3/C8 environment appears as a triplet at 32.4 ppm (J_{C-H} = 130.5 Hz) whereas the C4/C7 signal occurs at 28.2 ppm (J_{C-H} = 131.8 Hz). As expected, the J_{C-H} values for the COD methylene signals are approximately 35 Hz lower than those for the COD CH resonances. This is because the J_{C-H} coupling constant of a certain carbon atom is indicative of its hybridisation, and CH carbons are generally sp^2 hybridised, whereas CH_2 carbons are usually sp^3 hybridised.[34] There is more s-character in an alkene bond compared to an alkane group, therefore the J_{C-H} coupling constant is expected to be larger for a CH carbon than a CH_2 carbon. The HSQC spectrum (Figure 2.9) shows that the CH_2 at 32.4 ppm is correlated to the proton signals centred at ~2.72 and ~2.42 ppm, while the CH_2 at 28.2 correlates to the proton signals centred at ~2.60 and ~2.28 ppm.

As shown in Figure 2.1, COD can bind to platinum in two different ways to yield one of two possible symmetric conformers, each of which produces a distinct NMR pattern. To determine which of these is the actual conformer, the long-range couplings in the HMBC and H2BC are considered.

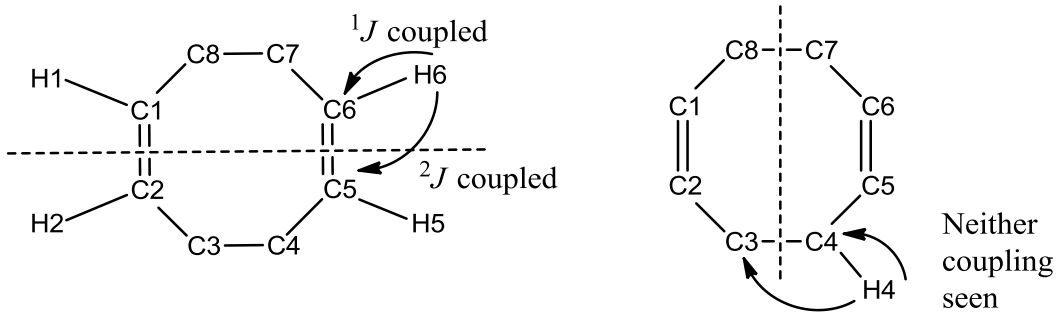

Figure 2.10: The two possible symmetric conformers of the COD ligand, depicted flat.

As depicted in Figure 2.11, the HMBC spectrum shows a residual coupled ^1J correlation from the H5/H6 to the C5/C6 signal together with a ^2J coupling to an olefinic carbon that produces the same chemical shift. This is indicative of the left-hand conformer in Figure 2.10.

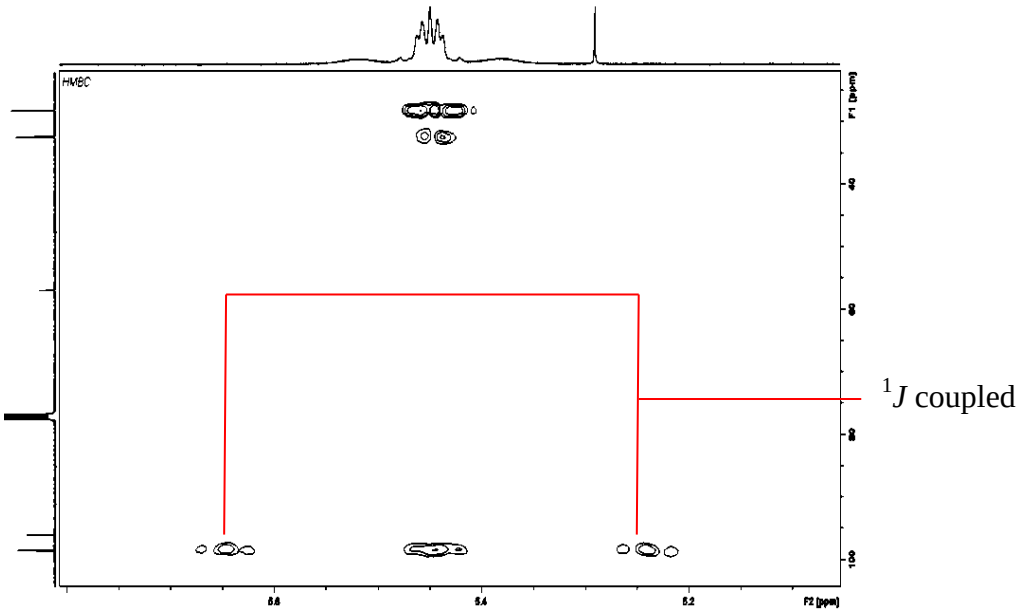

Figure 2.11: The HMBC of complex 2a shows the expected ^2J coupling of the H5/H6 protons to the C5/C6 environment and a residual ^1J coupling to C5/C6, as well as a strong ^2J coupling to the C4/C7 environment and a weaker ^3J coupling to the C3/C8 environment.

The H2BC spectrum (Figure 2.12) confirms this but only a ^2J coupling from the H5/H6 protons to the C5/C6 carbons is seen as the residual ^1J is more perfectly

cancelled. Additionally the H2BC shows a strong ^{2}J correlation from the H5/H6 environment to the methylene carbon at 28.2 ppm (C4 & C7) and a weaker ^{3}J coupling to the C3/C8 environment. These observations are consistent with the symmetric conformer on the left in Figure 2.10. If the complex displayed the alternative conformer, the resulting HMBC would show a residual ^{1}J coupling from H4 to C4 at 28.2 ppm, as well as a ^{2}J coupling to a carbon of the same chemical shift, neither of which is seen in the HMBC spectrum (Appendix IV).

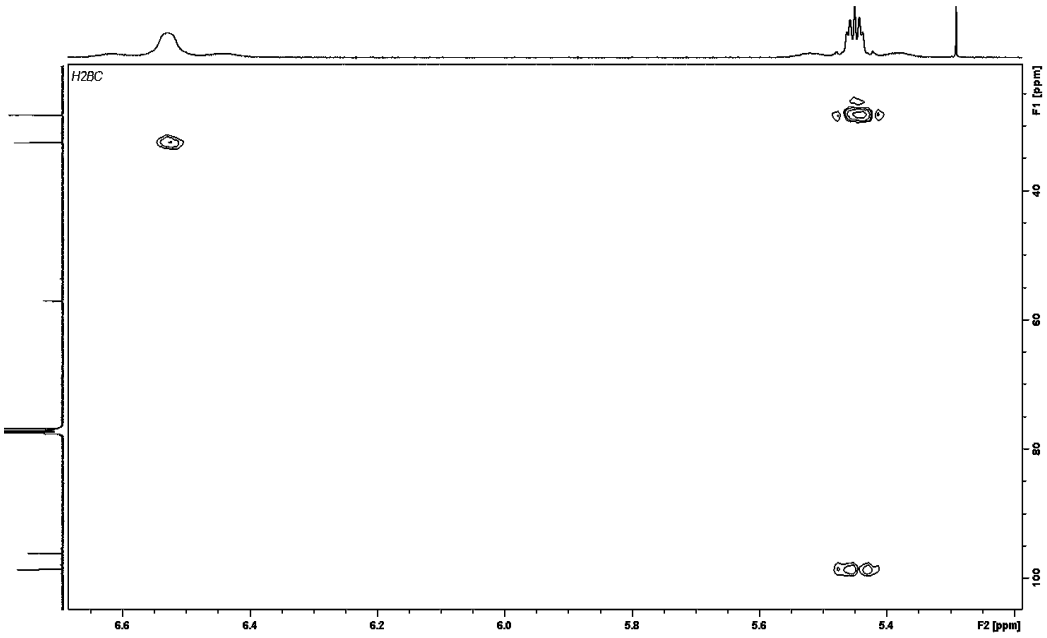

Figure 2.12: The H2BC of complex 2a confirms the symmetry of the molecule, by showing a ^{2}J correlation from the H5/H6 environment at 5.43 ppm to the C5/C6 environment at 98.2 ppm as well as a strong ^{2}J correlation to the C4/C7 signal at 28.2 ppm and a weaker ^{3}J coupling to the C3/C8 environment at 32.4 ppm.

As the proton signal at 6.51 ppm is attributable to the H1/H2 environment, the signals at 32.4 and 28.2 ppm can be assigned as C3 & C8 and C4 & C7 respectively. The metallacycle ring CH_2 carbon appears at 56.9 ppm as expected and exhibits broad shoulders due to coupling to ^{195}Pt ($^{2}J_{Pt\text{-}C}$ ~ 15.4 Hz).

2.2.3.2 NMR Spectroscopic Characterisation of **2b.1.5CH_2Cl_2**

^{1}H NMR

In comparison to its parent complex **2a**, the proton NMR spectrum of complex **2b** appears rather straightforward, with only two regions. The complex multiplet from 7.81-6.75 ppm corresponds to the aromatic protons, making interpretation difficult, and no further assignment was undertaken. The ring methylene signal at 4.16 ppm ($^3J_{Pt-H}$ ~ 40.8 Hz) comes at an expected chemical shift, and is slightly more downfield than that of the ring methylene in the parent complex **2a**, which comes at 4.03 ppm. However, it appears as a doublet, and this multiplicity may be due to coupling to the *trans* phosphine.

^{31}P NMR

The phosphorus NMR spectrum of complex **2b** shows two doublets at 9.2 ($^1J_{Pt-P}$ = 3058 Hz, $^2J_{P-P}$ = 23.7 Hz) and 4.8 ($^1J_{Pt-P}$ = 4031 Hz, $^2J_{P-P}$ = 22.7 Hz) ppm. Both of these show satellites from coupling to ^{195}Pt. It is known that, due to the *trans*-influence, ligands with their phosphorus *trans* to an oxygen have a larger $^2J_{P-P}$ coupling constant than ligands with their phosphorus *trans* to a nitrogen.[31] Hence it is easy to assign the doublet at 9.2 ppm to the phosphorus in environment L_A and the doublet at 4.8 ppm to the phosphorus in environment L_B on Figure 2.1.

2.2.3.3 NMR Spectroscopic Characterisation of **2c**

^{1}H NMR

The aromatic region of the proton NMR spectrum of complex **2c** is similar to that of **2b**, with all twenty-five aromatic protons appearing as a complex multiplet from 7.99-6.77 ppm. While some of these resonances may be resolved and assigned using 2D NMR techniques, they are of little interest to distinguish. The metallacycle CH_2 signal occurs at 4.03 ppm ($^{3}J_{Pt\text{-}H}$ ~ 18.3 Hz) as expected. The dppe CH_2 signals appear as two second order overlapping multiplets from 2.39-1.99 ppm and arise from four protons.

^{31}P NMR

Like **2b**, the ^{31}P NMR spectrum of **2c** displays two doublets at 37.4 ($^{1}J_{Pt\text{-}P}$ = 3085 Hz, $^{2}J_{P\text{-}P}$ = 12.4 Hz) and 28.1 ($^{1}J_{Pt\text{-}P}$ = 3876 Hz, $^{2}J_{P\text{-}P}$ = 12.1 Hz) ppm. Each of these has satellites due to coupling to ^{195}Pt. As stated earlier, the phosphorus signal with the larger $^{1}J_{Pt\text{-}P}$ coupling constant (28.1 ppm) is *trans* to the hippurate oxygen (L_A on Figure 2.1), while the signal with the smaller $^{1}J_{Pt\text{-}P}$ coupling constant (37.4 ppm) is *trans* to the hippurate nitrogen (L_B on Figure 2.1).

2.2.3.4 NMR Spectroscopic Characterisation of **2d**

^{1}H NMR

The proton NMR spectrum of **2d** displays three key signals. The first is a complex multiplet in the aromatic region of 7.35-7.27 ppm arising from five protons, as for the parent complex **2a**. The PTA methylene group resonances appear as a complex overlapping multiplet from 4.58-4.27 ppm. As for the other ligand-

substituted complexes (**2b, 2c** & **2e**), the metallacycle ring signal occurs as a doublet at 4.07 ppm and displays broad shoulders from coupling to ^{195}Pt ($^{3}J_{Pt\text{-}H}$ = 19.0 Hz).

^{31}P NMR

Much like the other ligand-substituted complexes (**2b, 2c** & **2e**), the ^{31}P NMR spectrum of complex **2d** shows two doublets, each with a pair of satellite lines due to coupling of the phosphorus to ^{195}Pt. The first occurs at -67.0 ppm ($^{1}J_{Pt\text{-}P}$ = 2799.7 Hz, $^{2}J_{P\text{-}P}$ = 22.0 Hz), while the second appears at -67.4 ppm ($^{1}J_{Pt\text{-}P}$ = 3483.7 Hz, $^{2}J_{P\text{-}P}$ = 21.7 Hz). Although these are very upfield chemical shifts, they compare well with that of other complexes where two *cis* PTA ligands are coordinated to platinum.[35] The signal at -67.0 ppm corresponds to the phosphorus of the PTA moiety *trans* to nitrogen as it has the lower $^{1}J_{Pt\text{-}P}$ coupling constant, whereas the -67.4 ppm signal is assigned to the PTA phosphorus *trans* to oxygen since it has the higher $^{1}J_{Pt\text{-}P}$ coupling constant. A representative ^{31}P NMR spectrum for phosphine-containing complexes **2b-e** is shown in Figure 2.13.

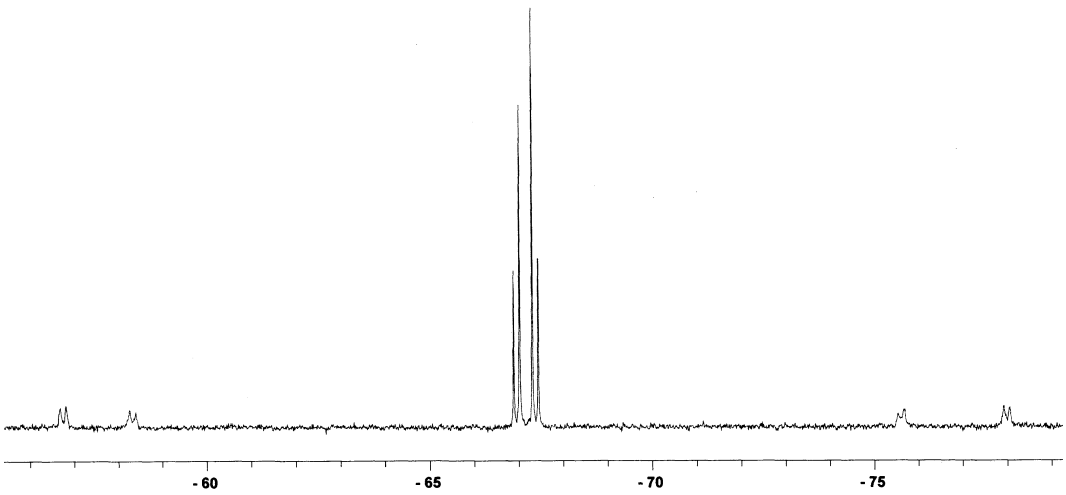

Figure 2.13: The ^{31}P NMR spectrum of 2d with the two doublets, each with a pair of ^{195}Pt satellites, typical of the phosphine-substituted complexes 2b-e.

2.2.3.5 NMR Spectroscopic Characterisation of **2e**

^{1}H NMR

Although the proton spectrum of **2e** (Figure 2.14) was recorded in both DMSO and $CDCl_3$, the discussion here is limited to the spectrum in DMSO, as it was the solvent used for the 2D spectra. This spectrum shows a number of interesting signals, and these are assigned to their various environments and summarised in Table 2.1.

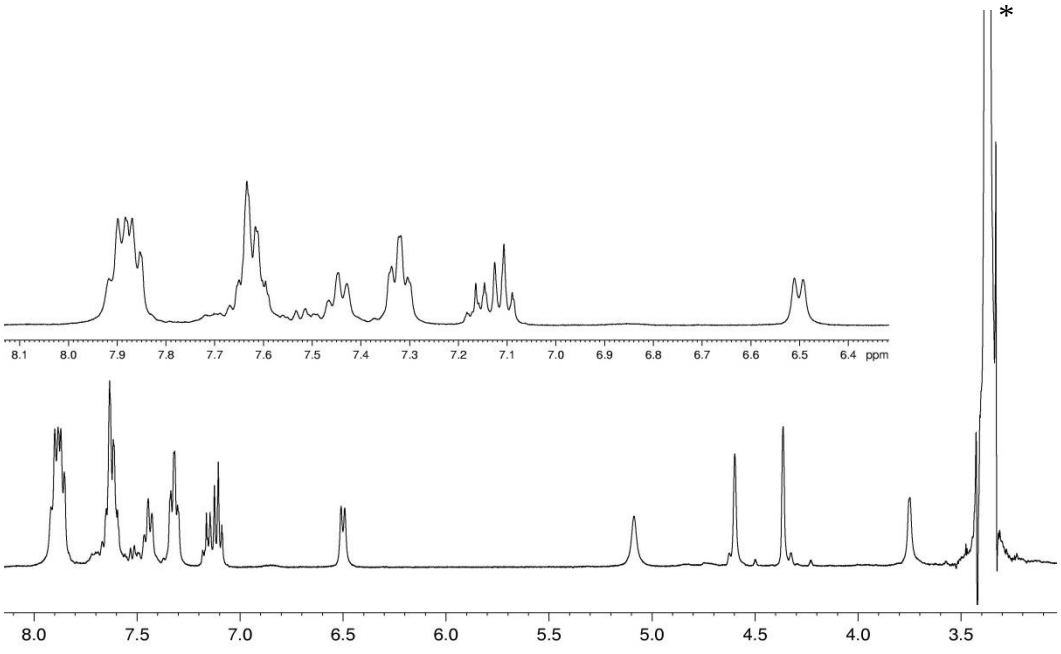

Figure 2.14: The ^{1}H NMR spectrum of 2e, with an expansion of the aromatic region across the top left of the figure (* represents the water due to wet DMSO solvent, which overlaps a ferrocene CH resonance).

Due to the symmetry of the two ferrocene rings in the dppf moiety, there are four proton signals attributable to the eight ferrocene CH protons on the dppf moiety. C1 is chemically equivalent to C2, C3 to C4, C5 to C6, and C7 to C8, as shown in Figure 2.15 (and consequently H1 & H2, H3 & H4, H5 & H6 and H7 & H8 are all chemically equivalent pairs). These appear as a broad singlet at 5.09 and three

sharper singlets at 4.60, 4.36 and 3.41 ppm. While the fourth ferrocene CH resonance may be hidden under the water peak (asterisked in Figure 2.14) due to wet DMSO in the ^{1}H spectrum, the high-resolution HSQC (Figure 2.16) indicates that the fourth signal comes at 3.41 ppm.

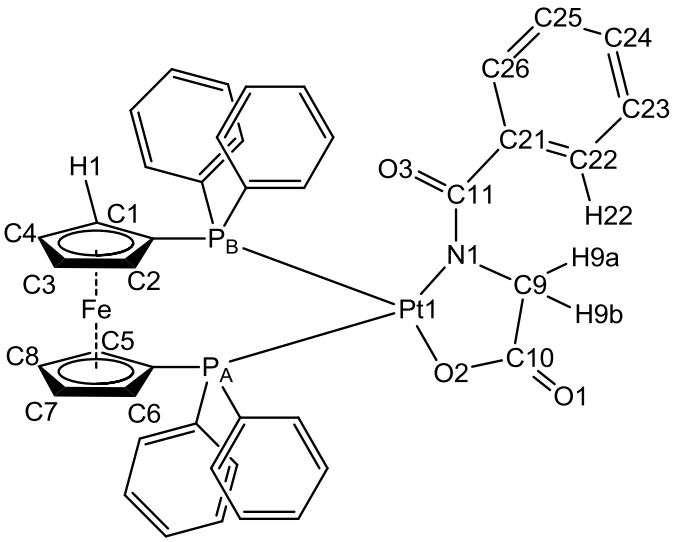

Figure 2.15: The numbering scheme of 2e, using the same numbering of the hippurate moiety as for 2a. The dppf phenyl rings are not labelled for simplicity. The diagram also highlights the symmetry of the ferrocene rings.

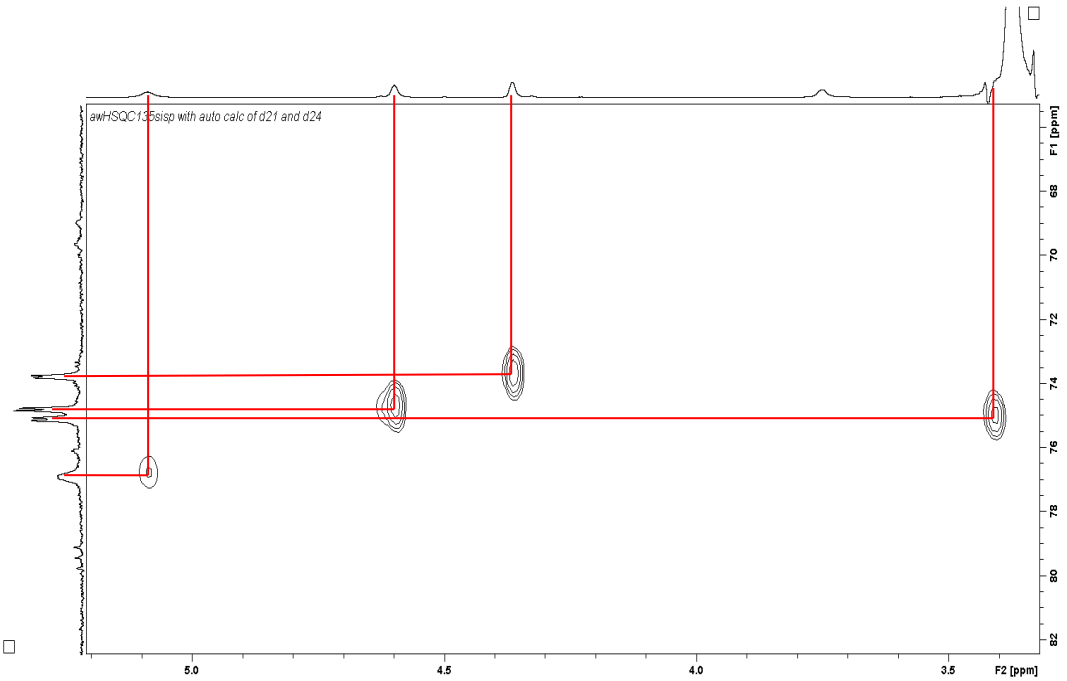

Figure 2.16: A high-resolution HSQC spectrum of 2e showing ^{13}C-^{1}H correlations enables assignment of the signal at 3.41 ppm hidden under the DMSO water peak as the fourth ferrocene CH resonance.

A high-resolution COSY spectrum (Figure 2.17) of this region shows correlations from the proton at 5.09 ppm to the proton at 4.60 ppm, and from the proton at 4.36 ppm to the proton at 3.41 ppm. This indicates that the 5.09 and 4.60 ppm protons are next to each other (i.e. on the same ring) whilst the protons at 4.36 and 3.41 ppm are alongside each other on the other ferrocene ring.

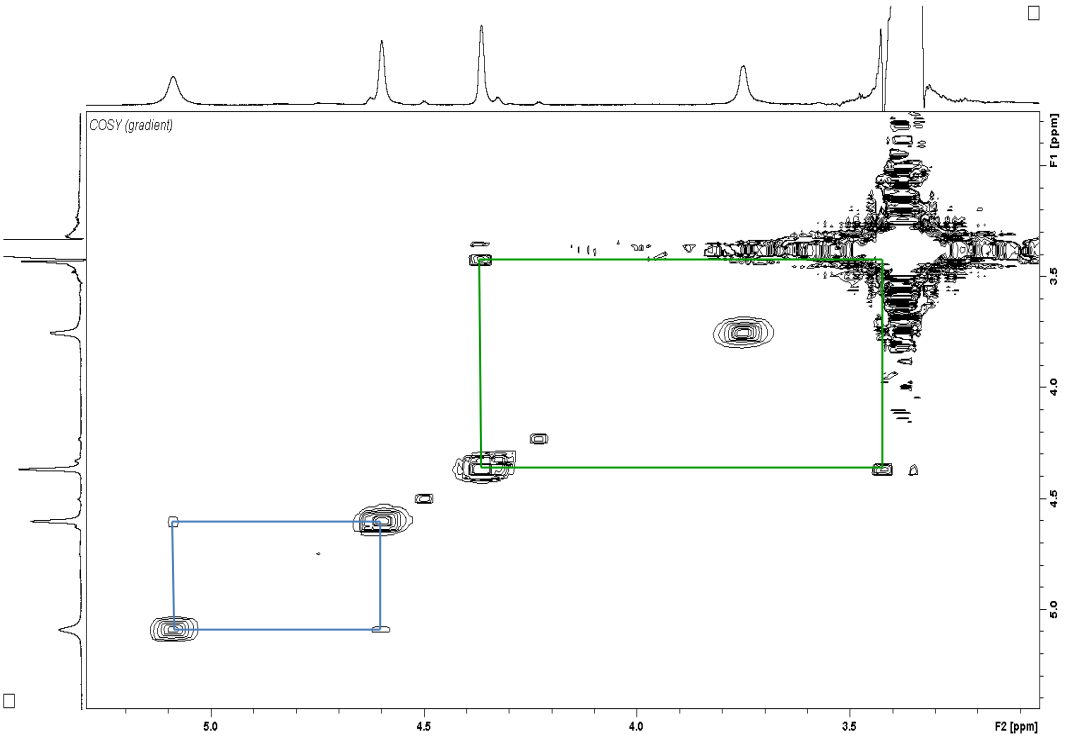

Figure 2.17: A high-resolution COSY showing correlations between the protons at 5.09 and 4.60 ppm (in blue), and 4.36 and 3.41 ppm (in green), respectively.

However, 2D NMR techniques did not enable full assignment of which proton corresponds to each environment in Figure 2.15. NMR spectra were calculated with DFT simulations to distinguish between these as for complex 2a. The four calculated chemical shifts for the ferrocene protons (when averaged to account for any vibrational movement during the time-scale of NMR spectroscopy) are 3.37, 4.58, 4.49 and 4.67 ppm (c.f. 3.41, 4.36, 4.60 and 5.09 ppm experimentally, respectively). The difference between the proton resonances for each ring is 1.21 and 0.18, while that of experimental NMR shifts is 0.95 and 0.48. While the first

three DFT-calculated resonances match the experimental chemical shifts well, caution must be exercised over assignment of the fourth NMR shift (4.67 ppm, compared to the corresponding experimental NMR shift of 5.09 ppm). Overall the DFT-calculated chemical shifts allow tentative assignment of H1/H2 at 3.41 ppm, H3/H4 at 4.36 ppm, H5/H6 at 4.60 ppm and H7/H8 at 5.09 ppm. These shifts are confirmed in the ^{13}C NMR section below, where interpretation of the HSQC spectrum using ^{13}C DFT-calculations allows for full assignment.

The signal for the metallacycle ring methylene is seen at 3.75 ppm as expected, and it displays broad shoulders from coupling to ^{195}Pt ($^{3}J_{Pt\text{-}H}$ ~ 50.7 Hz). As there is only one signal for the two protons, this suggests that – like parent complex **2a** - there is a plane of symmetry through the hippurate moiety which renders the two CH_2 protons chemically equivalent.

Table 2.2: The ^{1}H and ^{13}C chemical shifts of the various environments in complex 2e. Refer to Figure 2.15 for the atom numbering scheme‡.

Atoms	^{1}H chemical shift (ppm)	^{13}C chemical shift (ppm)
1, 2	3.41	75.1
3, 4	4.36	73.7
5,6	4.60	74.8
7,8	5.09	76.8
9	3.75	56.5
10	-	182.1
11	-	171.6
21	-	138.4
22-26 & dppf phenyl ring atoms	7.90 - 6.50	134.4 - 127.2 ppm

‡Note that assignment of ferrocene carbon and hydrogen atoms (atoms 1-8) are only tentative.

^{13}C NMR

The ^{1}H-decoupled ^{13}C NMR spectrum of **2e** (Figure 2.18) shows several resonances corresponding to the various environments in Figure 2.15 and are summarised in Table 2.2.

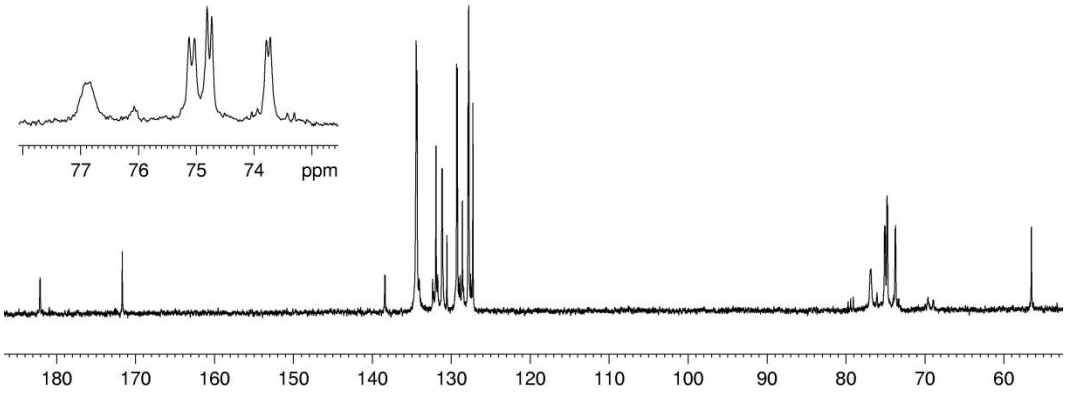

Figure 2.18: The ^{1}H-decoupled ^{13}C NMR spectrum of 2e showing an expansion of the 73-78 ppm region, which contains the ferrocene CH signals.

As seen in the expansion in the top left of the ^{1}H-decoupled ^{13}C NMR spectrum (Figure 2.18), there are four ferrocene CH resonances which all occur as doublets at 76.8, 75.1, 74.8 and 73.7 ppm respectively. These correspond to the C1/C2, C3/C4, C5/C6 and C7/C8 carbon environments. The bases of the doublets at 75.1 and 74.8 ppm overlap slightly. However the high-resolution HSQC spectrum (Figure 2.16) clearly indicates which protons are attached to the corresponding carbons: the proton at 5.09 ppm is attached to the carbon at 76.8 ppm, the proton at 4.60 ppm to the carbon at 74.8 ppm, the proton at 4.36 ppm to the carbon at 73.7 ppm, and the proton at 3.41 ppm to the carbon at 75.1 ppm. As the assignment of the ferrocene protons attached to these carbons is only tentative, ^{13}C DFT-calculations were used to substantiate the assignment of the ferrocene carbons. When averaged to allow for vibrational movement on the time-scale of

NMR spectroscopy, there are four calculated chemical shifts for the ferrocene CH environments; 82.0, 81.1, 83.5 and 82.3 ppm, compared to 75.1, 73.7, 74.8 and 76.8 (respectively) for experimental resonances. While these are significantly higher than the experimental chemical shifts, the difference in theoretical chemical shifts for each ring is in reasonable agreement with that of experimental: 0.95 and 1.24 compared with 1.4 and 2, respectively. Based on this, the ferrocene carbons can be assigned as follows: C1/C2 at 75.1 ppm, C3/C4 at 4.36 ppm, C5/C6 at 74.8 ppm and C7/C8 at 76.8 ppm.

The two carbonyl signals appear at 182.1 and 171.6 ppm, and based on chemical shifts of the parent complex **2a** the signal at 182.1 ppm can be assigned as the ring carbonyl neighbouring the metallacycle CH_2 (C10), while the 171.6 ppm signal can be attributed to the nitrogen-attached carbonyl (C11). The HMBC spectrum (Appendix V) confirms this, with the carbonyl signal at 171.6 ppm showing long-range coupling to aromatic protons. The metallacycle ring carbonyl is too far away to show any couplings to aromatic protons.

The aromatic ^{13}C signals occur in the 138.4-127.2 ppm region. While the singlet at 138.4 ppm can be tentatively assigned as the quaternary C21 based on its low intensity, the rest of the aromatic signals appear as a complex set of resonances, preventing further assignment.

The metallacycle ring methylene signal (C9) appears as a singlet at 56.5 ppm and shows satellite lines from coupling to ^{195}Pt ($^{2}J_{Pt\text{-}C}$ = 47.2 Hz).

^{31}P NMR

Similarly to the phosphorus NMR of the other three ligand-substituted complexes (**2b-d**), the ^{31}P NMR spectrum of complex **2e** shows two phosphorus signals at

9.44 ($^1J_{Pt\text{-}P}$ = 3131 Hz, $^2J_{P\text{-}P}$ = 22 Hz) and 6.47 ($^1J_{Pt\text{-}P}$ = 4102 Hz, $^2J_{P\text{-}P}$ = 23 Hz) ppm. The signal at 9.44 ppm can be assigned with the phosphorus environment *trans* to the metallacycle nitrogen atom due to its lower $^1J_{Pt\text{-}P}$ coupling constant, whereas the 6.47 ppm signal can be assigned to the phosphorus environment *trans* to the metallacycle oxygen.

2.2.4 Mass Spectral Analysis

All complexes except **2a** were successfully characterised by ESI-MS. They are all good candidates for mass spectrometry due to the presence of carbonyl groups, containing lone pairs on the oxygen which are easily ionised in ESI-MS.[36] Each complex (**2b-e**) shows a strong $[M+Na]^+$ peak, 22 mass units above that expected for $[M+H]^+$, as well as small $[M+H]^+$ and $[M+K]^+$ peaks in most cases. This was confirmed by adding a small amount of sodium chloride to each complex before analysis, the result being that only the $[M+Na]^+$ peak is observed for each complex. A representative spectra comparison is given in Figure 2.19, for complex **2b**.

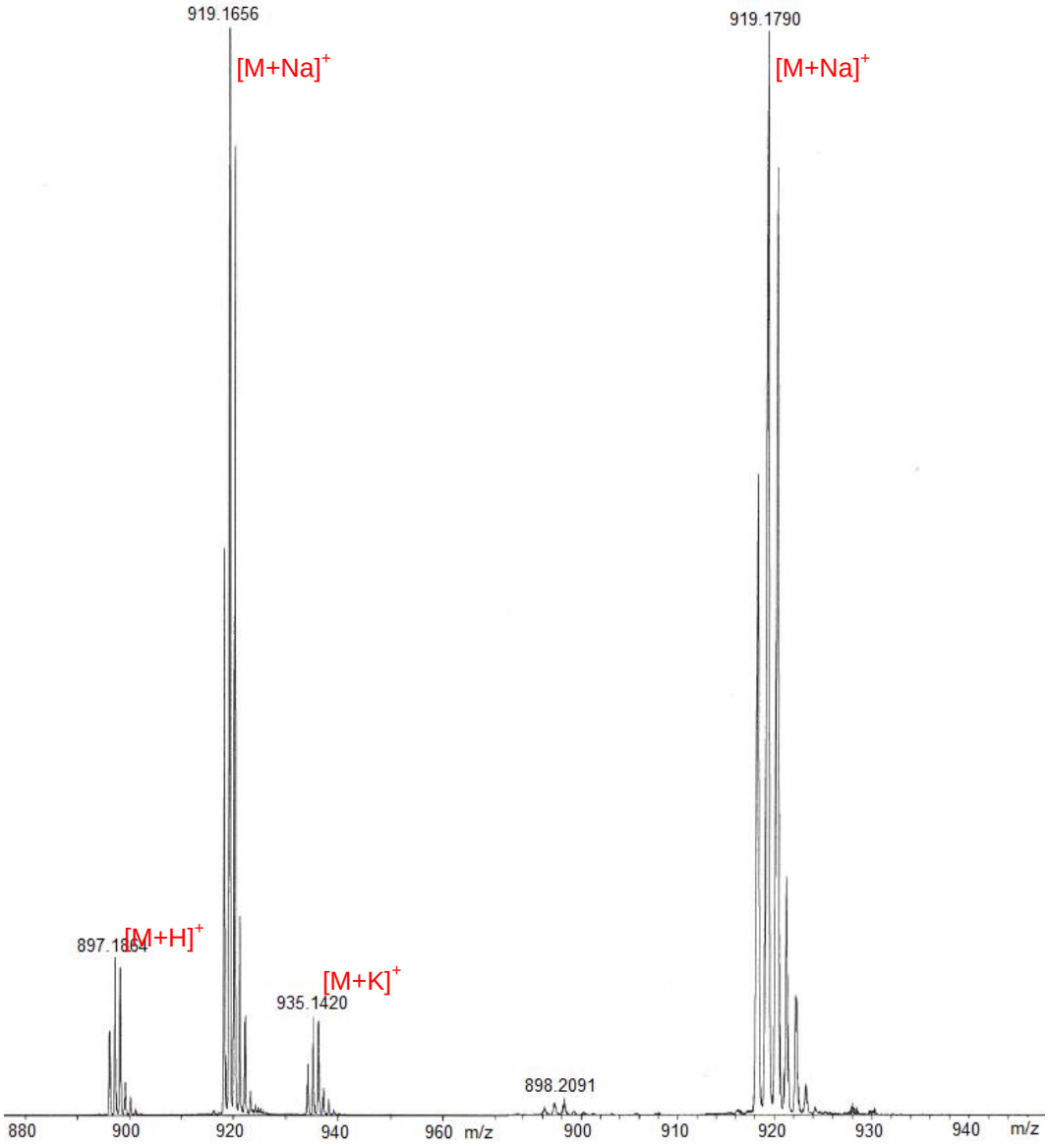

Figure 2.19: The left-hand mass spectrum shows the ions observed from the complex 2b, while the right-hand mass spectrum shows the ion observed from 2b with added sodium chloride.

2.2.5 IR Spectral Analysis

Complexes **2a-e** have interesting IR spectra. The starting material hippuric acid **102** has been characterised by IR previously,[37] and selected peaks for this are assigned to corresponding functional groups displayed in Table 2.3. Although Ramachandran & Natarajan tentatively assigned the peak at ~1180 cm^{-1} as a C-H ring deformation and the peak at ~1600 cm^{-1} as N-H bending, the IR vibrations

calculated using DFT simulations indicate that these vibrations are actually due to a C-N stretch and C=O stretch, respectively. Also of particular interest is the 1600-1760 cm^{-1} region, which contains the additional strong carbonyl stretch peak at 1751 cm^{-1}, which compares well to experimentally obtained values in Table 2.3.

However, on coordination to platinum in complex **2a** the carbonyl stretch peaks decrease to 1690 cm^{-1} and 1604 cm^{-1}. Table 2.4 shows selected IR peaks assigned to corresponding functional groups in both **2a** and the phosphine complex **2b**, and Figure 2.20 compares the IR spectra for hippuric acid, complex **2a** and the PPh_3-substituted complex **2b**.

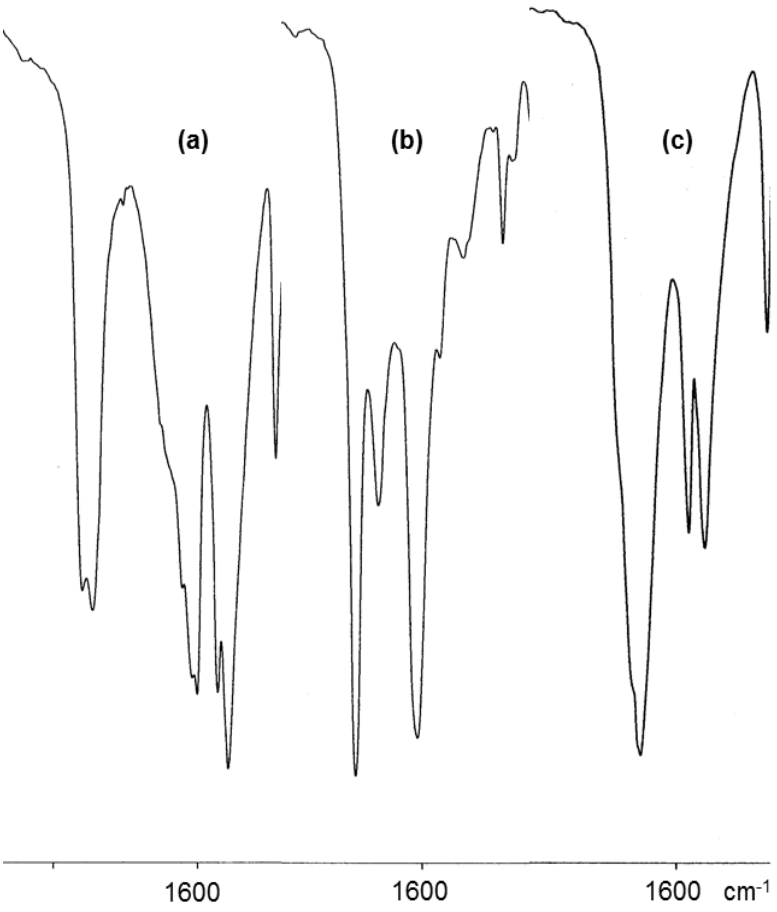

Figure 2.20: The IR spectra of (a) hippuric acid, (b) complex 2a and (c) the phosphine-substituted complex 2b, illustrating the changes in vibrations in the 1500-1800 cm^{-1} region.

The spectrum of complex **2b** [Figure 2.20(c)] is representative of all of the phosphine-substituted complexes **2b-e**; they all display a very strong C=O stretch at ~1650 cm^{-1}, and medium peaks at 1584 and 1563 cm^{-1} due to aromatic stretching in the multiple aromatic rings present.

Table 2.3: Selected IR absorptions obtained for hippuric acid compared to literature values.

Observed Wavenumber (cm^{-1})	Literature Wavenumber (cm^{-1}) [37]	Assignment
1760	1751	C=O stretch
1600	1608	C=O stretch‡
1183	1178	C-N stretch‡

‡Refer to text for explanation of assignment.

Table 2.4: Selected IR absorptions obtained for complex 2a and phosphine derivative 2b with assignments.

Complex	Wavenumber (cm^{-1})	Assignment
2a	1690	C=O stretch
	1604	C=O stretch
	1101	C-N stretch
2b	1647	C=O stretch
	1584 & 1563	Aromatic C=C stretch

2.2.6 Crystal Structure of 2a

The crystal structure of **2a** was carried out to determine the coordination geometry, bonding and orientation of the hippurate ligand around the platinum(II) centre. Several views of the structure are depicted in Figures 2.21-2.24, with the atom numbering scheme shown in Figure 2.21. A search of the CSD (Version 1.15) showed that there are no known crystal structures of transition metal complexes

containing the hippuric acid ligand. Only 3 structures of Pt-COD complexes containing N,O- ligands have been reported.[5,6]

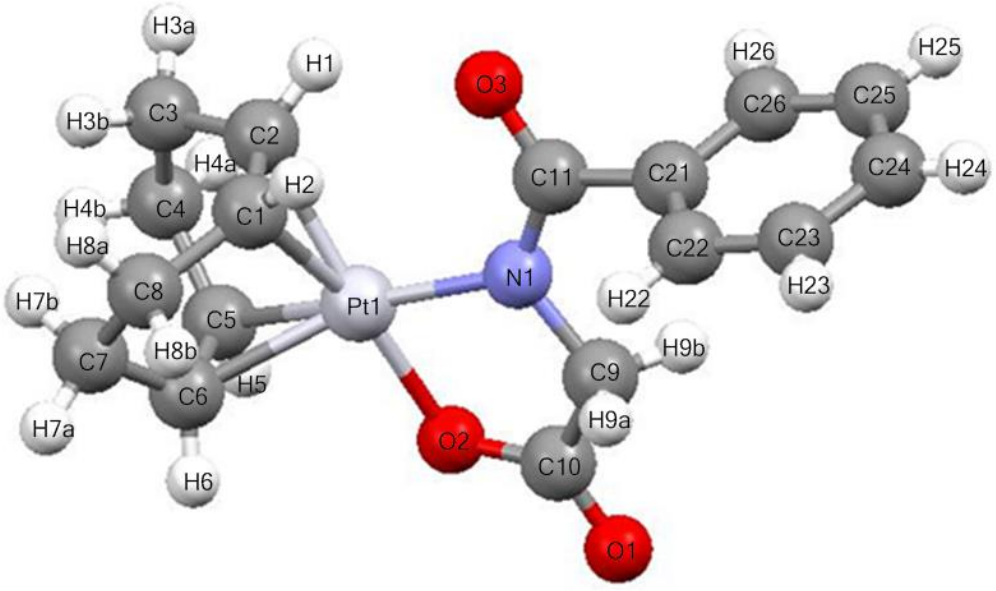

Figure 2.21: The crystal structure of 2a showing the complete numbering scheme for the complex.

The geometry about the platinum(II) atom is approximately square planar with minor deviations, however no atom diverges from the platinum-coordinated least-squares mean plane [defined by N1, O2, Pt1, C1/C2(midpoint) and C5/C6(midpoint)] by more than 0.05 Å. Bidentate coordination of the hippurate moiety to the platinum centre occurs via O2-Pt1-N1 bonds to give a 5-membered ring-system. This 5-membered metallacycle ring has an envelope conformation as seen in Figure 2.22, with a fold angle between the Pt1-N1-O2 and O2-C10-C9-N1 planes of 14.9°. The adjoined oxygen atoms (O1 and O3) deviate from the square plane of the envelope (defined by the plane N1-C9-C10-O2) by 0.457 Å and 0.592 Å, respectively. The phenyl ring plane (defined by C21-C22-C23-C24-C25-

C26) is at an angle of 83.85° to the 5-membered ring plane, defined by Pt1-N1-C9-C10-O2.

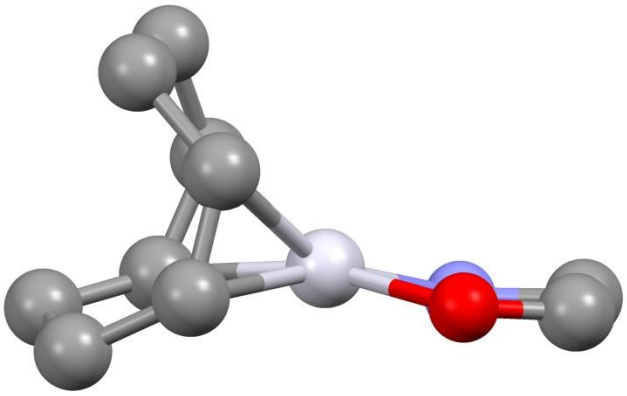

Figure 2.22: The crystal structure of 2a highlights the envelope conformation of the 5-membered ring. The square of the envelope is made up of the N1-C9-C10-O2 atoms, while the 'flap' consists of the N1-Pt1-O2 triangle.

As expected, the Pt1-C1/C2(midpoint) bond length *trans* to the metallacycle O2 atom (2.048Å) was slightly shorter than the Pt1-C5/C6(midpoint) bond length *trans* to the metallacycle N1 atom (2.068 Å), due to the hippurate oxygen having a smaller *trans* influence than the metallacycle nitrogen.[31]

When solving the crystal structure of **2a**, the C6 atom was refined isotropically due to a ripple effect from the attached platinum, hence length and angle comparisons to other platinum complexes containing a similar Pt-C bond may be slightly less certain for the Pt1-C6 bond. However the geometric parameters of the remaining Pt-C bonds (Pt1-C1, -C2 & -C5) can be evaluated definitively with regard to similar complexes. The Pt(^{t}BA^{F}Ph)(COD) complex [H_2^{t}BA^{F}Ph = 2-(2-trifluoromethyl)anilino-4,6-di-*tert*butylphenol] synthesised by Boyer et al. in 2009[5] is an appropriate complex for comparison, as it contains both a COD moiety coordinated to the platinum centre as well as a dianionic N,O-donor ligand.

As shown in Table 2.5, the two complexes have similar geometric parameters, despite having different groups attached to the 5-membered ring. As for **2a**, the Pt-C/C(midpoint) length *trans* to the oxygen is slightly smaller than the Pt-C/C(midpoint) bond *trans* to nitrogen in the Pt(^{t}BA^{F}Ph)(COD) complex due to oxygen having a larger *trans* influence. The angles for both complexes are all very comparable, as seen in Table 5.

Compared to the starting material [$PtCl_2$(COD)], complex **2a** has different bond lengths from the Pt(II) centre to the methyne carbons (C1, C2, C5 & C6).[38] In the starting material, the bond lengths corresponding to Pt1-C1 and Pt1-C2 are similar to those for **2a**, (2.154 and 2.172 Å respectively, compared to 2.155 and 2.170 Å for **2a**). However, the bond lengths corresponding to Pt1-C5 and Pt1-C6 are shorter in [$PtCl_2$(COD)] than in **2a** (2.178 and 2.176 Å compared to 2.181 and 2.187 Å for **2a**). This may be due to the larger *trans* influence of the nitrogen in the hippurate moiety in **2a** in contrast to that of the chlorine in [$PtCl_2$(COD)], causing slight lengthening of the Pt-C bond. The COD moiety in **2a** is also significantly more distorted from the normal gauche shape (as seen in Figures 2.23 and 2.24) than for the parent material, [$PtCl_2$(COD)].

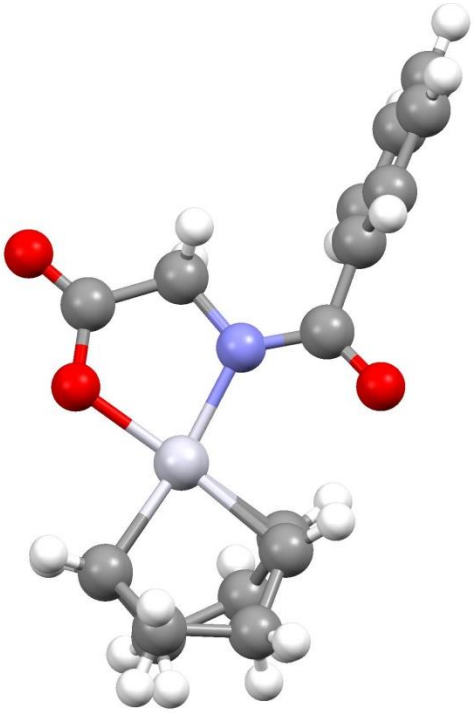

Figure 2.23: The crystal structure of 2a shows that the COD moiety is not completely symmetrical in its "boat" shape.

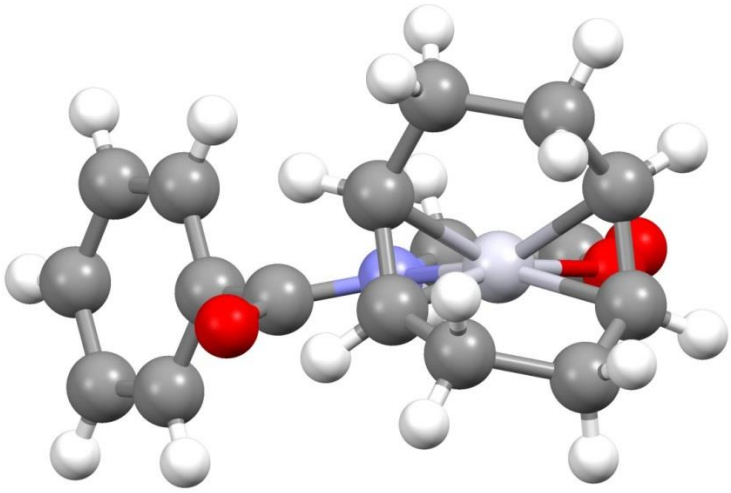

Figure 2.24: The top-view of the COD moiety in the crystal structure of 2a shows the distortion of the COD moiety.

The crystal structure of complex **2a** also shows significant differences to the hippuric acid starting material,[39] which forms the 5-membered metallacycle ring

on coordination. The lengths corresponding to N1-C9 and N1-C11 are both slightly longer in **2a** compared to hippuric acid (1.468 and 1.358 Å respectively, c.f. 1.446 and 1.342 Å in hippuric acid), as is the O2-C10 bond (1.324 Å c.f. 1.301 Å in hippuric acid).

The bite angle of the hippurate ligand (the N1-Pt1-O2 angle) is 81.83°, which is significantly smaller than the idealised 90° angle expected for a square planar complex. In the similar square planar *N*-acetylglycinato-platinum complex synthesised by Kemmitt et al. in 1992[3] the bite angle is even smaller (78.8°). This may be due to the bulky dppe ligand occupying a large amount of space, causing the N-Pt-O angle to appear smaller than expected. The Pt1-N1 (2.060 Å) and Pt1-O2 (2.097 Å) bond distances of the *N*-acetylglycinato-platinum complex are longer than those for complex **2a**, and the Pt1-N1 bond is slightly shorter than the Pt1-O2 bond, which is the opposite of those in complex **2a** (2.016 and 2.013 Å respectively). However these differences in Pt-N and Pt-O bonds may be due to the higher trans influence of the phosphine groups (compared to carbons in complex **2a**).

In each crystal, 4 molecules stack diagonally to each other. They are not very close together as there are no hydrogen-bonding interactions and the COD groups are too bulky to allow the platinum(II) centres to stack closely.

Table 2.5: Selected bond lengths and angles of complex 2a (estimated standard deviations given in parentheses) compared to the same key parameters in similar complex Pt(^{t}BA^{F}Ph)(COD).

	2a	**Pt(^{t}BA^{F}Ph)(COD)**
Bonds		
Pt1-C1	2.155(3)	2.154
Pt1-C2	2.170(3)	2.128
Pt1-C1/C2(midpoint)	2.048(3)	2.027
Pt1-C5	2.181(3)	2.144
Pt1-C6	2.187(4)	2.160
Pt1-C5/C6(midpoint)	2.068(3)	2.035
Pt1-O2	2.013(2)	1.962
Pt1-N1	2.016(3)	1.974
O2-C10	1.324(4)	1.334
N1-C9	1.468(4)	1.375
N1-C11	1.358(4)	1.407
C9-C10	1.520(4)	1.397
O1-C10	1.213(4)	-
O3-C11	1.231(4)	-
Angles		
C1/C2(midpoint)-Pt1-C5/C6(midpoint)	86.77(12)	87.33
N1-Pt1-O2	81.83(10)	81.87
C1/C2(midpoint)-Pt1-N1	100.14(11)	100.17
C5/C6(midpoint)-Pt1-O2	91.05(11)	90.58
Pt1-N1-C11	127.22(19)	126.83
Pt1-N1-C9	112.51(2)	112.58
Pt1-O2-C10	116.20(19)	113.80

2.3 Conclusion

Five novel platinum(II) hippurate complexes (**2a-e**) have been synthesised and characterised, with the X-ray crystal structure of complex **2a** being successfully obtained. These appear to be the first known platinum complexes of this type. Unfortunately the biological activities of these complexes are not yet known, as throughout the duration of this thesis there were no biological testing facilities available.

Chapter 3: Attempted Synthesis and Characterisation of Gold Hippurate Complexes

Note:

There are 2 sets of compound numbers; **3a**-**3d** discussed in Chapters 3-5 are separate from complex **3** mentioned in the introduction.

3.1 Experimental

3.1.1 Attempted synthesis of [Au{OC(O)CH$_2$N(COPh)}(2-anp)] (anp = anilinopyridyl) (3a)

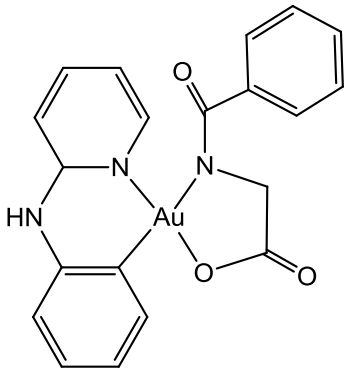

3a

Preparation of **3a** was attempted using a similar procedure for the synthesis of complex **2a**. Silver(I) oxide (624.6 mg) was added to a mixture of 2-anp-$AuCl_2$ (anp = anilinopyridyl) (203.5 mg, 0.466 mmol) and hippuric acid (110.9 mg, 0.619 mmol) in dichloromethane (30 mL), and the mixture was refluxed for 1 hour giving a black suspension. The mixture was cooled, filtered and rotary evaporated to ~5 mL and 95 mL petroleum spirits was added to precipitate potential product overnight (as for **1f**). Yellow crystals formed which were filtered, washed with petroleum spirits (~5 mL) and dried under vacuum overnight to give 160.1 mg of product. However, the NMR obtained for the expected complex was

not able to be rationalised, and the ESI-MS showed evidence of the formation of the unwanted product, as depicted on the left (**3c**) of Figure 3.4, at 566.04 *m/z*.

3.1.2 Attempted synthesis of [Au{OC(O)CH$_2$N(COPh)}(2-bp)] (bp = benzylpyridyl) (3b)

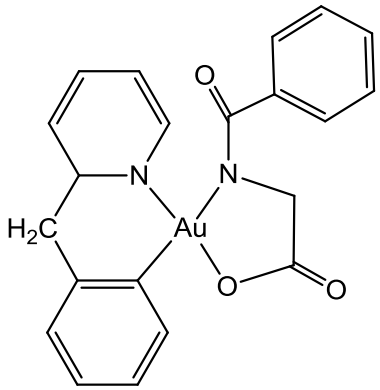

3b

Preparation of **3b** was attempted using a similar procedure for the synthesis of complex **2a**. Silver(I) oxide (626.2 mg, excess) was added to a mixture of 2-bp-$AuCl_2$ (bp = benzylpyridyl) (207.1 mg, 0.475 mmol) and hippuric acid (109.7 mg, 0.612 mmol) in dichloromethane (30 mL), and the mixture was refluxed for 1 hour giving a black suspension. After cooling to room temperature the mixture was filtered through glass fibre filter paper giving a yellow solution. This was rotary evaporated to remove the solvent to ~5 mL volume. Petroleum spirits (95 mL) was added and the mixture allowed to crystallise overnight, giving white crystals which were filtered off, washed with petroleum spirits (~5 mL) and dried under vacuum overnight to give 184.9 mg of product. However, the resulting product gave NMR that was not able to rationalised, and showed evidence in the ESI-MS of formation of the unwanted product depicted on the right (**3d**) in Figure 3.4, at 565.04 *m/z*.

3.2 Results & Discussion

3.2.1 NMR Spectroscopic Investigation of 3a and 3b

The reaction of hippuric acid with 2-bp-$AuCl_2$ and 2-anp-$AuCl_2$ gives air and water-stable yellow and white powders (respectively). However, the proton NMR spectra for both complexes showed extra signals which were unable to be rationalised, even when taking into account potential isomerism. This suggested the formation of a by-product.

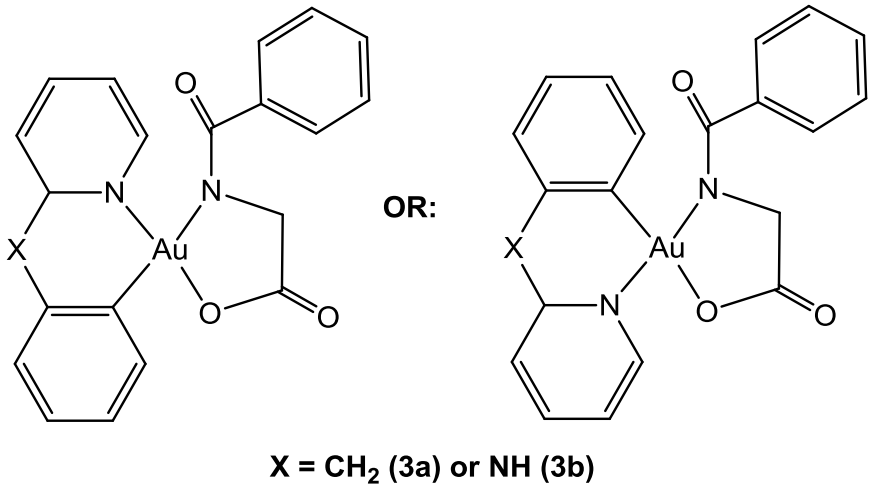

Figure 3.1: The two different ways that the 2-anp/2-bp ligand can coordinate leads to the possibility of two isomers for each 3a and 3b, which may be reflected in the NMR spectra for each.

Complexes **3a** and **3b** may exist as isomers, as shown in Figure 3.1. The planarity of the 2-anp/bp ligand also influences the number of proton signals seen in the CH_2 region (~3-5 ppm). While the 2-anp moiety is typically flat, the 2-bp ligand is often puckered, making the hippurate CH_2 protons inequivalent and doubling the number of signals seen. For the CH_2 (3.5-5 ppm) region of the ^1H NMR spectrum of **3a** (Figure 3.2), if only one isomer of **3a** is present and the 2-anp moiety is flat, one singlet for the hippurate CH_2 would be observed. If both isomers are present

and the 2-anp ligand is flat then there would be two singlets (CH_2 signals of different chemical shifts). However, after integration Figure 3.2 shows 3 doublets with similar intensities, a significantly smaller doublet and a broad singlet. The intensities of the integrations for each signal do not make sense or fit into any of the above scenarios, as each pair of doublets (for each isomer) would need to be the same intensity for the signals to be rationalised.

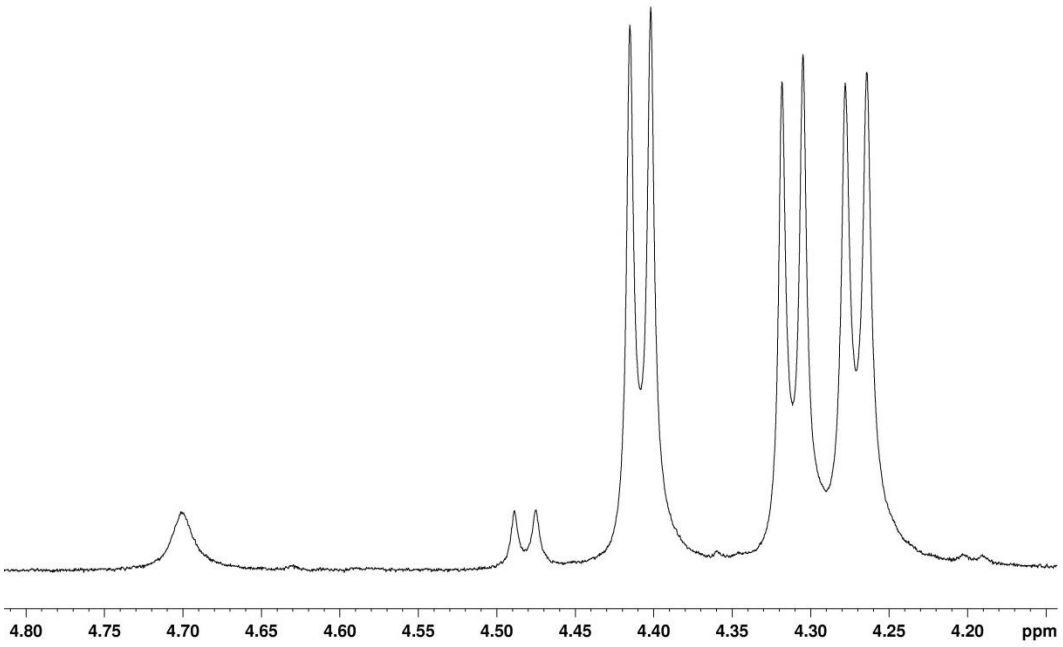

Figure 3.2: The CH_2 (4.2-4.8 ppm) region of the ^{1}H spectrum of 3a.

On the other hand, the 2-bp moiety is often puckered, which can lead to fluxional behaviour, doubling the amount of signals seen and leading to broad signals. When considering the CH_2 region of the proton spectrum of **3b** (Figure 3.3), there are the similar possible situations that will affect the number of signals in the CH_2 region, however there is an additional CH_2 in the 2-bp moiety. Hence for one isomer of **3b** with the 2-bp ligand flat a singlet for each CH_2 would be observed;

with the 2-bp ligand puckered and one isomer present there would be two doublets for each CH_2 (two different chemical shifts for each methylene proton, both coupled to each other); and if the 2-bp moiety is puckered and 2 isomers are present four doublets for each CH_2 would be seen. The 3.8-5.0 ppm region of the ^1H spectrum of **3b** (Figure 3.3) shows two doublets and a singlet, as well as two broad singlets which may be attributable to fluxional movement of the 2-bp ligand. However, after integration the broad signals have half the intensity of the doublets and singlet, and the numbers of signals present does not make sense for any of the scenarios discussed above, therefore the proton NMR was unable to be rationalised. This suggests that for each complex formed, there may be a mixture of compounds, rather than isolating **3a** and **3b** alone as expected.

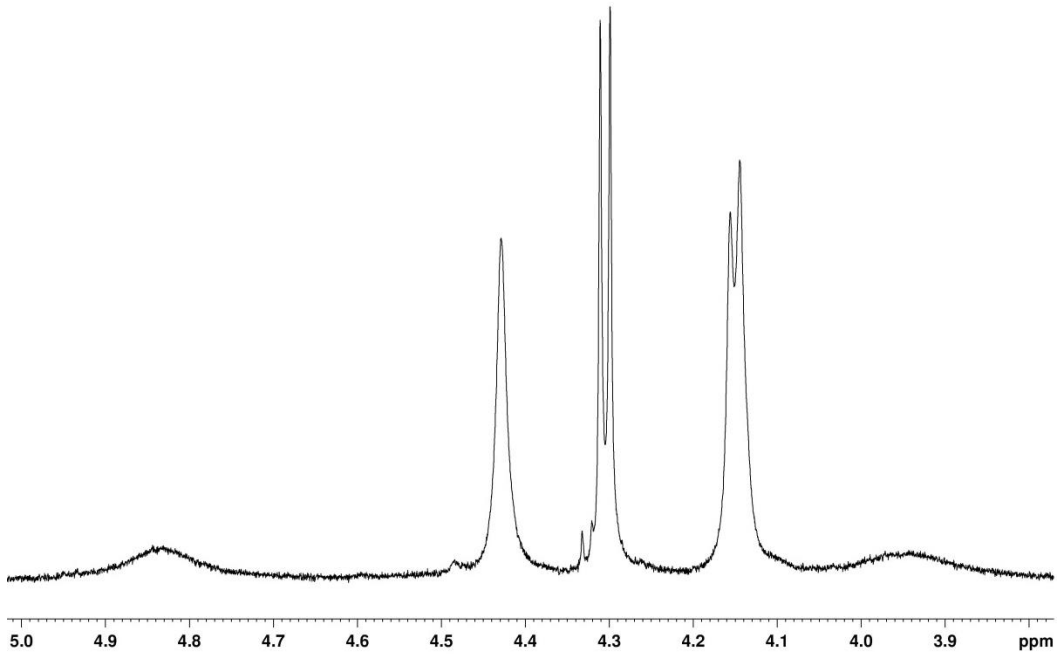

Figure 3.3: The CH_2 (3.8-5.0 ppm) region of the ^1H spectrum of 3b.

3.2.2 Mass Spectral Investigation of 3a and 3b

ESI-MS was useful in determining what had actually been produced. The expected M^+ ion for **3a** is 543.09, and for **3b** is *m/z* 542.09. However, the ions observed were at *m/z* 535.08 for **3a**, and 533.09 for **3b**, which correspond to the M^+ ion *m/z* values for **3c** and **3d**, respectively. Therefore, ESI-MS of both compounds showed evidence of the formation of bis-cycloaurated cationic complexes, outlined in Figure 3.4 below. The formation of this class of ions is not uncommon for gold syntheses, and has been reported before by Dinger & Henderson in 1998.[40]

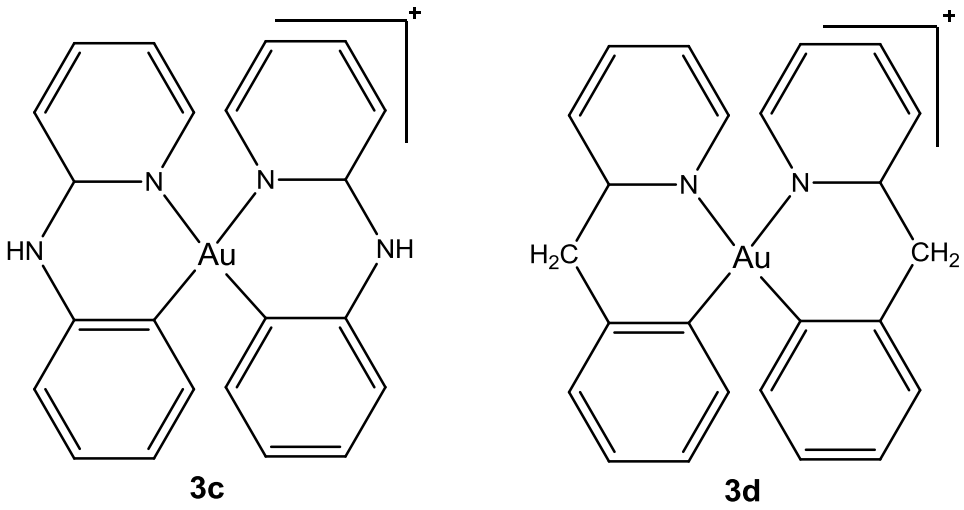

Figure 3.4: The bis-cycloaurated cations 3c and 3d above formed when attempting to synthesise 3a and 3b, respectively.

However, *m/z* values of 566.04 and 565.04 were also observed for **3a** and **3b**, which correspond to $[M+Na]^+$ for **3a** and **3b** respectively. The combination of ions observed in the ESI-MS along with the conclusions drawn from the NMR spectra suggests that the complexes formed are mixtures of **3a** & **3c**, and **3b** and **3d**.

3.3 Conclusion

During attempts to synthesise two gold(III) hippurate complexes (**3a** & **b**), two bis-cycloaurated cationic complexes **3c** and **3d** were produced. This was reflected in an unexpected extra set of signals in the ^{1}H NMR spectrum for each product, and in the ESI-MS spectra where *m/z* values were obtained which indicated the formation of these bis-cycloaurated ions. The impurities **3a** and **3b** may only be present in small amounts, yet might still give intense ESI-MS signals. No further attempts to characterise these complexes were made.

Chapter 4: Synthesis and Characterisation of a Platinum *N*-phenylanthranilate Complex

Note:

There are 2 sets of compound numbers; complex **4** discussed in Chapters 4-5 is separate from compound **4** mentioned in the introduction.

4.1 Experimental

4.1.1 Synthesis of [Pt{OC(O)(C_6H_4)N(Ph)}(COD)] (4a)

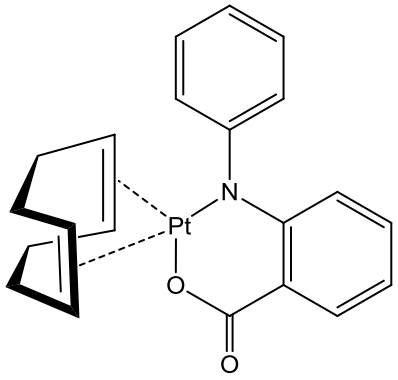

4a

Complex **4a** was prepared using a similar procedure to the preparation of **2a**. Silver(I) oxide (1529.8 mg, excess) was added to a stirred mixture of [$PtCl_2$(COD)] (500.4 mg, 1.337 mmol) and *N*-phenylanthranilic acid (295.2 mg, 1.384 mmol) in dichloromethane (30 mL), and the mixture was refluxed for 3.5 h giving a dark green-yellow suspension. After cooling to room temperature the mixture was filtered through glass fibre filter paper twice to remove any insoluble silver salts, and the filter paper washed with dichloromethane (~2 mL) each time, giving a brown-yellow solution which was rotary evaporated to ~5 mL. Petroleum spirits (~95 mL) was added and the mixture allowed to crystallise overnight, giving

green-yellow crystals which were filtered off, washed with petroleum spirits (5 mL) and dried under vacuum overnight to give 51% of **4a**.

mp = 155-157°C (decomp.)

Found: C, 48.3; H, 4.2; N, 2.6%. $C_{21}H_{21}NPtO_2$ requires C, 49.0; H, 4.1; N, 2.7%.

IR: υ(C=O) = 1616 cm^{-1}(vs).

ESI-MS: (capillary exit voltage = 160 V) *m/z* 515.17 (25%, $[M+H]^+$), calculated *m/z* for $C_{21}H_{21}NPtO_2.H$ = 515.12.

NMR: Refer to Figure 4.2 for the atom numbering scheme of **4a**.

^{1}H δ 8.26-5.90 (m, 9H, H12-H15 & H-22-H26), 5.42 (m, 2H, H5/H6, $^2J_{Pt-H}$ = 54.3 Hz), 4.42 (m, 2H, H1/H2, $^2J_{Pt-H}$ = 64.7 Hz), 2.70-2.56 (m, 4H, H3a, H4a, H7a & H8a), 2.27-2.11 [m, 4H, H3b, H4b, H7b & H8b] ppm.

^{13}C-{^{1}H} δ 166.2 (s, C9), 153.1 (s, C11), 150.2 (s, C21), 133.9 (s, C15), 131.5 (s, C13), 130.0 (s, C22/C26), 129.7 (s, C23/C25), 126.1 (s, C24), 116.4 (s, C14), 116.1 (s, C12), 114.7 (s, C10), 98.4 [s, $C5/C6_{A(trans\ N)}$, $^1J_{Pt-C}$ = 139.4 Hz], 93.7 [s, $C1/C2_{B(trans\ O)}$, $^1J_{Pt-C}$ = 197.6 Hz], 31.0 (s, C3/C8), 28.4 (s, C4/C7) ppm.

4.2 Results & Discussion

4.2.1 Syntheses

The reaction of $[PtCl_2(COD)]$ and *N*-phenylanthranilic acid in the presence of silver(I) oxide refluxing in refluxing dichloromethane gives, in reasonable yield and purity, complex **4a**, the first known complex of this type. **4a** is stable in air and water, and crystallises as a very intense green-yellow coloured solid. This – in contrast with the platinum hippurate complexes **2a-e**, which are all colourless

(excluding complex **2e**, which is intense yellow due to the presence of ferrocene) – suggests a highly delocalised conjugated system. It was therefore of interest to determine the crystal structure of **4a**, to determine if the entire metal-ligand system is planar. Crystals have been obtained which are expected to be suitable for X-ray structure determination, however the structure has not yet been determined at the time of completion of this thesis.

As for complex **2a**, complex **4a** did not give a simple ESI mass spectrum. This is once again interesting, as the majority of compounds containing carbonyl groups are usually excellent candidates for mass spectrometry due to their easily ionisable C=O moieties.[36] The reason for this is once again unknown, as similar COD-containing platinum complexes have shown to have excellent ESI-MS results.[28]

4.2.2 NMR Spectroscopic Characterisation

4.2.2.1 NMR Spectroscopic Characterisation of **4a**

^{1}H NMR

The proton spectrum of complex **4a** (Figure 4.1) shows a number of well-resolved signals corresponding to the environments shown in Figure 4.2.

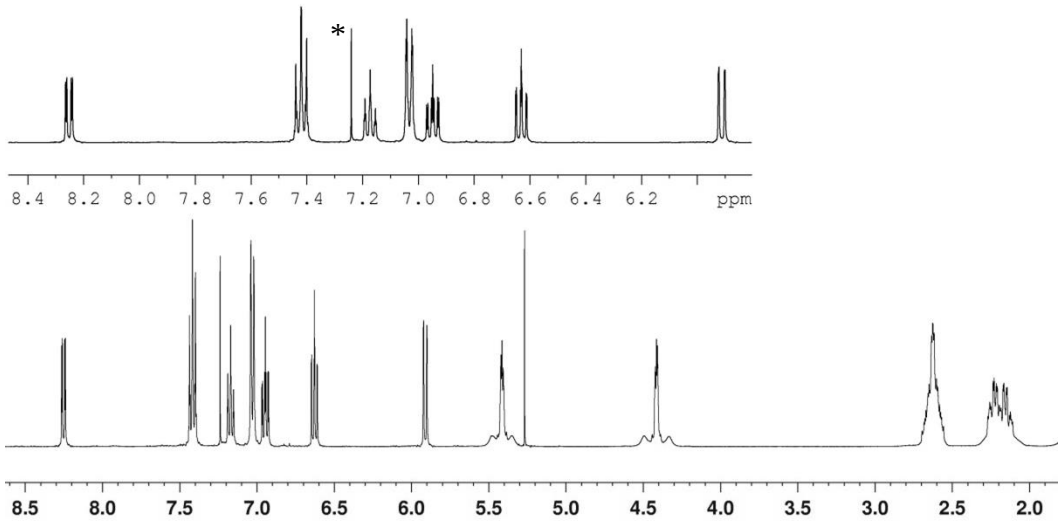

Figure 4.1: The ^{1}H NMR spectrum of complex 4a, showing signals corresponding to phenyl groups and the COD moiety (* represents traces of $CHCl_3$ in the $CDCl_3$ solvent). The top left shows an expansion of the phenyl region (5.9-8.4 ppm).

The signals which can be assigned to the assorted proton and carbon environments on Figure 4.2 are summarised in Table 4.1 at the end of this section.

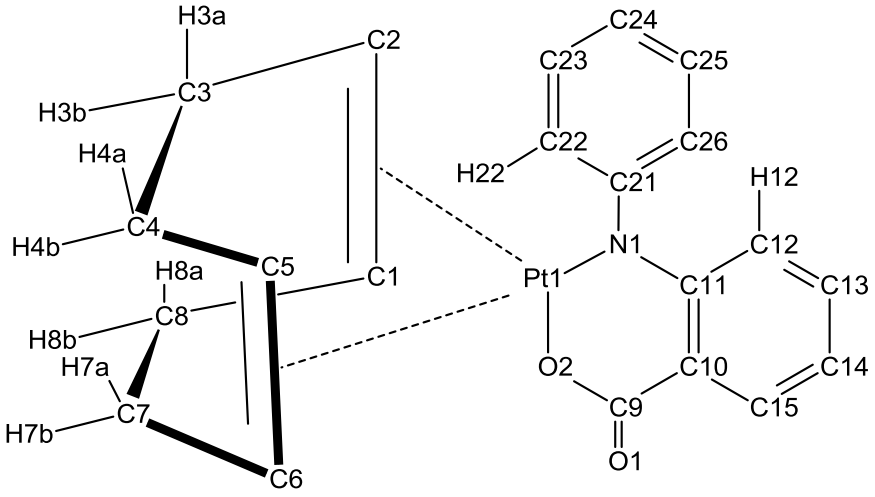

Figure 4.2: The assorted proton and carbon environments in complex 4a, giving rise to the signals seen in the ^{1}H and ^{13}C NMR spectra.

As for complex **2a**, the four COD methyne (CH) resonances are only seen as two signals in the proton spectrum of **4a**, since C1 and C2, C5 and C6 (and accordingly H1 and H2, and H5 and H6) are rendered equivalent due to the COD moiety being present in the gauche conformation it adopts upon coordination (as seen in Figure 4.2). The two COD methyne signals are observed as multiplets at 5.42 and 4.42 ppm, and both exhibit broad shoulders from coupling to ^{195}Pt ($^{2}J_{\text{Pt-H}}$ = 54.3 Hz and 64.7 Hz, respectively). The nitrogen and oxygen atoms attached to the platinum metal centre will exert differing *trans*-influences on the carbon atoms *trans* to each of these, resulting in different coupling constants.[31] Consequently, the signal at 4.42 ppm can be assigned as being *trans* to the Pt-attached oxygen (i.e. assigned to H1/H2), as it has the larger $^{2}J_{\text{Pt-H}}$ coupling constant, which indicates it is attached to the carbon *trans* to the oxygen (at 93.8 ppm, from the HSQC). In contrast, the signal at 5.42 ppm corresponds to the environment *trans* to the Pt-attached nitrogen (i.e. assigned to H5/H6) as it has the lesser $^{2}J_{\text{Pt-H}}$ coupling constant, which shows that it is attached to the carbon environment *trans* to the nitrogen (at 98.4 ppm, from the HSQC). These assignments are as anticipated, as the methyne protons *trans* to the metallacycle oxygen would be expected to be further downfield.[33] The DFT-calculated theoretical NMR shifts confirm these assignments, as they show two different proton environments (which are averaged to allow for NMR spectroscopy vibrational motion) that are 0.98 ppm apart (as shown by the red lines in Figure 4.3). This is in good agreement with the observed NMR shifts, which are exactly 1 ppm different. The H1/H2 signal is calculated to be at 4.20 ppm, which is 0.22 ppm lower than that of the observed resonance, while the H5/H6 shift is estimated to occur at 5.18 ppm (0.25 ppm lower than the observed chemical shift).

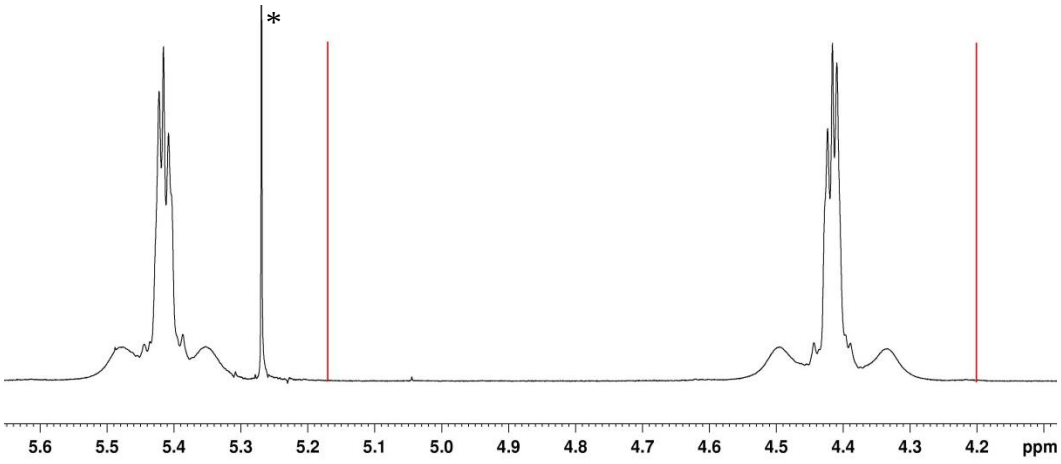

Figure 4.3: An expansion of the COD CH (4-6 ppm) region of the ^{1}H NMR spectrum of complex 4a, showing the observed and DFT-calculated resonances (red lines) for the COD methyne protons (* represents traces of CH_2Cl_2).

The eight COD methylene (CH_2) protons are slightly more complicated to assign. In the ^{1}H spectrum for 4a (Figure 4.1), they appear as two complex multiplets from 2.70-2.56 and 2.27-2.12 ppm. Due to the conformation of the COD moiety (highlighted in Figure 4.2), the H3a and H8a, H3b and H8b, H4a and H7a, and H4b and H7b protons of COD are rendered equivalent, giving only 4 signals for 8 protons. What makes the assignment of these even more difficult is that each multiplet appears to correspond to two different proton environments, each on different carbons, as seen in the HSQC experiment. Axial protons are generally higher in chemical shift than equatorial protons,[32] which aids in assignment. A selective 1D NOESY experiment was carried out on complex **4a**. In this, one signal becomes irradiated, and the proton signals closest to this are then seen as a result of through-space correlations. When the CH signal at 5.42 is irradiated, the initial correlation which appears is to the CH signal at 4.42 ppm (which shows that is the most spatially close signal). It then shows correlations to the CH_2 protons centred first at 2.63 and later at 2.22 ppm. This allows assignment for the **4a** and **7a** protons at 2.63 ppm and the **4b** and **7b** protons at 2.22 ppm, as these are

the closest environments spatially to the H5/H6 signal at 5.42 ppm. Therefore, by process of elimination the CH_2 signals centred at 2.62 and 2.16 ppm can be assigned to **3a**/**8a** and **3b**/**8b**, respectively.

There are two separate ring systems in complex **4a**; a 5-proton phenyl ring (attached to the nitrogen atom) with 2:2:1 proton intensities, and a 4-proton aromatic spin system with single proton intensities. Presuming that there is free rotation about the N-1-C21 bond which renders the C22 and C26 environments identical, there are three proton environments which arise from the N-substituted phenyl ring (assigned to H22/H26, H23/H25 and H24 on Figure 4.2). To initially differentiate between the two ring systems, the relative proton intensities can be used. Upon examination of the ^1H spectrum for complex **4a**, there is a triplet of doublets at 7.42 ppm and a doublet of doublets at 7.03 ppm which have twice the intensity of the rest of the phenyl signals, hence belong to the 5-proton phenyl ring. The H22/H26 signal is expected to be a doublet of doublets, as it has 1 nearest neighbour and long-range coupling from the conjugated ring system, and double the intensity for all phenyl signals except the H23/H25 signal. The high-resolution NOESY spectrum (Figure 4.4) confirms assignment of the doublet of doublets at 7.03 ppm as the H22/H26 proton signal, as it shows a strong correlation from the signal at 7.03 ppm to the ring-substituted phenyl proton H12 at 5.91 ppm.

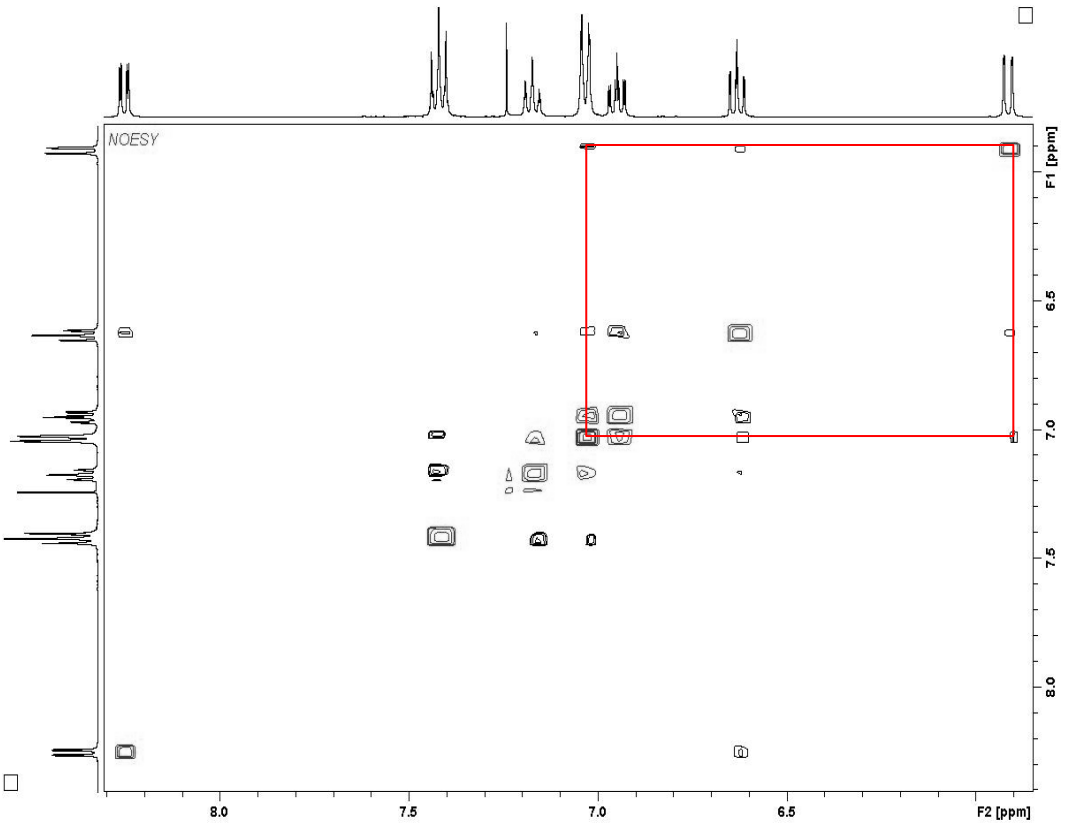

Figure 4.4: The high-resolution NOESY spectrum of the phenyl (5.9-7.5) region of complex 4a shows through-space correlations from the H12 signal at 5.91 ppm to the H22/H26 signal at 7.03 ppm (shown by the red lines).

The triplet of doublets at 7.42 ppm can be assigned to the H23/H25 environment due to its double intensity. A high-resolution COSY spectrum (Figure 4.5) of the 7-7.5 ppm region confirms this assignment, showing a strong ^{3}J correlation from the H22/H26 signal at 7.03 ppm to the triplet of doublets at 7.42 ppm. The same COSY (Figure 4.5) also allows assignment of the single-intensity triplet of doublets at 7.17 ppm as the H24 proton, as it shows correlations from both the H23/H25 signal at 7.42 ppm (^{3}J couplings) and the signal at 7.03 ppm (^{4}J couplings).

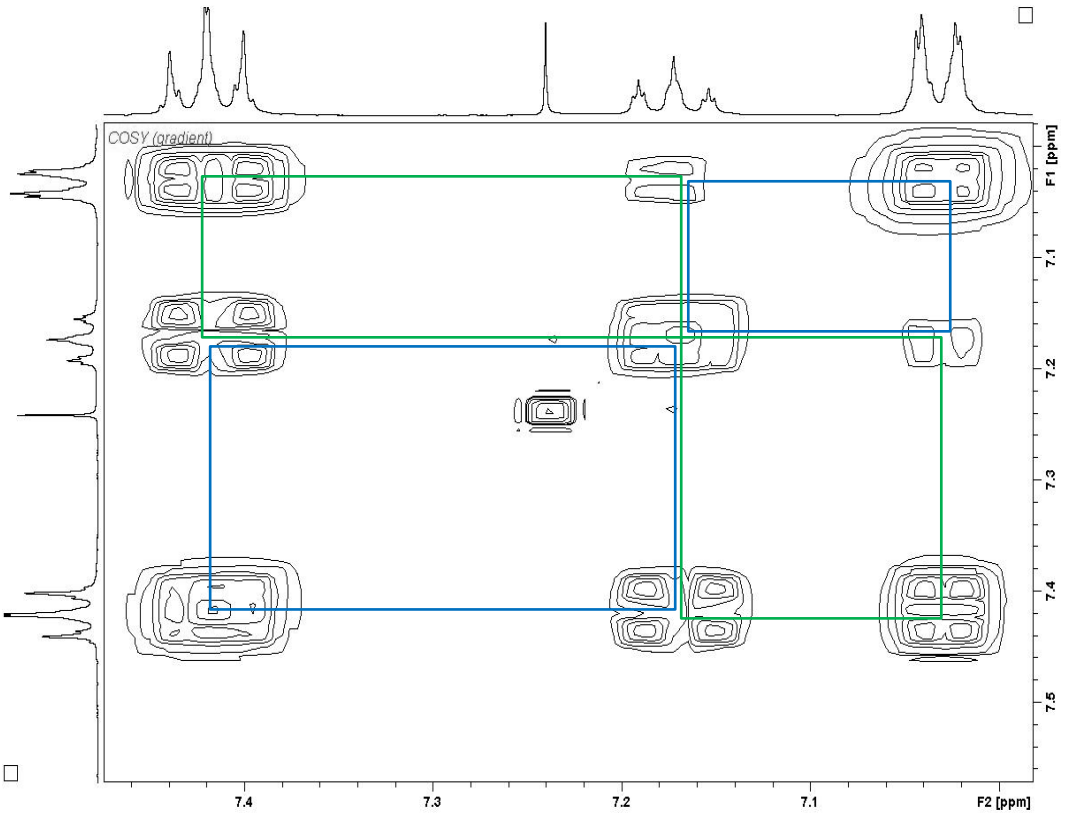

Figure 4.5: The high-resolution COSY spectrum of the 7-7.5 ppm region of 4a shows 3 and 4-bond ^{1}H-^{1}H couplings. The green lines indicate ^{3}J couplings between the signals at 7.17 and 7.42 ppm, while the blue lines show ^{4}J couplings between the triplet at 7.17 and doublet at 7.03 ppm.

There are four non-equivalent proton signals that can be attributed to the ring-substituted phenyl ring (consisting of protons H12 to H15). Both protons H12 and H15 are seen as a doublet of doublets at 8.25 and 5.91 ppm, which is the expected multiplicity of a proton with 1 nearest neighbour along with longer-range ring coupling. Typically, an HMBC experiment would be used to distinguish between H12 and H15 as it usually shows 2 and 3-bond couplings. However, the recorded HMBC spectrum also showed some 4-bond couplings due to long-range coupling through the conjugated ring system, so this could not be used to distinguish between H12 and H15. A unique solution to this was to use a through-space NOESY experiment (Appendix VI) to see if either signal showed correlations to the N-substituted phenyl ring, hence allowing assignment of the signal in the H12

environment. The high-resolution NOESY spectrum of **4a** (Figure 4.4) shows a correlation from the proton signal at 5.91 ppm to the phenyl ring H26 proton at 7.03 ppm, allowing assignment of the proton at 5.91 ppm as H12. Therefore, by process of elimination the remaining doublet of doublets at 8.25 ppm can be assigned as H15.

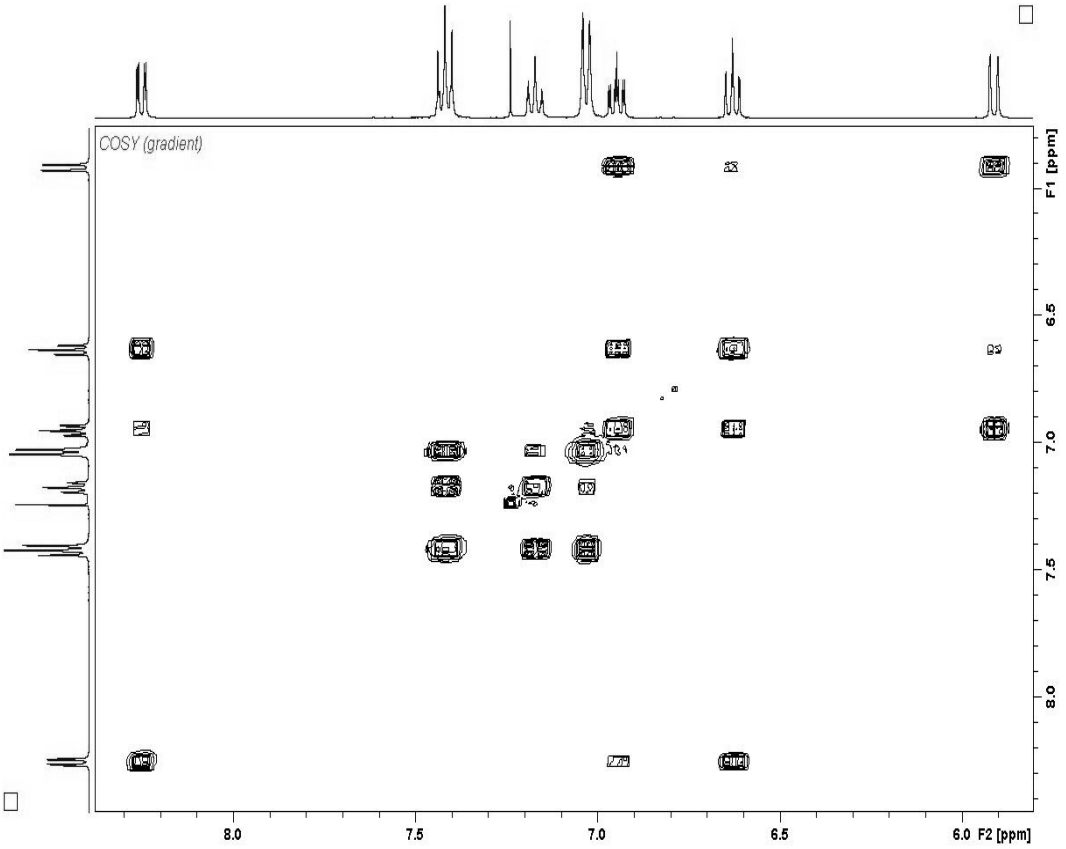

Figure 4.6: A high-resolution COSY spectrum of the phenyl region (5.9-8.5 ppm) of complex 4a shows 3 and 4-bond ^{1}H-^{1}H correlations. For simplicity, correlation lines have been omitted.

The remaining two environments in the 4-proton ring system (H13 and H14) are seen as triplets of doublets at 6.95 and 6.93 ppm. The high-resolution COSY spectrum of the phenyl region (5.9-8.5 ppm) of **4a** (Figure 4.6) allows differentiation between H13 and H14 by showing ^{3}J and ^{4}J couplings to the

protons H12 and H15. Figure 4.6 shows a ^{3}J coupling from the H12 proton at 5.91 ppm to the signal at 6.95 ppm as well as a ^{4}J coupling from the H15 proton at 8.25 ppm, which allows assignment to the H13 environment. Similarly, a ^{3}J coupling from the H15 proton at 8.25 ppm to the signal at 6.63 ppm is seen, with an additional ^{4}J coupling from the H12 proton at 5.91 ppm, enabling assignment of the H14 proton.

Table 4.1: The various proton and carbon signals assigned to each of the ^{1}H and ^{13}C chemical environments for 4a.

Atoms	^{1}H chemical shift (ppm)	^{13}C chemical shift (ppm)
1, 2	4.42	93.8
3, 8	~2.62 (**a**), ~2.16 (**b**)	31.0
4, 7	~2.63 (**a**), ~2.22 (**b**)	28.4
5, 6	5.42	98.5
9	-	166.2
10	-	114.7
11	-	153.1
12	5.91	116.1
13	6.95	131.5
14	6.63	116.4
15	8.25	133.9
21	-	150.2
22, 26	7.03	130.0
23, 25	7.42	129.7
24	7.17	126.1

^{13}C NMR

The ^{13}C NMR spectrum of complex **4a** (Figure 4.7) gives a number of signals corresponding to the 15 different NMR environments shown in Figure 4.2, and these are assigned in Table 4.1.

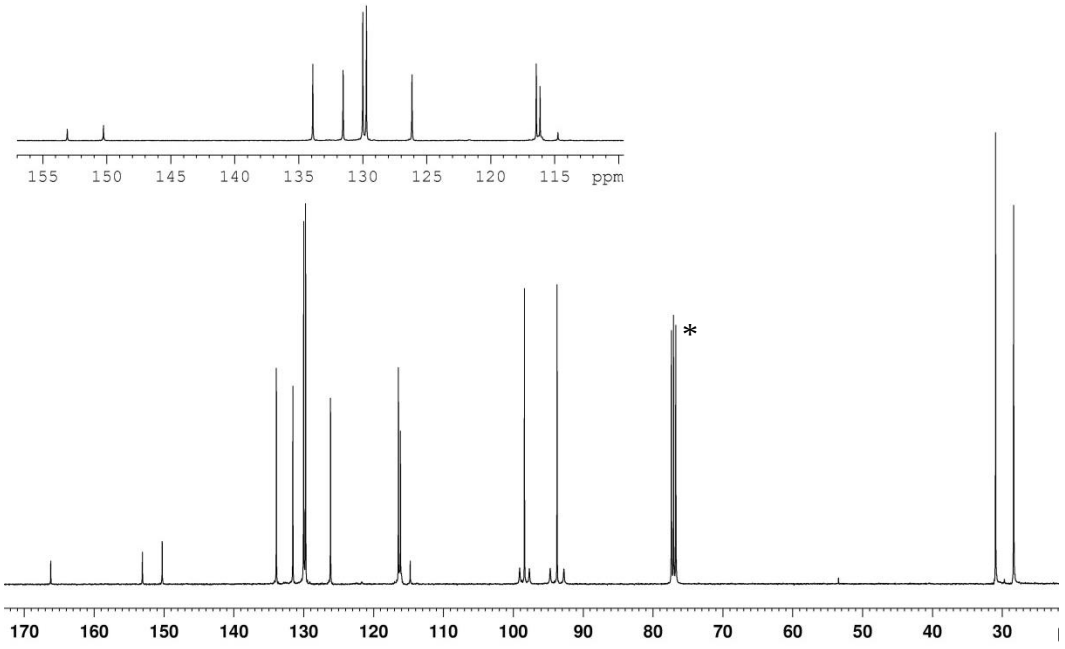

Figure 4.7: The ^{13}C NMR spectrum of complex 4a shows a number of signals which correspond to the various carbon environments (* represents $CDCl_3$). The top left shows an expansion of the phenyl and carbonyl region (110-170 ppm).

The COD methyne (CH) resonances are observed at 98.4 and 93.8 ppm, and both exhibit satellites from coupling to ^{195}Pt ($^{1}J_{Pt\text{-}C}$ = 139.4 and 197.6 Hz, respectively). These two signals correspond to either the C1/C2 or C5/C6 environments. The NOESY spectrum (Appendix VI) shows a stronger through-space correlation from the signal at 93.8 ppm to the nitrogen-attached phenyl ring signals at 7.03 and 7.42 ppm (in the H22/26 and H23/25 positions) than the signal at 94.8 does, hence the signal at 93.8 ppm can be assigned to the C1/C2 environment. Therefore by process of elimination, the resonance at 98.4 ppm can be assigned to

the C5/C6 environment. The COD region of the HSQC spectrum (Figure 4.8) confirms these assignments, as it shows that the signal at 98.4 is correlated to the H5/H6 proton signal at 5.42 ppm, while the signal at 93.8 ppm shows correlations to the proton signal at H1/H2 resonance at 4.42 ppm.

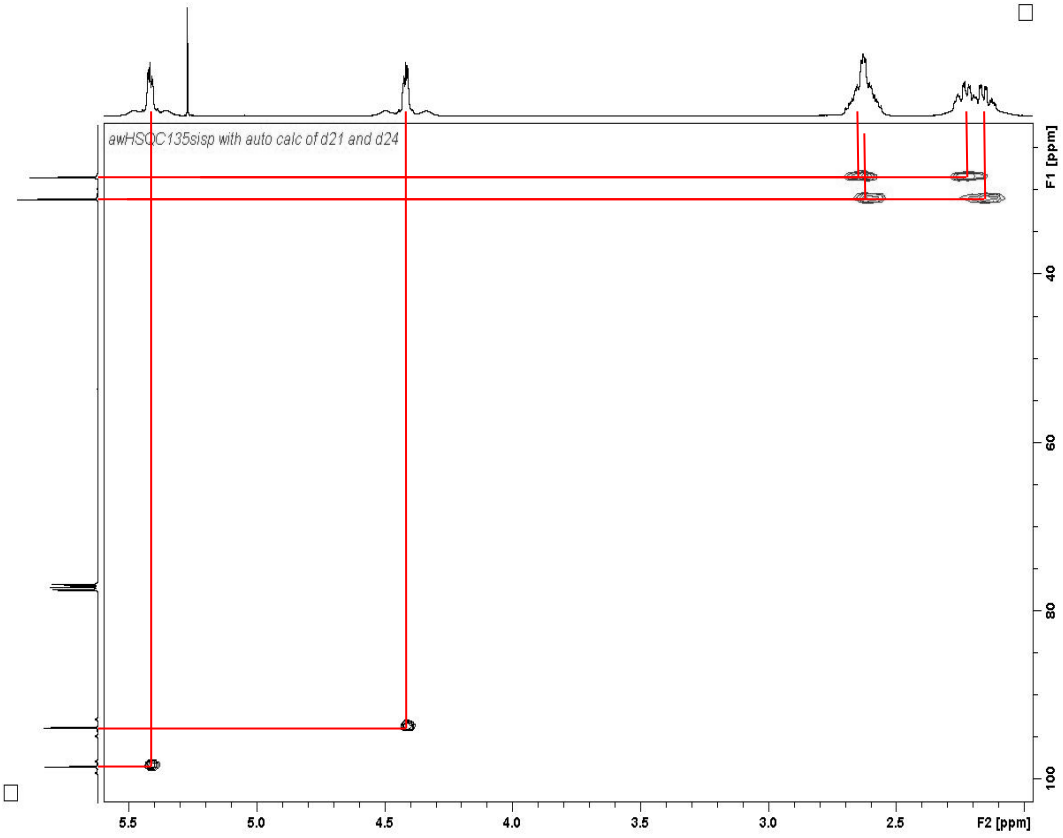

Figure 4.8: The COD region of the HSQC spectrum of complex 4a, showing ^{13}C-^{1}H correlations (using red lines) between the COD carbons and protons.

The COD CH_2 signals appear at 31.0 and 28.4 ppm. The HSQC of the COD region (Figure 4.8) indicates that the 31.0 signal shows coupling to the proton signals at ~2.62 and ~2.16 ppm, while the resonance at 28.4 ppm shows correlations to the proton signals at ~2.63 and ~2.22 ppm. The H2BC spectrum of complex **4a** enables assignment of each COD methylene, as it displays 2-bond ^{13}C-^{1}H couplings from the previously assigned COD CH carbons. The COD section of the H2BC spectrum of complex **4a** (Figure 4.9) shows a 2-bond

coupling from the C1/C2 proton at 4.42 ppm to the carbon at 31.0 ppm, hence this can be assigned as the C3/C8 environment. Similarly, Figure 4.9 displays a 2-bond coupling from the C5/C6 proton at 5.42 ppm to the carbon at 28.4 ppm, enabling assignment of this carbon as the C4/C7 environment.

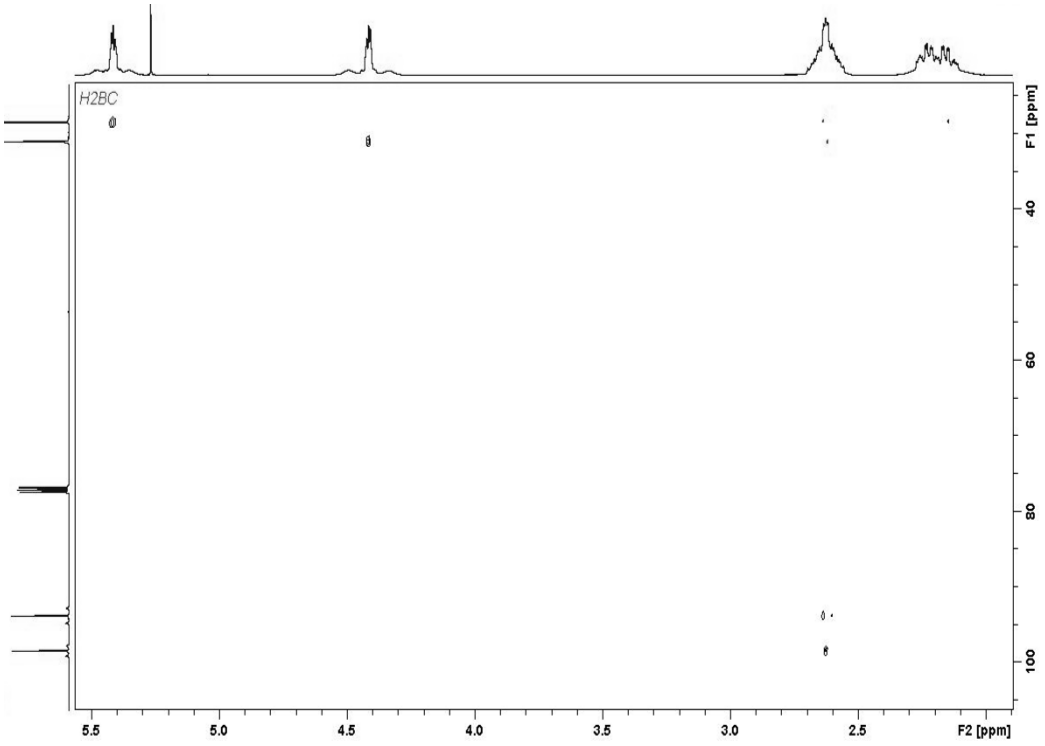

Figure 4.9: The H2BC spectrum of the COD region of complex 4a shows 2-bond ^{13}C-^{1}H couplings between the COD methyne and methylenes, allowing assignment of the two CH_2 carbons.

The HMBC experiment confirms that, as for complex **2a**, the symmetry adopted by the COD moiety is that of the left conformer in Figure 2.10. The HMBC of the COD CH region of complex **4a** (Figure 4.10) shows not only residual ^{1}J couplings from the C1/C2 and C5/C6 carbons at 98.4 and 31.0 ppm to the protons at 5.42 and 4.42 ppm (respectively), but also displays 2-bond ^{13}C-^{1}H correlations from each carbon resonance to an olefinic proton of the same chemical shift. This verifies that the COD moiety of complex **4a** adopts the left hand symmetrical

conformer in Figure 2.10, and that C1 and C2; C5 and C6; C3 and C8, and C4 and C7 are all chemically equivalent.

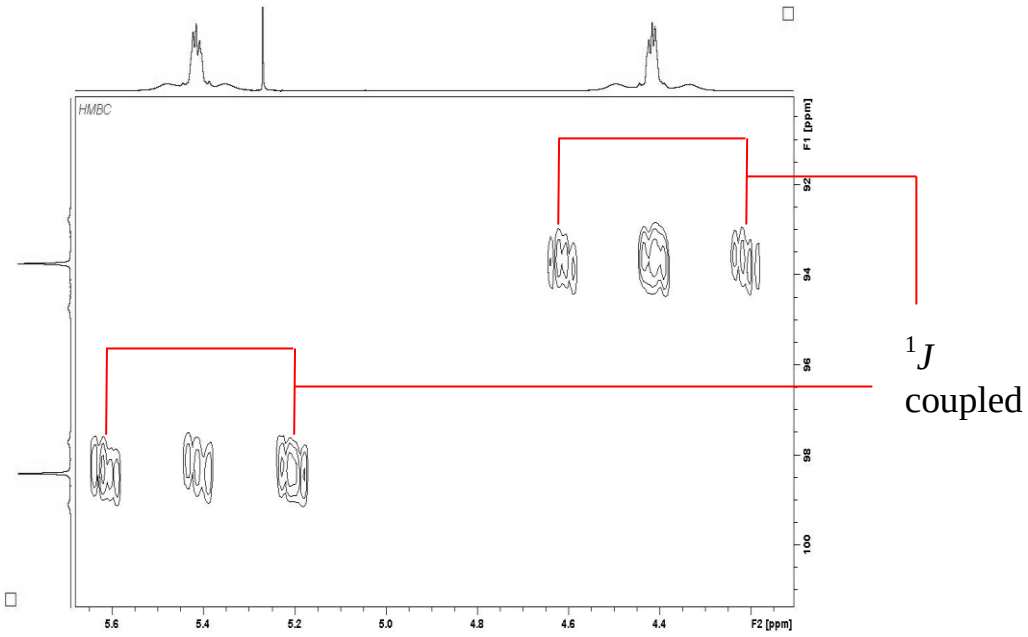

Figure 4.10: The COD CH region of the HMBC spectrum of complex 4a shows both residual ^1J and ^2J couplings, confirming the symmetrical conformation the COD moiety adapts in the complex.

Assuming that there is free rotation about the N1-C21 bond which makes the C22 and C26 environments equivalent, there are four ^{13}C environments in the nitrogen-attached phenyl ring (C22/C26, C23/C25, C24 and quaternary carbon C21). The phenyl region of the HSQC spectrum (Figure 4.11) proved very useful in assigning the remaining protonated carbons in complex **4a**. Figure 4.11 allows identification of the carbon signals at 130.0, 129.7 and 126.1 ppm as the environments C22/C26, C23/C25 and C24 (as they are attached to H22/H26 at 7.03 ppm, H23/H25 at 7.42 ppm and H24 at 7.17 ppm, respectively).

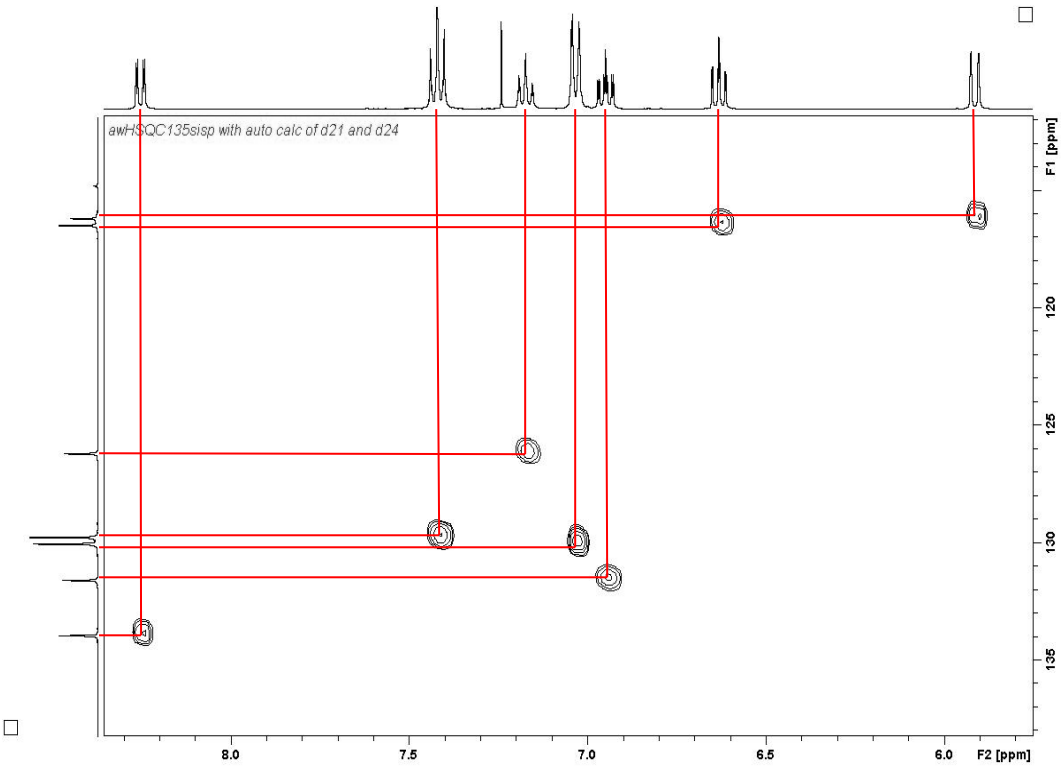

Figure 4.11: The phenyl region of the HSQC NMR spectrum of complex 4a, showing ^{13}C-^{1}H correlations which allow assignment of protonated phenyl carbons.

The remaining quaternary carbons can all be assigned using chemical shift and an HMBC experiment. Due to its chemical shift, the carbonyl in the C9 position is expected to be the quaternary carbon with the highest ppm (166.2 ppm). The phenyl region of the HMBC spectrum (Figure 4.12) confirms this assignment as it shows a strong ^{3}J coupling from the carbon at 166.2 ppm to the H15 proton at 8.25 ppm, a slightly weaker ^{4}J coupling to the H12 proton at 5.91 ppm and a very weak ^{4}J coupling to the H14 proton at 6.63 ppm. The H2BC spectrum further substantiates this assignment, as it shows no 2-bond ^{13}C-^{1}H couplings from the signal at 166.2 ppm (as expected).

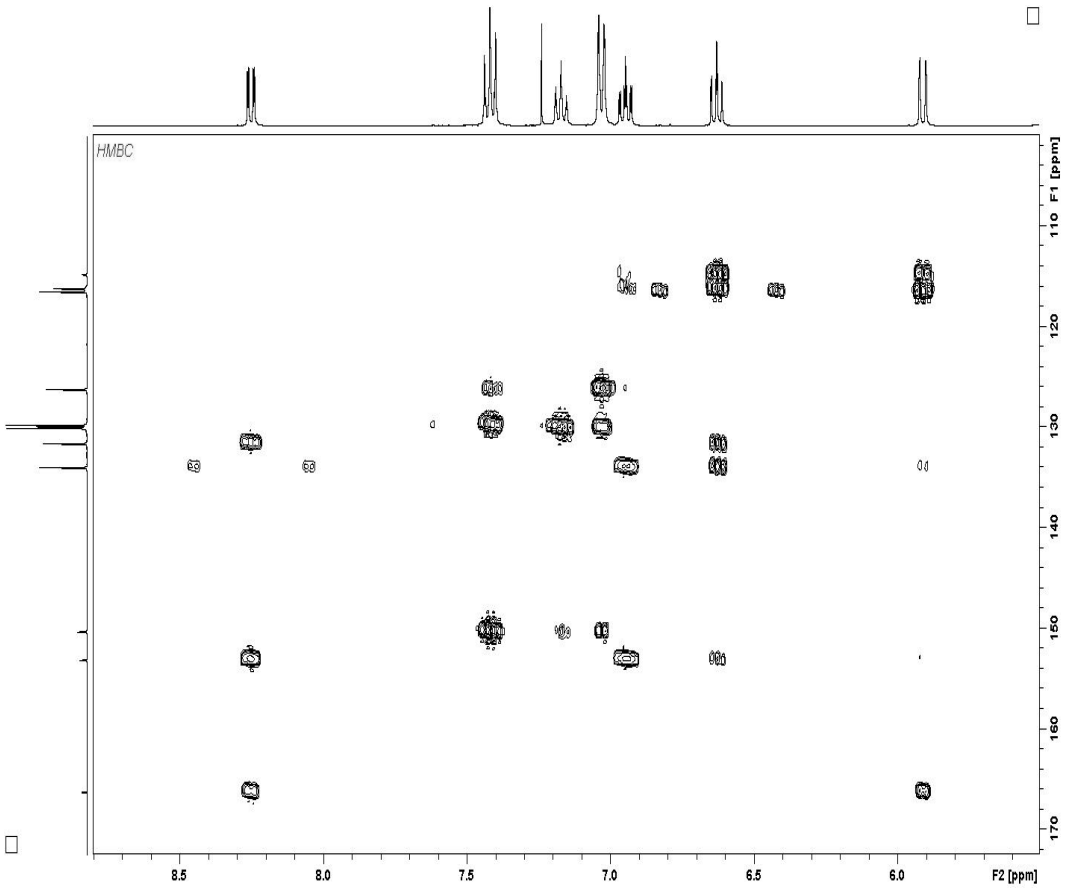

Figure 4.12: The phenyl region of the HMBC spectrum of complex 4a shows long-range ^{13}C-^{1}H couplings, and is particularly useful in assigning the quaternary carbons.

In aromatic systems, 3-bond ^{13}C-^{1}H couplings in long-range heteronuclear experiments tend to be stronger than 2-bond correlations. The quaternary carbon at 150.2 ppm shows a strong ^{3}J coupling to the H23/H25 proton signal at 7.42 ppm, as well as a weak 2-bond coupling to the H22/H26 proton signal at 7.03 ppm and an even weaker ^{4}J correlation to the H24 resonance at 7.17 ppm. This enables assignment of the quaternary carbon at 150.2 ppm to the C21 environment.

Commonly, the chemical shift of a carbon neighbouring a carbonyl group (such as C10) is lower than for a standard quaternary carbon in a ring system, while that of

a carbon two positions from a carbonyl (for example, C11) is higher. This suggests that the carbon at 114.7 ppm arises from the C10 environment, while the signal at 153.1 ppm may be the C11 carbon. The HMBC spectrum (Figure 4.12) confirms these assignments. It shows a strong ^{3}J coupling from the carbon at 114.7 ppm to the H14 proton at 6.63 ppm, and an additional relatively strong 3-bond correlation to the H12 signal at 5.91 ppm. Similarly, the spectrum shows a strong 3-bond coupling from the carbon at 153.1 ppm to the H14 resonance at 6.95 ppm and another strong ^{3}J correlation to the H15 proton signal at 8.25 ppm. Hence the quaternary carbons at 114.7 and 153.1 ppm can be assigned as the C10 and C11 environments, respectively.

4.2.3 IR Spectral Analysis

The IR spectra of complex **4a** and its parent acid differ to that of **2a** significantly. The parent material *N*-phenylanthranilic acid **124** has a very strong C=O stretch at 1660 cm^{-1}, as well as a very strong C-N stretch at 1263 cm^{-1}. These decrease to 1616 cm^{-1} and increase to 1338 cm^{-1} respectively upon coordination to the platinum(II) metal centre to form complex **4a**. The 1500-1700 cm^{-1} region is of particular interest, as it shows the key changes in peaks following reaction of the parent acid to form the complex. This is highlighted in Figure 4.13, and a comparison in assigned frequencies between the two outlined in Table 4.2. DFT calculations were carried out to calculate vibrations for both *N*-phenylanthranilic acid and complex **4a**, which aided the assignment of peaks in the spectra.

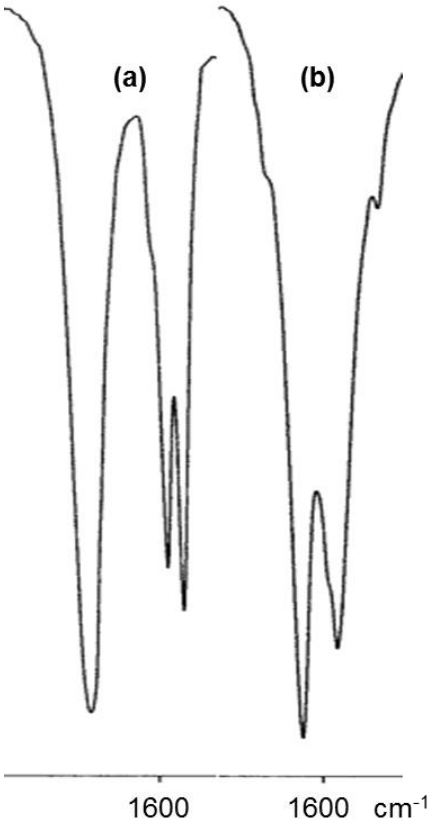

Figure 4.13: The IR spectra of (a) *N*-phenylanthranilic acid and (b) complex 4a, illustrating the changes in vibrations in the 1500-1700 cm^{-1} region.

Table 4.2: Selected IR absorptions obtained for starting material *N*-phenylanthranilic acid and complex 4a

Compound	Wavenumber (cm^{-1})	Assignment
***N*-phenylanthranilic acid**	1660	C=O stretch
	1590 & 1577	C=C stretch (asym.)
4a	1616	C=O stretch
	1587	C=C stretch

4.3 Conclusion

A platinum(II) complex containing a 6-membered ring which utilises the N,O-donor ligand *N*-phenylanthranilic acid has been successfully synthesised and characterised. This extends the range of N,O-donor ligands that can be successfully coordinated to a platinum(II) metal centre, using silver(I) oxide as a mediator for the reaction. A variety of 1D and 2D NMR techniques have been used to provide full spectral assignment. The crystal structure for this has not yet been acquired, although crystals expected to be suitable for X-ray determination have been grown. Like the platinum-hippurate complex **2a**, the presence of the labile COD moiety suggests that a range of phosphine-substituted derivatives should be easily produced via straightforward ligand substitution reactions.

Chapter 5: Further Recommendations

5.1 Experimental Recommendations

It is of interest to determine the crystal structures of complexes **2b**-**e** and particularly **4a** (to investigate its planarity), as only one crystal structure for complex **2a** was determined in the duration of this thesis due to time constraints.

Biological testing has not yet been carried out on any of the novel complexes (**2a**-**e** and **4a)**, as biological testing facilities were unavailable during the period of this project. Biological testing would be of interest in future, as platinum(II) complexes have attracted much attention as probable anti-cancer agents since 1969.[1]

Future research of this type should focus on investigating more N,O-donor ligands, with both 5 and 6-membered ring systems. It would be relevant to attempt to coordinate existing and new dianionic N,O-donor ligands to other precious metal centres such as gold, ruthenium and rhodium. Although attempts to coordinate two N,O-donor ligands to a gold(III) metal centre did not work in this thesis, attempts using new ligands (or the same, under different conditions) may be successful.

5.2 Theoretical Recommendations

Because this was a primarily synthetic thesis, there were limited opportunities to do a thorough investigation as to the most accurate level of theory possible for the

DFT-calculations. Therefore, any discrepancy between theoretical and experimental results may be due to this. However, a sensible method and basis set was chosen for each calculation based on the literature and previous work carried out on similar complexes. It would be preferable to carry out a more thorough basis set for future work. Some calculations were attempted using the more accurate aug-cc-pVTZ basis set, but convergence issues were encountered, which may have been resolved with more time.

References

1. Rosenberg, B.; Vancamp, L.; Trosko, J. E.; Mansour, V. H. Platinum compounds: a new class of potent antitumour agents. *Nature* **1969**, *222*, 385-386.

2. Nance, L. E.; Frye, H. G. Preparation and infrared analysis of some dipeptide complexes of Zeise's salt. *J. Inorg. Nucl. Chem.* **1976**, *38*, 637-639.

3. Kemmitt, R. D. W.; Mason, S.; Fawcett, J.; Russell, D. R. Synthesis and reactivity of N-acetylamino acidate(2-) and related complexes of platinum(II). *J. Chem. Soc., Dalton Trans.* **1992**, 1165-1176.

4. Fehn, A. Crosslinkable polyorganosiloxane compositions. EP1672031A1, **2006**.

5. Boyer, J. L.; Cundari, T. R.; DeYonker, N. J.; Rauchfuss, T. B.; Wilson, S. R. Redox activation of alkene ligands in platinum complexes with non-innocent ligands. *Inorg. Chem.* **2008**, *48*, 638-645.

6. Laurent, P.; Veyre, L.; Thieuleux, C.; Donet, S.; Coperet, C. From well-defined Pt(ii) surface species to the controlled growth of silica supported Pt nanoparticles. *Dalton Trans.* **2013**, *42*, 238-248.

7. Liu, Y.; Li, D.; Sun, S. Pt-based composite nanoparticles for magnetic, catalytic, and biomedical applications. *J. Mater. Chem.* **2011**, *21*, 12579-12587.

8. Tang, Z.; Kotov, N. A. One-dimensional assemblies of nanoparticles: preparation, properties, and promise. *Adv. Mater.* **2005**, *17*, 951-962.

9. Astruc, D. Front Matter. In *Nanoparticles and Catalysis*; Wiley-VCH Verlag GmbH & Co. KGaA, **2008**.

10. Kemmitt, R. D. W.; Mason, S.; Russell, D. R. The synthesis and reactivity of N-bonded η1-1-azaallyl type complexes of platinum(II) and palladium(II). Crystal structure of [Pt{CH=C(NHCOMe)C(O)O}(PMe_2Ph)$_2$]. *J. Organomet. Chem.* **1991**, *415*, C9-C13.

11. Petrosyan, V. S.; Permin, A. B.; Bogdashkina, V. I.; Krut'ko, D. P. Alkyl derivatives of platinum and rhodium as intermediates in homogeneous reactions of olefin hydrogenation and isomerisation. *J. Organomet. Chem.* **1985**, *292*, 303-309.

12. Bauer, W.; Prem, M.; Polborn, K.; Suenkel, K.; Steglich, W.; Beck, W. Organometallic complexes of iridium, palladium, chromium, and iron from 2-phenyl-5(4H)-oxazolones - organometallic labeled dipeptides. *Eur. J. Inorg. Chem.* **1998**, 485-493.

13. Chaudhuri, S. R.; Kaludjerovic, G. N.; Bette, M.; Schmidt, J.; Schmidt, H.; Paschke, R.; Steinborn, D. Synthesis, characterization and cytotoxicity studies of platinum(II) complexes with amino acid ligands in various coordination modes. *Inorg. Chim. Acta* **2013**, *394*, 472-480.

14. Gong, Y.-Q.; Cheng, Y.-F.; Gu, J.-M.; Hu, X.-R. Synthesis and characterization of N-benzoyl-DL-α-valinato complexes of palladium(II), platinum(II). Crystal structure of a complex with deprotonated nitrogen coordinating to the palladium(II). *Polyhedron* **1997**, *16*, 3743-3746.

15. Zeng, H. Benzoisoselenazole derivatives with anti-inflammatory, antineoplastic, and antithrombotic activity. CN1511835A, **2004**.

16. Zeng, H. Bisbenzisoselenazolonyl derivatives having antineoplastic, antiinflammatory and antithrombotic activities, and their therapeutic use. US20090123567A1, **2009**.

17. Gabano, E.; Cassino, C.; Bonetti, S.; Prandi, C.; Colangelo, D.; Ghiglia, A.; Osella, D. Synthesis and characterisation of estrogenic carriers for cytotoxic Pt(II) fragments: biological activity of the resulting complexes. *Org. Biomol. Chem.* **2005**, *3*, 3531-3539.

18. Sengupta, S.; Jordan, V. C. Selective estrogen modulators as an anticancer tool: Mechanisms of efficiency and resistance. *Adv. Exp. Med. Biol.* **2008**, *630*, 206-219.

19. Zhang, J.; Wang, L.; Li, L.; Qin, X.; Li, X. Medicinal composition of platinum coordinated complex, and its application in the preparation of antineoplastic drug. CN101891769A, **2010**.

20. Zhang, J.; Zhang, F.; Wang, L.; Du, J.; Wang, S.; Li, S. Synthesis, characterization, and cytotoxicity of complexes of platinum(II) with 2,2'-bipyridine and N-benzoyl-L-amino acid dianion. *J. Coord. Chem.* **2012**, *65*, 2159-2169.

21. Sankhla, N. K.; Kanungo, P. K.; Mehta, R. K. Alpha-picoline and ethylenediamine adducts of Ni(II), Cu(II), Pd(II) and Pt(II) complexes with ortho-(2-pyrrolideneimino)benzoic acid and 3-(2-pyrrolideneimino)propionic acid. *Indian J. Chem. A* **1979**, *17*, 422-424.

22. Singh, P.; Pokhariyal, G. P.; Singh, V.; Singh, S. C.; Agrawal, G. K. Studies on Pt(IV), Rh(III) and Co(III) complexes of Schiff-bases. *Acta Chim. Hung.* **1980**, *104*, 63-67.

23. Pokhariyal, G. P. Some square-planar complexes of platinum(II) with 2,5-dihydroxyacetophenone and N-4-methylphenylglyoxal Schiff-bases. *J. Indian Chem. Soc.* **1985**, *62*, 11-13.

24. Gade, D.; Puri, L. Synthesis and spectral studies of platinum complexes with amide-group containing ligands. *Transit. Metal Chem.* **1989**, *14*, 203-205.

25. Xie, X.-h.; Chen, J.-y.; Xu, W.-q.; He, E.-x.; Zhan, S.-z. Design, synthesis and reactivity with dichloro-bis(triphenylphosphine) platinum(II) of two triazenide compounds. *Inorg. Chim. Acta* **2011**, *373*, 276-281.

26. Ruiz, J.; Lopez, J. F. J.; Rodriguez, V.; Perez, J.; de Arellano, M. C. R.; Lopez, G. Synthesis and characterization of chelate and bridging triazenide complexes of palladium and platinum. Stereoselective oxidative addition of chlorine or

iodine to [NBu_4][Pt(C_6F_5)$_2$(η_2-PhNNNPh)]. *J. Chem. Soc. Dalton Trans.* **2001**, 2683-2689.

27. Oliver, D. L.; Anderson, G. K. Substitution reactions of (diphosphine)palladium(II) and -platinum(II) chloride and triflate complexes. *Polyhedron* **1992**, *11*, 2415-2420.

28. Henderson, W.; K. Nicholson, B. Synthesis and electrospray mass spectrometry of platinum(II) complexes derived from thiourea dianions and the x-ray structure of [Pt{NMeC(=NCN)S}(COD)] (COD = Cyclo-octa-1,5-diene). *Polyhedron* **1996**, *15*, 4015-4024.

29. Cairns, M. A.; Dixon, K. R.; Smith, M. A. R. A new synthesis of platinum—carbon bonds. *J. Organomet. Chem.* **1977**, *135*, C33-C34.

30. Daldy, J. A.; Fawcett, J.; Henderson, W.; Kemmitt, R. D. W.; Russell, D. R. Cyclopentadiene-, furan- and thiophene-derived 1,2-dioxolene complexes of platinum(II) and the crystal structure of [Pt{OCC(CO_2Me)CH_2C(CO_2Me)CO}(PPh_3)$_2$]. *J. Chem. Soc. Dalton Trans.* **1994**, 3383-3387.

31. Appleton, T. G.; Clark, H. C.; Manzer, L. E. The trans-influence: its measurement and significance. *Coordin. Chem. Rev.* **1973**, *10*, 335-422.

32. Silverstein, R. M.; Webster, F. X.; Kiemle, D. J. *Spectrometric identification of organic compounds*; 7th ed.; John Wiley & Sons: Hoboken, NJ, **2005**.

33. Balci, M. *Basic 1H- and 13C-NMR Spectroscopy*; Elsevier Science & Technology: Amsterdam, NLD, **2005**.

34. Berlin, A.; Bradamante, S.; Ferraccioli, R.; Pagani, G. A. Trigonal configuration of disulphonyl carbanions. *J. Chem. Soc. Chem. Comm.* **1986**, 1191-1192.

35. Otto, S.; Roodt, A.; Purcell, W. Synthesis and characterisation of water soluble Pt(II) complexes of 1,3,5-triaza-7-phosphaadamantane (PTA). Crystal and molecular structure of {cis-[$PtCl_2$($PTA)_2$]}$_2$ · H2O. *Inorg. Chem. Comm.* **1998**, *1*, 415-417.

36. Henderson, W.; MacIndoe, J. S. *Mass spectrometry of inorganic, coordination and organometallic compounds : tools, techniques, tips*; Wiley: Chichester, **2005**.

37. Ramachandran, E.; Natarajan, S. Crystal growth of some urinary stone constituents: II. In-vitro crystallization of hippuric acid. *Cryst. Res. Technol.* **2002**, *37*, 1274-1279.

38. Syed, A.; Stevens, E. D.; Cruz, S. G. Reexamination of the pi-bonding in dichloro(cycloocta-1,5-diene)platinum. *Inorg. Chem.* **1984**, *23*, 3673-3674.

39. Currie, M.; Macdonald, A. L. Hippuric acid: a neutron diffraction analysis. *J. Chem. Soc. Perkin Trans. 2* **1974**, 784-787.

40. Dinger, M. B.; Henderson, W. Organogold(III) metallacyclic chemistry. Part 4. Synthesis, characterisation, and biological activity of gold(III)-thiosalicylate and -salicylate complexes. *J. Organomet. Chem.* **1998**, *560*, 233-243.

41. Chatt, J.; Hart, F. A. *J. Chem. Soc. Dalton Trans.* **1960**, 1378.

42. Daigle, D. J.; Pepperman Jr, A. B.; Vail, S. L. Synthesis of a monophosphorous analog of hexamethylenetriamine. *J. Heterocyclic Chem.* **1974**, *11*, 407-408.

43. Bishop, J. J.; Davison, A.; Katcher, M. L.; Lichtenberg, D. W.; Merrill, R. E.; Smart, J. C. Symetrically disubstituted ferrocenes: 1. The synthesis of potential bidentate ligands. *J. Organomet. Chem.* **1971**, *27*, 241-&.

44. Fuchita, Y.; Ieda, H.; Kayama, A.; Kinoshita-Nagaoka, J.; Kawano, H.; Kameda, S.; Mikuriya, M. Cycloauration of 2-substituted pyridine derivatives. Synthesis, structure and reactivity of six-membered cycloaurated complexes of 2-anilino-, 2-phenoxy- and 2-(phenylsulfanyl)-pyridine. *J. Chem. Soc. Dalton Trans.* **1998**, 4095-4100.

45. Cinellu, M. A.; Zucca, A.; Stoccoro, S.; Minghetti, G.; Manassero, M.; Sansoni, M. Synthesis and characterization of gold(III) adducts and cyclometallated derivatives with 2-substituted pyridines. Crystal structure of $[Au\{NC_5H_4(CMe_2C_6H_4)\text{-}2\}Cl_2]$ *J. Chem. Soc. Dalton Trans.* **1995**, 2865-2872.

46. Frisch, M. J.; Trucks, G. W.; Schlegel, H. B.; Scuseria, G. E.; Robb, M. A.; Cheeseman, J. R.; Scalmani, G.; Barone, V.; Mennucci, B.; Petersson, G. A.; Nakatsuji, H.; Caricato, M.; Li, X.; Hratchian, H. P.; Izmaylov, A. F.; Bloino, J.; Zheng, G.; Sonnenberg, J. L.; Hada, M.; Ehara, M.; Toyota, K.; Fukuda, R.; Hasegawa, J.; Ishida, M.; Nakajima, T.; Honda, Y.; Kitao, O.; Nakai, H.; Vreven, T.; Montgomery, J. A., Jr.; ; Peralta, J. E.; Ogliaro, F.; Bearpark, M.; Heyd, J. J.; Brothers, E.; Kudin, K. N.; Staroverov, V. N.; Kobayashi, R.; Normand, J.; Raghavachari, K.; Rendell, A.; Burant, J. C.; Iyengar, S. S.; Tomasi, J.; Cossi, M.; Rega, N.; Millam, N. J.; Klene, M.; Knox, J. E.; Cross, J. B.; Bakken, V.; Adamo, C.; Jaramillo, J.; Gomperts, R.; Stratmann, R. E.; Yazyev, O. A.; A. J.; Cammi, R.; Pomelli, C.; Ochterski, J. W.; Martin, R. L.; Morokuma, K.; Zakrzewski, V. G.; Voth, G. A.; Salvador, P.; Dannenberg, J. J.; Dapprich, S.; Daniels, A. D.; Farkas, Ö.; Foresman, J. B.; Ortiz, J. V.; Cioslowski, J.; Fox, D. J. Gaussian 09. Gaussian Inc.: Wallingford, CT, **2009**.

Appendix I

General Experimental and Theoretical Procedures

All reactions were carried out without attempts to exclude light or air. [$PtCl_2$(COD)],[3] dppe,[41] PTA,[42] dppf,[43] 2-anp$AuCl_2$,[44] and 2-bp$AuCl_2$[45] were prepared using literature methodology. Silver(I) oxide (BDH), hippuric acid (Sigma), filter aid (Ajax), triphenylphosphine (BDH) and *N*-phenylanthranilic acid (BDH) were used as supplied. All solvents were drum grade, with the exception of dichloromethane, which was passed through a solvent purification system to remove water, air and stabilisers.

All 1D and 2D nuclear magnetic resonance (NMR) spectra (^{1}H, ^{13}C & ^{31}P, COSY, NOESY, DEPT, HSQC, HMBC and H2BC) were recorded on a Bruker AVIII-400 spectrometer in $CDCl_3$ or DMSO (as specified in-text) using BBI or BBFO probes, depending on the nucleus of the sample. NMR spectra were referenced to tetramethylsilane at 300K. Standard Bruker supplied pulse programmes were used for each experiment, with parameters including spectral window, number of increments, pulse angle and repetition rate altered as appropriate for each specific sample.

Infra-red (IR) spectra were recorded as KBr discs on a Perkin Elmer Spectrum 100 FT-IR spectrometer.

Electrospray ionisation mass spectrometry (ESI-MS) was performed on a Bruker MicroTOF mass spectrometer, with acquisition in methanol using the positive ion

mode. Calibration was carried out before each set of analyses using sodium formate in positive ion mode.

Elemental analyses were completed in duplicate by the University of Otago Microanalytical Laboratory (Chemistry Department). Melting points were recorded as finely ground samples in capillary tubes on a Buchi M-560 Melting Point instrument.

Unit cell dimensions and reflection data for **2a** were collected at the University of Waikato on an Agilent supernova diffractometer. Empirical absorption corrections were made using spherical harmonics. The structure was solved by direct methods and routine development and refinement was used. Refinement was based on F^2, and all hydrogen atoms were placed in calculated positions. The SHELXS-97 and SHELXL-97 programs were used with the latter for refinement.

Density functional theory (DFT) calculations were completed using Gaussian 09.[46] Unless specified, all calculations were completed using the B3LYP functional and the 6-311++G(2d,2p) basis set for all atoms excluding Pt and Au. For Pt and Au, the LANL2DZ basis set and effective core potential was used instead. Geometry optimisations were completed for all compounds. For compounds that NMR shifts were calculated for, geometry optimisations were also carried out using chloroform as the solvent (unless otherwise specified). NMR chemical shifts were calculated using the GIAO approach with TMS as a reference. The geometrical optimization and NMR chemical shifts of **2e** were calculated using DMSO as the solvent. The structure of **2e** was reoptimized with the smaller 6-31G(d) basis set to allow harmonic frequencies to also be calculated.

Appendix II

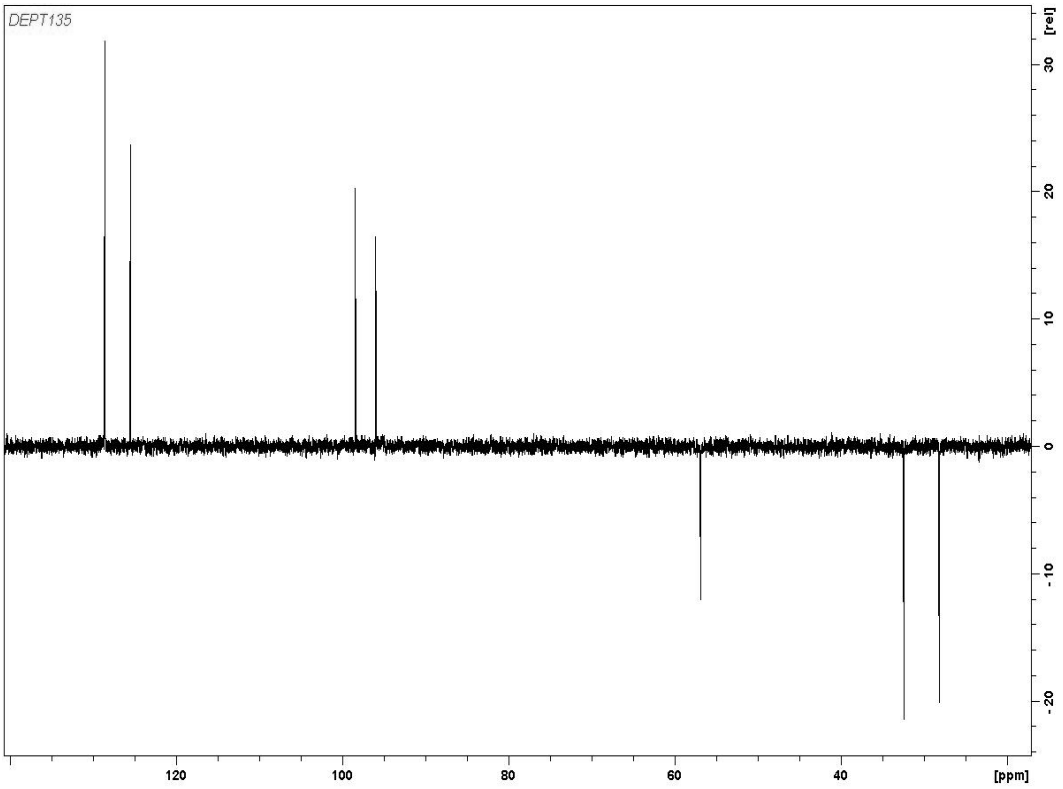

The DEPT135 NMR spectrum of complex 2a shows the ring methylene signal and the COD CH_2 signals as negative, with the CH and CH_3 signals shown as positive.

Appendix III

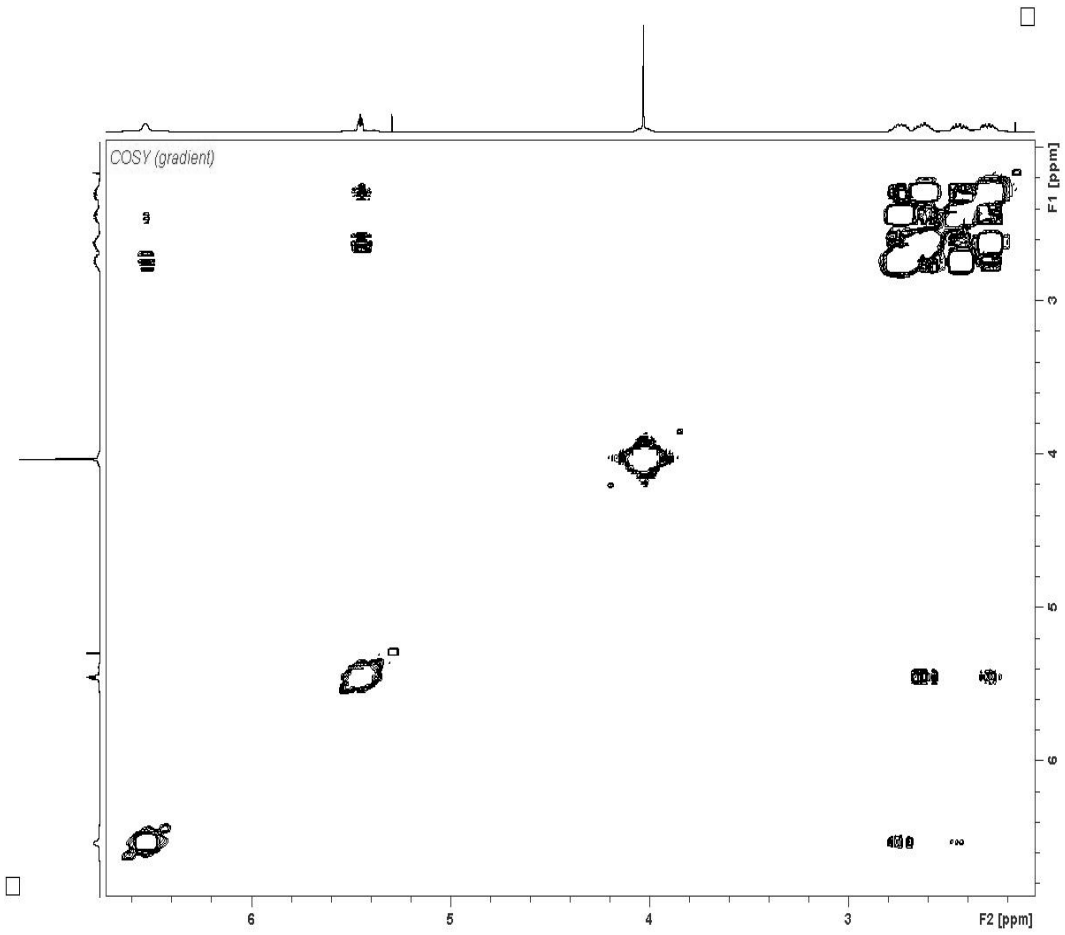

The COSY spectrum of 2a showing correlations from alkene protons to methylene protons. Correlations from the proton at alkene proton at 6.51 ppm to the methylene protons at ~2.72 and ~2.42 ppm are shown in orange, while correlations from the alkene proton at 5.43 to the methylene protons at ~2.60 and ~2.28 ppm are shown in purple. Correlation lines are drawn directly from alkene to methylene for clarity.

Appendix IV

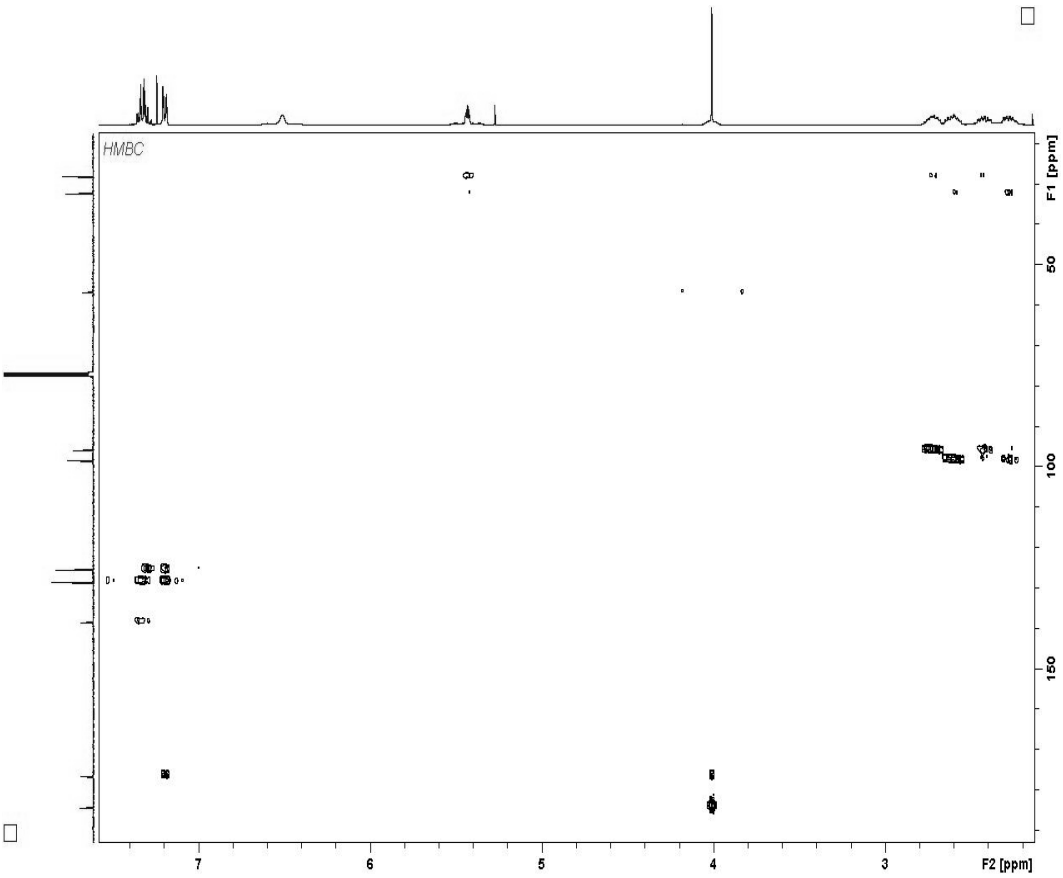

The HMBC spectrum of complex 2a showing correlations from the nitrogen-attached carbonyl at 176.6 ppm to the aromatic protons. The spectrum also shows a lack of ^{2}J coupling from the carbon at 28.2 ppm to a proton attached to a carbon of the same chemical shift, confirming the symmetry of 2a as the left conformer in Figure 2.10.

Appendix V

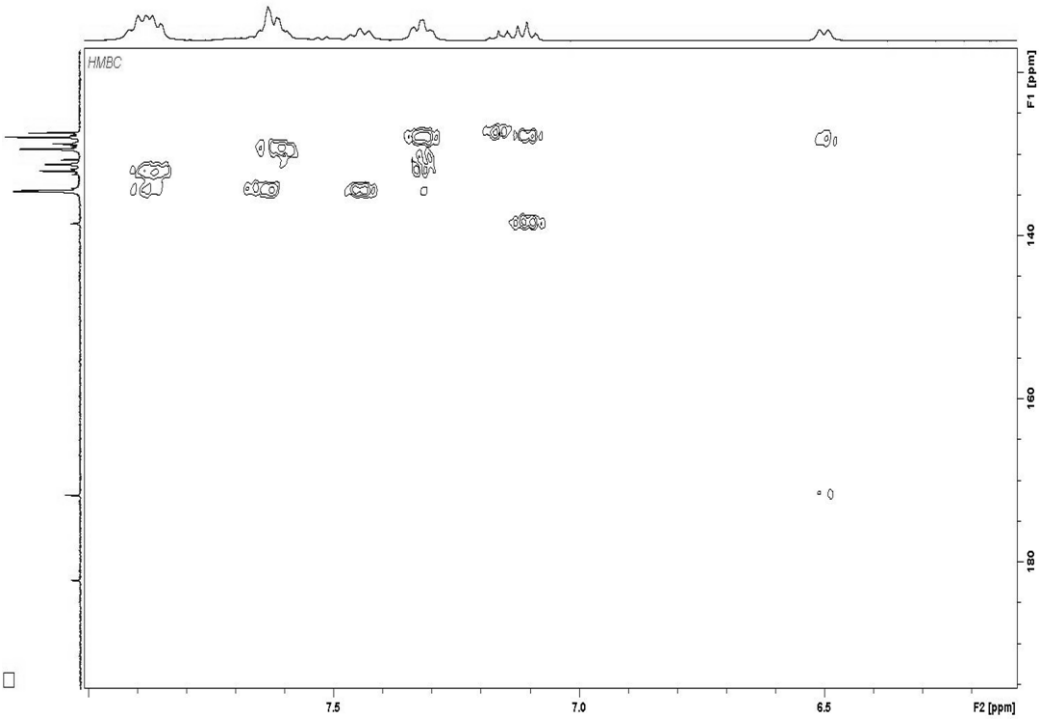

The HMBC spectrum of the carbonyl and aromatic ^{13}C region of complex 2e. The metallacycle carbonyl at 182.1 ppm shows no long-range couplings to the aromatic protons as it is too far away.

Appendix VI

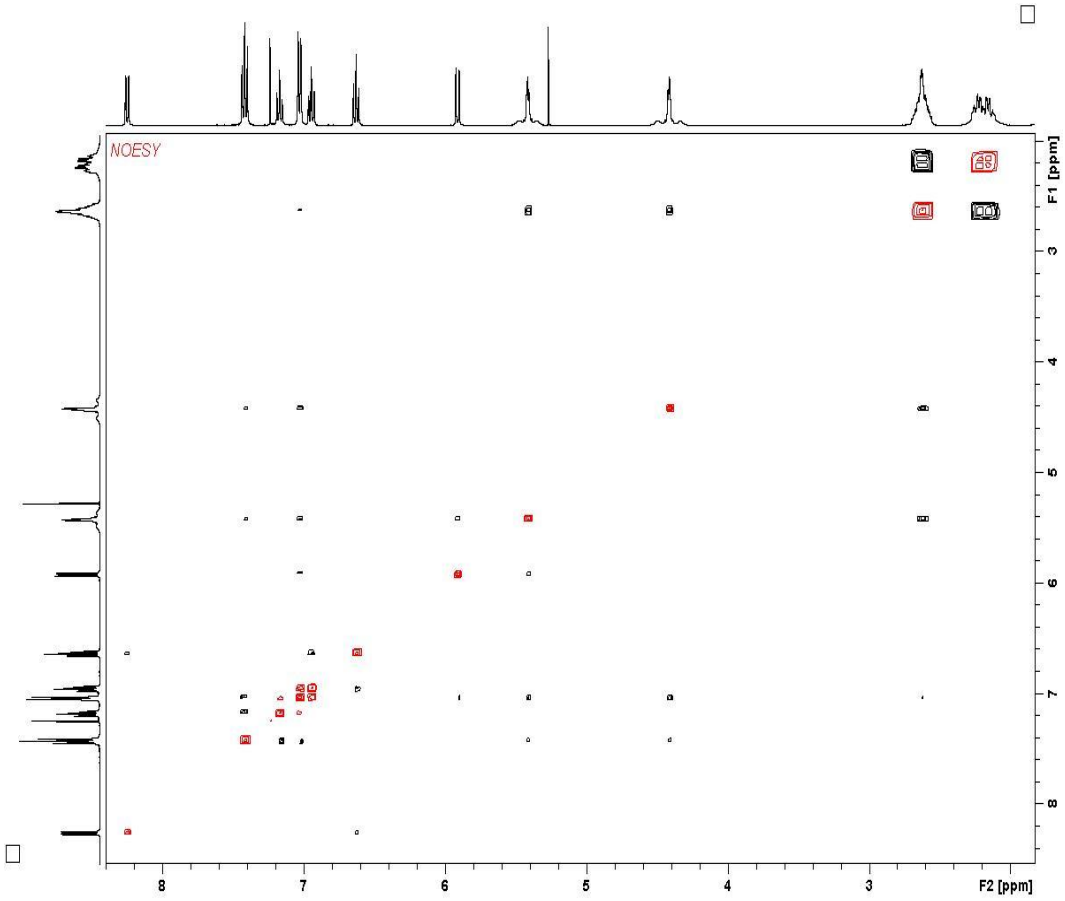

The NOESY spectrum of complex 4a, showing through-space ^{1}H-^{1}H correlations.